RUSSIAN JOURNAL OF EARTH SCIENCES, VOL. 6, NO. 6, PAGES 391–456, DECEMBER 2004

Continuous record of geomagnetic field variations during cooling of the Monchegorsk, Kivakka and Bushveld Early Proterozoic layered intrusions

D. M. Pechersky[1], V. S. Zakharov[2], A. A. Lyubushin[1]

Abstract. A continuous record of the geomagnetic field direction during of cooling of the Monchegorsk (2.5 Ga), Kivakka (2.45 Ga) and Bushveld (2.06 Ga) layered intrusions was conducted for the first time. The low-Ti titanomagnetites (T_c = 530–580°C) are the main natural remanent magnetization (NRM) carriers. The high temperature NRM component according to petromagnetic characteristics is thermoremanent and was acquired at the cooling phase of the intrusion. The magnetic grains above 540°C are close to a single-domain state. The temperature versus time and cooling velocity versus temperature and time dependences during cooling of intrusions were calculated on the basis of solution of the Stefan problem and the nonstationary heat conduction problem. The geothermal gradient value was taken as 20° km^{-1}. The unblocking temperatures in the course of thermal demagnetization of samples (T_d) and the blocking temperatures during cooling from high temperatures (T_b) rate dependences were used for conversion of the T_d to T_b [*Dodson and McClelland,* 1980]. A detailed thermal demagnetization at 2°–3° interval from 530°C up to 580°C was made and a pattern of behavior of the geomagnetic field direction was obtained (a) for the time of "running" the Curie points over the section and (b) for the cooling time of the intrusion at each sampling point from T_b = 580°C. A wavelet analysis has been used to study the field variation etc. The main rhythms of the direction variation spectrum are 3–4.5, 5–7, 8–10, 12, 15–17, 19–20, 30–40, 50–60, and 90–100 kyr and they change in time. The length of rhythms is different and ranges from 1–2 oscillations ("splashes") up to 10–12. The **Monchegorsk intrusion**. The pole 265.3°E, 1.3°N. The length of record is ∼70 kyr. The geomagnetic excursion of the reversal polarity lasting for less than 2000 years and the R-subchron of ∼60 kyr were recorded. **Kivakka intrusion.** The A_1 prefolded and A_2 synfolded components which occurred at the stage of cooling of the intrusion are isolated. The body started to tilt approximately 85 kyr after intrusion emplacement and it lasted for 20–25 kyr. The pole of the A_1 is 17.8°S and 247°E. Duration of the record is 35 kyr and only one R-polarity existed during this period. **Bushveld intrusion.** Orientation of the horizontal plane of the samples has been restored from viscous magnetization and a paleomagnetic pole (12°N, 35.4°E) has been determined from a high-temperature N-component of the NRM. A paleomagnetic record for ∼500 kyr was obtained; polarity of the field has changed only once during this period.

Introduction

A fine structure of the geomagnetic field is commonly studied from paleomagnetic records in sections of the sedimentary and volcanogenous deposits. The overwhelming majority of such sections, even the most "continuous" have gaps and, consequently, the paleomagnetic records of the geomagnetic field are discontinuous. The gaps are not always detected and they cover time intervals of several years to

[1] Institute of Physics of the Earth, Russian Academy of Sciences, Moscow, Russia
[2] Moscow State University, Moscow, Russia

Paper number TJE04158.
ISSN: 1681–1208 (online)

The online version of this paper was published 12 January 2005.
URL: http://rjes.wdcb.ru/v06/tje04158/tje04158.htm

a few million years and their distribution along sections is usually irregular.

Only the cooling magmatic bodies ranging from lava flows (cooling time of days, months and years) to large intrusive bodies, whose cooling time covers dozens of thousands and millions of years, represent an actual continuous record of the geomagnetic field behavior. Samples from such bodies yield two versions of continuous records: 1) detailed sampling from the contact to the inner zone of the body; the isotherm the Curie point of magnetic minerals which are present in the body shifts from the contact, where the cooling is relatively fast, to the maximum time approximately in the center of the body (one should have in mind that by the time of record the contact zone and the enclosing rocks are heated noticeably and the cooling pattern may be either uniform or reverse); 2) detailed thermal demagnetization applied to each sample will make it possible to read the record of the geomagnetic field behavior at the sampling point during cooling of the magmatic body at the sampling point from the Curie point of a magnetic mineral present in the sample to the blocking temperature, at which a significant portion of the thermoremanent magnetization is still recognizable within the accuracy of measurements. The theoretical and experimental paleomagnetic investigation of the artificial and natural samples containing the magnetite grains of different size, from single-domain to multidomain [*Pechersky et al.,* 2002, 2004; *Shcherbakov and Shcherbakova,* 2002] have shown that "time" (temperature) of the field direction variations in the pTRM directions is retained during the thermal demagnetization, whereas amplitude of the direction variations reduces notably with respect to actual value (90°) from the single-domain (error is close to zero) to 40° in the case of the multidomain grains. Consequently, presence of the single-domain grains is required in the second version for a reliable record.

An important point is the choice of a body for a thermophysical calculation of its cooling process without a notable participation of fluids ("dry" melt) at all the stages. The latter accelerate considerably the cooling process and add complexity to the pattern. The heterophase and single-phase change of the primary magnetic minerals at different stages of existence of the body make the record still more complicated.

All the above considered, the gabbro-pyroxenite layered intrusions reasonably uniform by the magmatic conditions (nearly dry magma) and cooling, which is close to conductive, are the most favorable object. The cumulative parts of the complex are most favorable from the paleomagnetic point of view. They do not contain the primary igneous magnetic minerals, but magnetic minerals appear as inclusions in pyroxenes, olivines and plagioclases as a result of exsolution during the cooling phase, approximately from 550–600°C, i.e., during the cooling of a nearly homogeneous solid body. These inclusions are dominated by nearly single-domain low-Ti titanomagnetite and magnetite grains. It is important to select bodies that show no evidence of hydrothermal and similar alterations during both the cooling and subsequent existence of the body.

This is the *first* study of a *continuous record of paleovariations* of the geomagnetic field on the whole and, in particular, conducted on such objects, which are described in this article. There are some publications devoted to records of geomagnetic reversals in cooling magmatic bodies. This is mostly the first version of a record of an NRM component isolated at a temperature close to the Curie point of magnetite. For example, researchers have obtained fairly detailed records of the geomagnetic field before, during and after reversals during the cooling of the Miocene granitoid intrusions of Tatoosh (∼17–18 Ma) and Loreal Hill (∼8 Ma) in the northern USA [*Dodson et al.,* 1978] and the Agno diorite intrusion (∼15 Ma) on Luzon Island, Philippines [*Williams and Fuller,* 1982]. It was shown that the primary thermoremanent magnetization is associated with low-Ti titanomagnetite and magnetite. Being a carrier of a stable NRM component, the magnetite occurs as fine inclusions in silicates, products of their exsolution. As a rule, more than 90% of the NRM is unblocked in a range 540–580°C. Based on several thermophysical models, the cooling times of the intrusions in this temperature range and, accordingly, the duration of transitional zones were roughly estimated at less than 6000 to 14000 years, depending on whether water was involved or the cooling was purely conductive. Detailed sampling of a drill core from the Tatoosh intrusion revealed (against the background of appreciable noise) variations in the direction and value of magnetization; the vector rotates counterclockwise, producing variously shaped loops similar to secular variations.

Coe and Prevot [1989] and *Coe et al.* [1995] described a case of a very rapid geomagnetic reversal that was also discovered by the first method in the cooling record of a lava flow on Mount Steens. This interpretation, however, is not indisputable, because it was shown that this feature may have resulted from remagnetization of the upper part of the flow due to its heating by the overlying flow that erupted when the geomagnetic field had an opposite polarity. This is supported by the existence of a similar situation (high-temperature NRM components of opposite polarities present in one flow) observed, first, in lava flows on La Palma Island, where the Matuyama-Brunhes reversal was recorded, and second, in the Gamarri lavas in Ethiopia [*Valet et al.,* 1998]. Paleomagnetic, petromagnetic and other detailed studies proved that this is a result of the remagnetization of basalts by an overlying flow.

There are examples of the second version of record of the geomagnetic reversals found in samples containing single-domain pyrrhotite from Jurassic sedimentary sequence in the western Alps that slowly cooled in the Miocene and underwent deformations and metamorphism at temperatures of 300°C to 350°C in the Oligocene [*Crouzet et al.,* 2001a; *Rochette et al.,* 1992] and in the Himalayas where carbonates underwent metamorphism in the Tertiary period [*Crouzet et al.,* 2001b]. It is revealed a record of up to ten reversals in the course of detailed thermal demagnetization of NRM of each sample [*Crouzet et al.,* 2001a]. A correlation of magnetic chrons between samples and sampling points was then performed. As a result, a magnetostratigraphic section comprising 21 polarity reversals was constructed. The thermomagnetic study showed that the pyrrhotite grains have a single-domain structure and obey the law of additivity and independence of partial thermal magnetizations. The tem-

perature range within which the magnetic chrons was identified from unblocking temperatures was 302–182.5°C, and the record was ∼4 Myr long.

Finally, first paleomagnetic and thermophysical investigation of a typical layered gabbro-pyroxenite Monchegorsk intrusion were conducted [*Pechersky et al.,* 2002, 2004]. A magnetochronological pattern (Figure 1) was obtained for each sample taken from selected section 375 m thick for the second method used. The blocking temperature intervals were translated into the relative cooling time so to construct magnetochronological columns of magnetic polarity during cooling of the intrusion [*Pechersky et al.,* 2002, 2004]. Figure 1 shows that all the columns begin from N-polarity (chron $N1$) and at T_d = 550–560°C the boundary is between the N and R polarity, the N-polarity in columns (samples) covers an interval of 30–40 kyr. This pattern is seen from the base of the section up to ∼250 m, and behind the fault, which is between samples 43 and 45, stops sharply and only N-polarity ($N2$) is reliably noted. Evidently, a certain shift occurred along the fault, which interrupted a continuous record and a more high horizons of the section are fixed behind the fault. At later portions of the columns (T_d < 540° C) either partial remagnetization or unblocking temperatures are above 500°C (multidomain grains). In the latter case conversion of the unblocking temperatures (T_d) into blocking temperatures (T_b), and, consequently, estimation of the cooling time is not correct. Therefore, only unblocking temperatures above 530°C are used for magnetochronological assessment. A summary magnetochronological column from the moment of cooling of intrusion from 580°C looks as follows: $N1$-chron – from 0 to 30–40 kyr, R-chron – from ∼50 to ∼130 kyr, $N2$-chron – from 130 kyr and further. The reversed polarity duration is similar to the late Cenozoic subchrons.

This paper is dedicated, first of all, to continuation of the paleomagnetic and thermophysical study of the Monchegorsk intrusion and of two more intrusions of Kivakka and Bushveld. The main purpose of this is to obtain a paleomagnetic record of the geomagnetic field direction variations. We preferred to conduct this type of investigation with a rather ancient objects not only because they meet the aforementioned conditions, but also due to the fact that no sections of sedimentary and volcanogenous deposits are available in the Early Proterozoic for the study of the fine structure of the geomagnetic field.

Brief Geological Description

All three foregoing intrusions are typical layered gabbro-pyroxenite magmatic bodies, of a different age, located in different geological structures and even on different continents. All of them, despite their ancient age, are well preserved.

A. **The Monchegorsk pluton** is a part of the large layered Early Paleoproterozoic Monchegorsk intrusive complex, located in the central part of the Kola Peninsula. The age of the Monchegorsk intrusion is ∼2.5 Ga [*Amelin et al.,* 1995; *Balashov et al.,* 1993]. As a result of intensive collision processes, which accompanied the Svecofennian Ocean closure in the central part of the Baltic Shield about 2.0–1.9 Ga, this craton was separated into several tectonic blocks and was subjected to metamorphism: metamorphism weakens from the western boundary to the east from granulite to the greenstone facies. The Monchegorsk pluton was slightly affected by tectonic and metamorphic processes; metamorphic alterations localize here mainly in fault zones. The primary bedding of the intrusive rocks has been left intact, and minor variations in the layering attitude are primary.

The Monchegorsk pluton has an arcuate (in plan) shape; one of its two branches is elongated in a NE direction and the other trends E-W (Figure 2). The total area of the intrusion is about 55 km^2. Its W-SW continuation is break off by the Monche-Tundra fault; its southern continuation is buried under Early Paleoproterozoic volcanic-sedimentary rocks of the Imandra-Varzuga group, partially thrusting on the intrusion. The primary intrusive relationships have been preserved only in the northern part of the intrusion, where a rapidly cooled marginal zone consisting mainly of fine-grained norites and gabbro-norites exists all along the contact. Thickness of the zone ranges from 10 m to 100 m. A layer of peridotites (dunite cumulates) 100 m to 200 m thick is observed over gabbroids of the lower marginal zone. This layer is overlain by a 250 m to 400 m thick zone of rhythmically alternating peridotites, olivine orthopyroxenites, and orthopyroxenites. This zone underlies a layer of bronzitites 300 m to 700 m thick, which consists further of norites (plagioclase-orthopyroxene cumulates) and gabbro-norites (plagioclase-orthopyroxene-clinopyroxene cumulates). The only ore mineral observed in thin sections is chromite (in peridotites). The reconstructed total thickness of the intrusion is about 3 km; its upper part (∼1 km) was eliminated by erosion. The formation depth of the intrusion is 10–15 km (4–4.5 kbar), as indicated by very scarce evidence of the reaction between basic plagioclases and olivines, which proceeds at a pressure of at least 5 kbar.

Oriented samples were selected from outcrops along the eastern crest of Mountain Nittis. Rocks exposed here belong to the endocontact zone of rhythmically alternating peridotites (bronzitites) replaced in the upper part of the section by monotonous bronzitites of the pyroxenite zone.

Samples were collected uniformly from the base of the mounting to the top at 10 m intervals (vertically). The total thickness from which the samples were collected was 375 m. A total of 39 samples were collected from the intrusion, and 14, from its surrounding Archean gneisses. Aside of this, 46 samples were collected every 1–2 m in the interval from 100 m to 161 m from the lower contact.

B. **The Kivakka intrusion** (Figure 3) belongs to the Olang group of coeval layered plutons located within the Pyaozersk-Tiksheozersk uplift (Northern Karelia). The initial phase of the Proterozoic activity has shown in formation of the granite intrusions of the Nuorunen-Karmanka type, whose age is 2450±72 Ma [*Buiko et al.,* 1995] and 2449.3±3.7 Ma [*Levchenkov et al.,* 1994]. Intrusion of the layered plutons and gabbro-norites dikes was controlled by a series of the N-W deep faults [*Saltikova,* 1991; *Silvennoinen,* 1991]. The Kivakka intrusion isotope age is 2445±3.4 Ma [*Balashov et al.,* 1993]. A younger geological age of the layered plutons as compared with granites is confirmed by the

Figure 1. Magnetochronologic columns, arranged according to data of the component analysis of the difference vectors of the NRM in the process of the detailed thermal demagnetization [*Pechersky et al.*, 2004]. Blue color – normal (N) magnetic polarity, primary cooling intervals – bright color, weak color – partial or complete more young remagnetization; red color – reverse (R) polarity, bright color – primary cooling intervals, weak color – partial or complete more young remagnetization; white color – unreliable intervals. Fully unreliable samples are not included into the figure. Distance between columns is proportional to the vertical distance between the samples. The time scale is made on the basis of the thermophysical calculations. The "zero" point (magnetite Curie temperature) shifts from the base of the section to the top (375 m) for approximately 10 thousand years. T_d – NRM unblocking temperature during the laboratory thermal demagnetization, T_b – NRM blocking temperature in the process of cooling of the Monchegorsk intrusion, °C. Time is in kyr. Figures on the top of the columns are sample numbers.

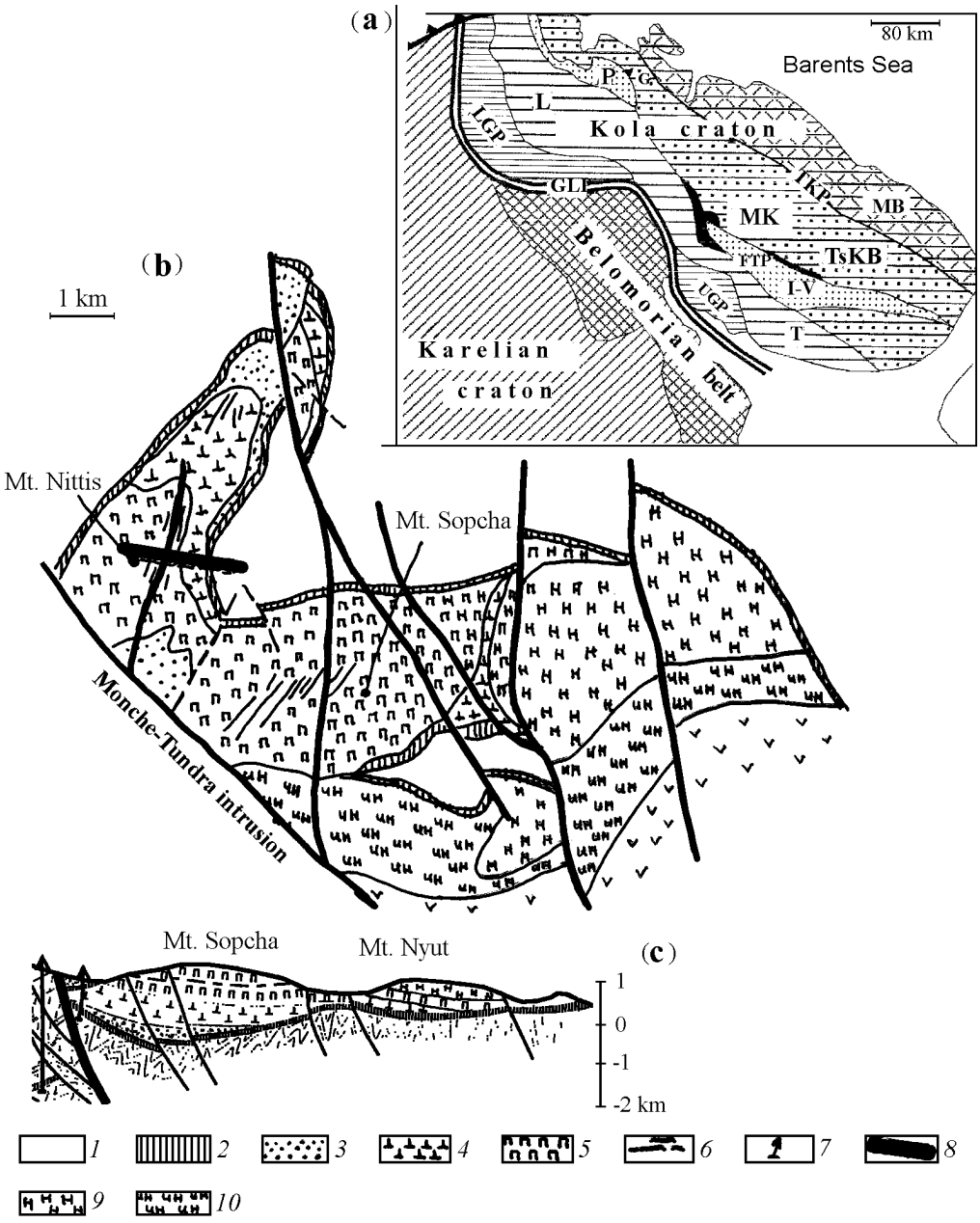

Figure 2. Diagram of the geological structure of the Monchegorsk pluton [*Sharkov,* 1980] a) Position of the Monchegorsk complex in the main tectonic structures of the N-E part of the Baltic shield. MB – 1 – Murmansk block; TsKB – Central Kola block; T and L – Tersk and Lottinsk fragments of the Tersk–Lottinsk block; P and I-V – Pechenega and Imandra-Varzuga structures of the Pechenega-Varzuga volcanogenic-sedimentary belt; LGP and UGP – Laplandia and Umbina fragments of the Laplandia–Umbina granulite belt; GLR – Laplandia main deep fault; MK – Monchegorsk complex. b) Diagram of the geological structure of the Monchegorsk pluton 1 – host diorite-gneiss, crystalline schist of the Kola series and other rocks of the recent Archean; 2 – peripheral endocontact zones of the intrusion; 3 – dunite, peridotite; 4 – rhythmic interbedding of dunite, peridotite, olivine bronzitite and bronzitite; 5 – predominantly bronzitite; 6 – zones of the sulphide mineralization; 7 – position of the core holes; 8 – area for taking oriented samples for the paleomagnetic study; 9 – norite; 10 – altered norite, 11 – faults.

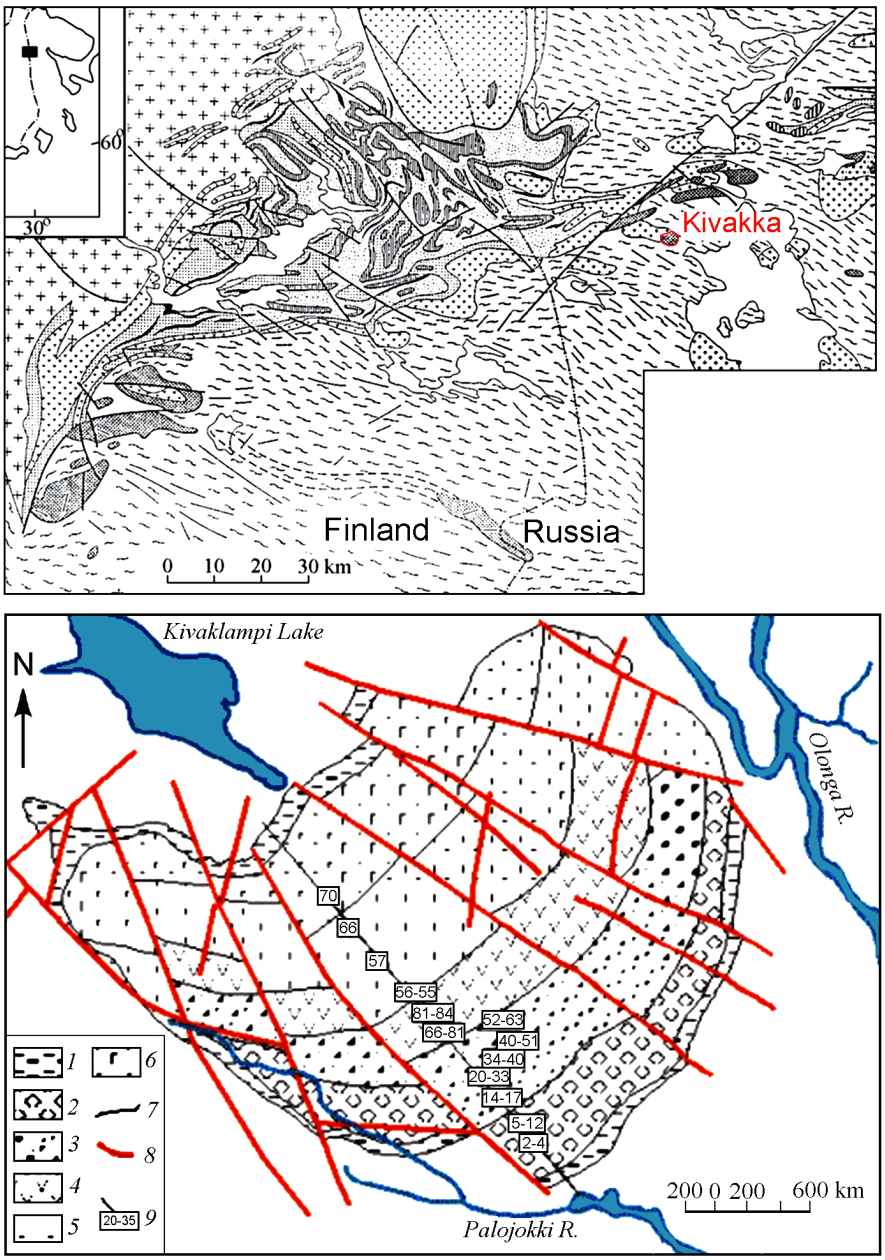

Figure 3. a) Schematic geological map of development of the North Karelia layered intrusions (lattice) and Kivakka intrusion position. b) Scheme of the geological structure of the Kivakka intrusion [*Koptev-Dvornikov et al.,* 2001]. 1 – contact zone rocks; 2 – peridotite of the olivinite zone; 3 – norite with pyroxenite horizons; 4 – norite; 5 and 6 – gabbro-norite; 7 – geological boundaries; 8 – faults; 9 – sampling profile of oriented samples, sampling points and sample number.

intersecting contacts of the gabbro-norites dikes.

The Svecofennian tectonomagmatic activity within the Pyaozersk-Tiksheozersk uplift is noted by intrusion of multiphase alkaline-ultrabasic bodies and metamorphic events in the interval of ~2–1.5 Ga [*Amelin and Semenov,* 1996; *Amelin et al.,* 1995; *Kogarko,* 1995].

The Kivakka massif has a truncated ellipse shape (in plan) with 4.9 km and 3.15 km semi-axes. An overturned circular cone with initially vertical axis is proposed as a model. Height of the cone is 3.9 km, the vertex angle is 40°, diameter is 6.5 km, volume of the cone is 44 km^3 [*Khvorov et al.,* 2000; *Koptev-Dvornikov et al.,* 2001]. It is presumed that the intrusion has developed as a result of a single injection of magma and its further differentiation in a chamber at the formation place [*Koptev-Dvornikov et al.,* 2001]. According to the modeling the geostatic pressure at the place of for-

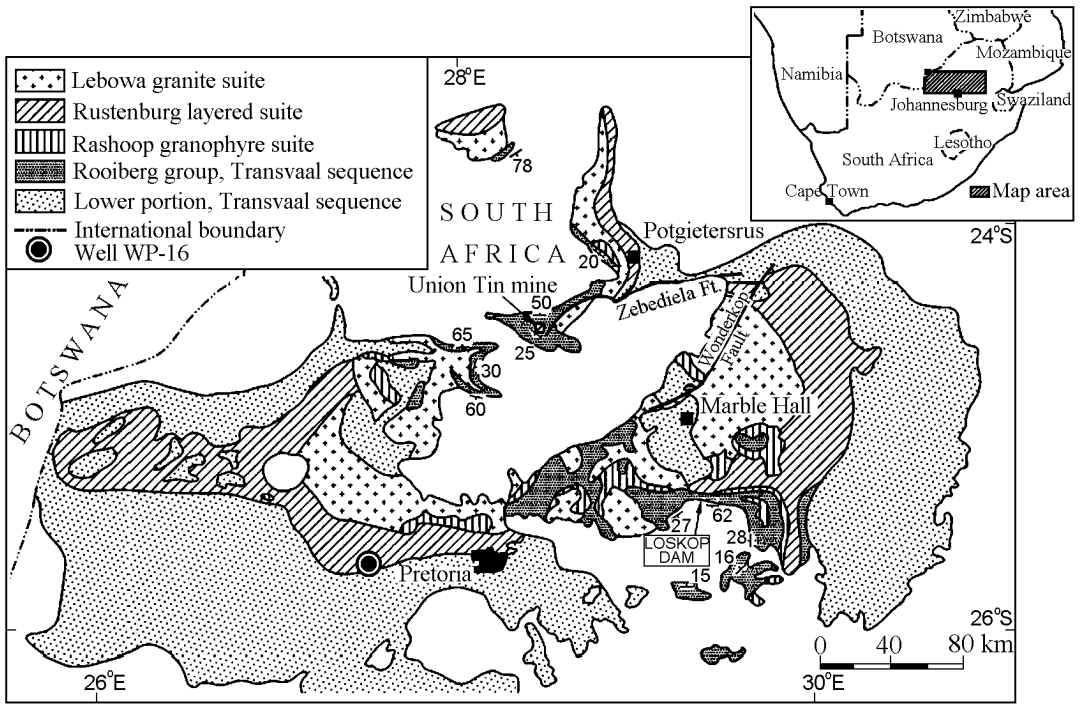

Figure 4. Geological scheme of the Bushveld intrusion [*Buchanan and Reimold,* 1998]. Red circle shows position of well WP-16.

mation of the intrusion was about 3 kbar that corresponds to a depth of ∼10 km, the magma initial temperature was 1380–1400°C, crystallization of magma was under dry conditions [*Khvorov and Azzuz,* 2003]. Features of insignificant local hydrothermal manifestation as fine quartz-chlorite veins whose formation temperature does not exceed 350°C show up much later (M. V. Borisov, verbal information, 2003). No other secondary alterations in the intrusion rocks were found.

The massif is divided into several blocks by a series of faults (the dip azimuth is 210°–220°, angle of dip is 70°–80°) and is tilted to the NW. The bedding elements of the primary magmatic lamination vary insignificantly and the average dip azimuth is 306° and the angle of dip is 35°. The dolerite dikes, which intruded to the rocks of the layered complex, have retained the primary bedding and are not disturbed by deformations. The contact zones and the layered series reflecting the order of alternation of cumulative paragenesises are distinguished in the vertical section of the Kivakka intrusion [*Lavrov,* 1979]. Thickness of the contact zone of the intrusion does not exceed 100 m and it is composed mainly of norites and pyroxenites. Olivinites and olivine-bearing pyroxenites 400 m thick occur in the base of the layered series. A 700 m thick packet of norites thick builds up the section; the lower part of this packet contains a group of coarse-grained pyroxenites. Sometimes small horisonts of olivine norites and gabbro-norites occur among norites. Banded rocks is a characteristic feature of the norite packet. A gabbro-norite layer 420 m thick is overlying the latter. The gabbro-norite with pigeonite stratum 320 m thick ends the section. Rocks of the layered intrusion complex do not contain primary magmatic magnetic minerals, i.e. minerals which crystallized from the melt. This is typical of the cumulative part of layered intrusions. The top 50 m of the upper zone are composed of minerals which characterize the residual melt of the basalt magma differentiation. The melt accumulates the iron group elements and, accordingly, an increased titanomagnetite content is observed.

The most complete section of the layered series is represented in the central block of the Kivakka intrusion (Figure 3). Thickness of the section reach to 1800 m. Oriented 70 samples were collected in a well exposed interval from 330 m to 1650 m of the section transversely to the strike of the magmatic lamination for petromagnetic and paleomagnetic study (Figure 3). Sampling began in the olivine zone where 7 samples of peridotites were collected. Two portions of the section were characterized in more detail. The first portion up to 300 m thick covers several bands of norites, plagioclase-bearing pyroxenites and gabbro-norites in the zone of a contrast lamination of the central part of the section. The second portion covers several bands at the top of the norite zone. Several samples were collected from massive gabbro-norites close to the intrusion roof.

C. **The Bushveld intrusion** (Figure 4) [*Eales and Cawthorn,* 1996; *Sharkov,* 1980; *Wager and Brown,* 1970] is located in the center of the South African Shield, on the southern periphery of an arcuate East-African rift. The intrusion is cup-shaped with the concave bottom (lopolith). The series of layered rocks falls inside the massif, the lamination dip angles 10°-15°prevail; they become greater towards the lateral contacts. The massif (in plan) is elongated in

the latitudinal direction. Its longer axis is 480 km and the cross-section dimension is about 80 km. A total thickness of the intrusion is 7–9 km. The intrusion penetrated into the upper part of the Lower Proterozoic Pretoria suite which was underlying at that time sediments and vulcanite of the Megalisburg and Rooiberg series. Thickness of the Rooiberg series lying on the roof of intrusion is about 3 km maximum, i.e. thickness of the Bushveld intrusion roof during its penetration did not exceed 3 km and, consequently, depth of the intrusion during its cooling was in the interval from 3 km to 10–12 km. The roof during formation of the intrusion raised and melted partially. This palingenous acid magma could have remained liquid throughout the period of crystallization of basic rocks of the massif. Judging from associations of the contact-metamorposed rocks, pressure in the intrusion walls varied from 2 kbar to 3 kbar [*Engelbrecht,* 1990], i.e., in case of a geostatic pressure the depth was 6–10 km ignoring pressure of magma onto surrounding rocks and this does not contradict the geological estimation of depth of formation of the intrusion.

Age of the Rooiberg vulcanites is 2.06 Ga, age of the Bushveld complex is 2.06 Ga [*Buick et al.,* 2001], age of 4 pyroxenites from different levels of the Merensky reef, which was determined by the Re-Os isochronous method is 2043±11 Ma, age by the Rb-Sr method is 2061±27 Ma [*Schoenberg et al.,* 1998]. The Makhuzo granites (a final granite magmatism) form small stocks, sills and dikes; the Pb-U and Rb-Sr-isochronous age is about 2050 Ma. Age of the red granites intruded the Busveld massif according to the Rb-Sr isochroous method is 1950±50 Ma. The latitude strike dikes of the Karoo age intruded the Busveld massif.

Majority of researchers give preference to a hypothesis of the layered magmatic rock formation as a result of crystallization differentiation of the basalt magma during one magmatic phase within a vast magmatic chamber. Another hypothesis suggests multiple injections of magma so close to each other in time, that the previous portion of magma had no time to differentiate. It is an important statement for our problem that in all variants of the Bushveld intrusion formation model all actions of intrusion or mixing of melts occurred at the magmatic phase; at the cooling phase below 600°C the Bushveld massif was a single, sufficiently solid body.

All rocks of the Bushveld complex are exceptionally fresh and not deformed. No signs of hydrothermal phenomenon were discovered; only two cases of a local minor quantity of the secondary amphibole have been noted. Alkaline intrusions and the red granite intrusions breaking through rocks of the Bushveld complex are at least 50 km away from the point of drilling the well WP-16. Their influence (heating) must not have a serious effect on the paleomagnetic results.

The well WP-16 (25°42′ S and 27°31′ E) was drilled in the south of the western part of the Bushveld intrusion (Figure 4). Section of the intrusion in the region of the well is represented by five zones: 1) marginal zone (norites); 2) lower zone consists of rhythmically alternating pyroxenites and harzburgites (820 m thick); 3) critical zone is characterized by a distinct fine lamination and it consists of pyroxenites and norites (1300 m); 4) main zone consists of norites, gabbro-norites and anorthosites (3100 m), a fine rhythm is weakly expressed; rocks of zones 2–4 are cumulative crystallization products; 5) upper zone is a final product of crystallization differentiation; total thickness of this zone is 1700 m.

The well and the oriented core samples for the paleomagnetic study cover upper 240 m of the critical zone and lower 540 m of the main zone, 173 specimens altogether. The well section is composed of norites (72% of the thickness), anorthosites (22% of the thickness) and pyroxenites (6% of the thickness). The main rock-forming minerals in the rocks of the well section are bronzite and basic plagioclase, clinopyroxene is rare in occurrence, olivine occurs sporadically, occurrence of biotite and amphibole is even more rare, the ore minerals are represented by chromite.

The main and the critical zones are separated by the Merensky reef. It is 2–6 m thick. This is a layer of a porphyrite pyroxenite, which includes two interlayers of chromite 1–5 cm thick (near the lower contact) and 20–50 cm (below the upper contact). A sulfide mineralization is concentrated near the upper contact. The pegmatite veins sometimes with a massive sulphide mineralization occur in rocks of the reef. These veins outcrop rapidly at transition from the reef into overlying and underlying anorthosites.

According to this publication [*Hattingh,* 1986a, 1986b], the electron-microscopic study of rocks of the main and critical zones, products of high-temperature exsolution were found in the pyroxene and plagioclase grains; these were thin acicular inclusions of magnetite of 1–1.5 μm average width. The single-domain and pseudosingle-domain magnetic state of such grains is most likely and a natural remanent magnetization associated with this magnetite is considered, in paleomagnetic terms, as primary. Isolated fine grains of magnetite are few and far between. Aside of this, there are grains of ilmenite, in a more rare case these are thin acicular inclusions, more frequently there are isolated grains up to 100 μm, gematite lamellae occur inside these. Composition of isolated grains of ilmenite $x \approx 0.85$. Iron sulphide grains, mainly in narrow layers of the ore zones occur less frequently than ilmenite. A part of these grains are identified as pyrrhotite.

Rocks of the intrusion in the region of the well (but not in the well proper) here and there are replaced by holocrystalline magnetite-pyroxene pegmatoids. No alterations in the rocks enclosing pegmatites and baked contacts are seen, i.e. this is an in-situ replacement process without addition and evacuation of material, without metamorphism.

Techique of Paleomagnetic and Petromagnetic Measurements

The natural remanent magnetization (NRM or J_n) value and direction were measured in all samples with a JR-4 magnetometer, and the magnetic susceptibility κ and its anisotropy, with KLY-2 measuring instrument. The magnetic susceptibility was measured after regular heating in the laboratory to control mineralogical alterations. For a series of representative samples, we performed a ther-

momagnetic analysis in the laboratory of the Institute of Physics of the Earth and in the Borok observatory (with the vibromagnetometers and magnetometers designed by N. M. Anosov, K. S. Burakov and Yu. K. Vinogradov) of saturation magnetization J_s, saturation remanent magnetization J_{rs} and thermoremanent magnetization J_{rt} (TRM), coercive force H_c and remanent coercive force H_{cr} were measured. Paramagnetic minerals were excluded from values J_s and H_c of weakly magnetic samples according to magnetization curves or according to correlation of J_n and κ. Thus, a set of pyroxenite samples with $J_n < 0.1$ mA m^{-1} has $\kappa \approx 4 \times 10^{-4}$ SI units. This value was adopted as a paramagnetic susceptibility of pyroxenites and peridotites κ_p, and it was subtracted from the total value of magnetic susceptibility to determine ferrimagnetic susceptibility and, accordingly, the Koenigsberger ratio for the ferrimagnetic fraction of material: $Q_{nf} = J_n/50\kappa_f$, where $\kappa_f = \kappa - \kappa_p = \kappa - 400$.

Preliminary thermal demagnetization from 120°C to 580°C (12–15 steps) was performed on duplicates of all samples. A detailed thermal demagnetization of the Monchegorsk intrusion samples from 440°C to 600°C (thermal demagnetization step of 5°) and for samples collected every 1–2 m – from 540°C to 580°C (2–3° step) was performed to study the geomagnetic field record in the course of cooling of intrusive body. For samples from the Kivakka intrusion thermal demagnetization was performed from 420°C to 530°C (5° step) and from 530°C to 580°C (2°–3° step). The thermal demagnetization interval was selected on the basis of preliminary experimental investigations on artificial and natural samples [*Pechersky et al.,* 2002; *Shcherbakov and Shcherbakova,* 2002] and on data of the preliminary thermal demagnetization. Results of the latter have shown that below 400°C contribution of unblocking temperatures even in the case of single-domain grains is nearly the same as the accuracy of measurements with the JR-4 magnetometer. Specific character of collection of samples from the Bushveld intrusion is first, in their size and second, in their orientation. These are cubes 1×1 cm at the bottom and 1–0.4 cm high. Two cubes represent each level usually. The top and bottom of these cubes are known (the plane in some samples is not strictly horizontal) and their orientation in the horizontal plane is unknown. We were unable to conduct various paleomagnetic and petromagnetic experiments with the samples in their natural state because of their small size and quantity. By heating up to 200–300°C we tried to extract the NRM viscous component so as to restore through it orientation of samples in the horizontal plane. The core was lifted in 1995 and we received it in 2002. It is reasonable that samples changed their position more than once and every time they acquired a new viscous magnetization. To remove at least partially the "parasitic" viscous components, samples were kept for about a year in a permalloy screen and only after that they were subjected to thermal demagnetization. Declination was restored in the following way: declination of the difference vector $J_{n20} - J_{n200,300}$ was subtracted from declination of the ancient NRM component. Inclination of the difference vector, which had to be negative and close to inclination of the recent magnetic field of the Earth at the point of drilling of well WP-16 (-44°), served as a control of the fact that we deal with a viscous component generated by a recent geomagnetic field at the time of lifting the core from the well. Restoration of declination of the NRM primary component is important for the analysis of behavior of a complete vector of the geomagnetic field. Due to a reason mentioned above, however, the "restored" inclination has a wide scatter and is no good for the analysis of a fine structure of the geomagnetic field in the first version. Therefore, analysis of behavior of the geomagnetic field in the first version was according to inclination only. In the second version it is possible to analyze a completer magnetization vector, if to consider only relative variations of declination in the course of a detailed thermal demagnetization. The restored declination was of use to determine the mean paleomagnetic direction of the whole collection. It coincides practically with the paleomagnetic direction in samples from natural outcrops, collected in the same locality [*Hattingh,* 1986a]. Based on results of preliminary thermal demagnetization, samples were chosen for a detailed thermal demagnetization wit a three degrees step and interval for their thermal demagnetization was selected from 520°C to 580°C to analyze components associated with magnetic minerals, which are close to magnetite.

Titanohematite with T_c = 600–660°C is present in some samples of all collections. Time and temperature of its origination are not known (it is present more frequently in ilmenite as lamellae [*Hattingh,* 1986a, 1986b]), therefore, the NRM component associated with titanohematite is not used in the analysis of the geomagnetic field behavior.

To reduce contribution of magnetic soft multidomain grains, all samples from 5 mT to 30 mT underwent an alternating magnetic field demagnetization (AF demagnetization) on the unit designed by D. Kevlashvili (IFZ RAS), before the detailed thermal demagnetization. The amount of 10–15 mT will suffice for majority of samples to get a stable NRM component.

Samples were heated in a furnace placed into a four-layer screen of annealed and AF cleaned permalloy; the magnetic field inside the furnace did not exceed 10 nT.

The blocking temperature of the remanent magnetization depends strongly on the cooling rate [*Dodson and McClelland-Brown,* 1980; *Pullaiah et al.,* 1975]. In case the intrusive body cools slowly the blocking temperature (T_b) of the natural thermoremanent magnetization will differ considerably from the unblocking temperatures (T_d) of the natural remanent magnetization in the course of thermal demagnetization of samples in a laboratory. We used the plots of T_b and T_d versus the cooling rate for single-domain magnetite particles, presented in [*Dodson and McClelland-Brown,* 1980] (Figure 5). In order to use these plots, it is necessary to choose the samples whose carrier of the given NRM component is the single-domain magnetic mineral (in our case it is magnetite and a low-Ti titanomagnetite). In case of a noticeable role of the multidomain grains all magnetization will take place near the Curie point. If there are several magnetic minerals with different Curie points in the sample it becomes difficult to translate temperatures into time.

To estimate the NRM nature a set of indicators is used. These are the magnetic hardness expressed in terms of H_{cr},

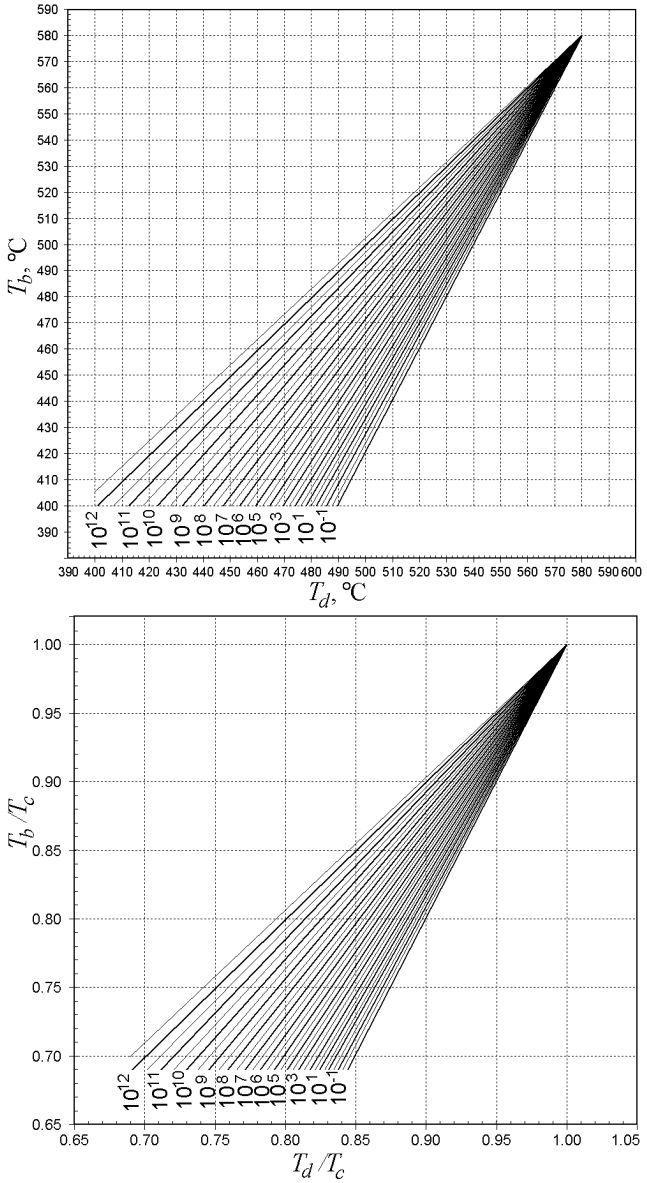

Figure 5. Diagram of dependence for unblocking temperature T_d and blocking temperature T_b curve of the thermoremanent magnetization of the single-domain grains a) magnetite and b) titanomgnetite at different velocities of cooling of the body [*Dodson and McClelland-Brown,* 1980]. Numbers at the lines are cooling velocity (°/Myr).

H_{cr}/H_c, Q_n, Q_{nf}, the shape of the curve $J_n(T)$, the linearity of the Arai–Nagata diagrams ($dJ_n - dJ_{rt}$), the similarity of variations in dD and dI between several neighboring samples, and the ratio J_{rt}/J_{ri}. It is known [*Sholpo,* 1977] that, in an ensemble of multidomain grains, the ratio $J_{rt}/J_{ri} \approx 3$ and decreases with an increase of single-domain particles in the ensemble of magnetic grains. However, in the case of crystallization magnetization, we have $J_{rk}/J_{ri} \approx 1$ [*Nguen and Pechersky,* 1985]. Therefore, if J_n and J_{rt} are acquired in similar external magnetic fields, J_n/J_{ri} and $J_{rt}/J_{ri} \approx 3$, this will indicate that J_n is mostly associated with multidomain grains and is a thermoremanent magnetization; if $J_{rt}/J_{ri} \approx 3$, and $J_n/J_{ri} \approx 1$, this means that J_n is likely to be of the crystallization or chemical origin (in the latter case, usually $J_{rc}/J_{ri} < 1$ [*Nguen and Pechersky,* 1987]).

The component analysis based on the thermal demagnetization data was performed with the use of the program developed by *Enkin* [1994] was applied to single out the NRM components obtained in the course of thermal demagnetization and to determine mean paleomagnetic directions.

Petromagnetic Results

A. **The Monchegorsk intrusion.** According to the thermomagnetic analysis of J_s, J_{rs}, J_{rt}, rocks of the intrusion are clearly dominated by magnetite with T_c = 550–585°C and occasionally contain pyrrhotite with T_c = 325°C. In contrast, pyrrhotite prevails in the host rocks and is the only magnetic mineral in some gneiss samples.

According to a hyperbolic form of $J_s(T)$ the paramagnetic contribution is substantial in rocks of the intrusion. The great majority of samples are dominated by paramagnetic κ. Judging from the susceptibility and saturation magnetization, rocks of the intrusion contain commonly <0.1% of magnetite. In general, the magnetization of periodites is higher than that of pyroxenites (Table 1). The distribution of κ and NRM along the section is mainly controlled by distribution of periodites, which are predominant in the lower part of the intrusion. The rocks are little affected by heating: the susceptibility κ_T measured after heating of samples to 540–580°C changes insignificantly, and the κ_T/κ_0 ratio varies from 0.8 to 1.08, averaging 0.98. Only in samples containing appreciable amounts of iron sulfides, in particular, pyrrhotite, does κ_T/κ_0 reach 1.8 (sample 44). This ratio is even higher in the surrounding gneisses, where the main magnetic mineral is pyrrhotite.

The magnetic hardness of rocks was estimated from H_{cr}, it varies from 12 mT to 37 mT, irrespective of the rock composition, concentration of magnetic minerals, and, κ, variation, and likely reflects the predominance of nearly single-domain and multidomain grains.

The rocks above the edge zone of the intrusion are isotropic, the maximum-to-minimum susceptibility ratio of the sample is A_κ = 1.0–1.08 (averaging 1.02); in the edge zone A_κ reaches 1.19 and averages 1.1 in the lower 100 m of the section. Such behavior of the magnetic anisotropy is common for magmatic bodies whose magnetic fabric forms in their peripheral zones at the stage of crystallization. Higher anisotropy is inherent to a more magnetic samples, i.e., is associated with magnetic minerals, whereas weakly magnetic pyroxenites, whose susceptibility is predominantly paramagnetic, are as a rule, nearly isotropic. The magnetic anisotropy of the host gneisses is A_κ = 1.02–1.19, averaging 1.12.

As seen from the J_n/J_{ri} and J_{rt}/J_{ri} values and the Q_{nf} values correlating with these ratios (Table 2), the main contribution to J_n and J_{rt} at room temperature is made by multidomain grains, and J_n is a thermoremanent magnetization in ∼70% of samples. Evidently, magnetic grains in

Table 1. Magnetization of Monchegorsk intrusion rocks

Rock	no.	κ, 10^{-4} SI units		J_n, mA m^{-1}		Q_{nf}	
		average	range	average	range	average	range
Peridotite	8	16.8	9.2–153	90.4	50–1850	11.7	1.5–60
Pyroxenite	29	8.9	4.0–59.3	26.6	<0.1–285	6.5	1.0–278

the interval 540–580°C are close to the single-domain state. Below this interval they are close to the mulltidomain state, as is seen from the NRM direction, which practically does not change within the measurement error, in the course of the thermal demagnetization up to 500–530°C (see below).

B. **The Kivakka intrusion.** Rocks of the intrusion are weakly magnetic, as a rule, (Table 3) the feature which is usual for cumulative rocks. Figure 6 shows typical curves of $J_{rs}(T)$. One can see the heating stability of the magnetic material (Figure 6, Table 3). According to data of the thermomagnetic analysis (Table 3) the Curie point vary from 525°C to 560°C, and this corresponds to concentration of titanomagnetite with $x = 0.11$–0.05. The saturation magnetization of such titanomagnetites averages approximately 415×10^3 A m^{-1}. The saturation magnetization of the investigated samples does not exceed 10^3 A m^{-1}, accordingly, their titanomagnetite content is no more than 0.3%; in most cases it is less than 0.1% and frequently it is less than 0.01%. Some samples contain the magnetic phase, which disappears

Table 2. Magnetic properties of the Monchegorsk intrusion rocks

no.	J_{rt}/J_{ri}	J_n/J_{ri}	Q_{nf}	Domain state	J_n origin	Main T_d
2	2.45	2.1	17.9	MD+SD	TRM	575 (585)
3	3.65		9	MD	TRM	575 (585)
4	3.89	11.4?	25.8	MD	TRM?	575 (585)
5	2.39	5.1	26.4	MD+SD	TRM	575
6	3.47	3.6	17.5	MD	TRM	575 (585)
7	1.9	6.9?	19.3	SD+MD	TRM	575
9	2.4	0.52	1.4	MD+SD	CRM?	555, 575
10	4.6	3.8	6.3	MD	TRM	545
12	3.13	4.6	13.2	MD	TRM	560
30	2.17	7.7?	42.7	MD+SD	TRM	565, 580
33	2.4	1.4	23.8	MD+SD	KRM+TRM	565
35	5.4	2.7	12	MD	TRM	565
37	4.3	0.84	4	MD	KRM	565
38	2.24	0.65	3.2	MD+SD	CRM?	545(560, 80)
39	3.14	1.07	2.1	MD	KRM	565
40	4.7	0.6	1	MD	CRM?	545 (560)
42	3.5	3.26	15	MD	TRM	575 (585)
43	2.3	4.2	<0.5	MD+SD	TRM?	575
45	2.1	0.33	0.6	MD+SD	CRM?	585
46	2.65	0.66	3.2	MD	CRM	545, 565 (580)
47	6.2?	9.2?	116	MD	TRM	545(560, 585)
48	2.64	6.5?	19	MD	TRM	545, 565
49	2.96	0.72	1.5	MD	CRM	545? 585?
51	1.92	2.16	16	MD+SD	TRM	565 (580)
53	1.9–2.4	3.4–4.3	29	MD+SD	TRM	560

Note: TRM, KRM, and CRM are the thermal, crystallization, and chemical remanent magnetizations, respectively. Higher values of the ratios are possibly due to an incomplete creation of the anhysteretic remanence in an alternating field of 90 mT and other factors; in the case of high ratios J_n/J_{ri}, this can be related to anomalously high NRM values in the region 540–550°C and an inaccurate NRM interpolation. Q_{nf} is the Koenigsberger factor ($J_n/50_\kappa$) for the ferrimagnetic part of the susceptibility κ_f that is the difference between the measured value of susceptibility and its paramagnetic part (about 4×10^4 SI units); the Q_{nf} and NRM values are interpolated in samples with NRM splash. MD and SD are multi- and single-domain grains. respectively. The main values of T_d are unblocking temperatures of NRM close to Curie points, and the T_d values given in parentheses account for an insignificant portion of the NRM value. Large determination uncertainties in J_n/J_{ri} and Q_{nf} in sample 43 are possibly due to a very small value of J_n (<0.1 mA m^{-1}).

Table 3. Magnetic properties of the Kivakka intrusion rocks

no.	rock	J_{rs}	H_{cr}	J_s	H_c	H_{cr}/H_c	J_{rs}/J_s	κ	Q_n	A_κ	Tc_1	Tc_2	J_{rst}/J_{rs}	T_d
4a41	norite	0.0056	581	0.022	144	4	0.26	219	3.45	1.01	280(30)540	540	1.46	560
11a36	harzb	0.086	22	0.518	15	1.53	0.17	4530	2.27	1.33	560	540	1.2	555
16b32	harzb	0.0027	141	0.042	43	3.3	0.064	245	5.96	1.004	525	520	1.19	555
20s1l	norite	0.0039	72	0.0173	32	2.28	0.225	305	31.2	1.017	530	530	1.09	555, 575
25s3u	bronz	0.075	32	0.858	12	2.73	0.09	3847	3.8	1.375	240(14)540	530	1.02	575
26s4l	norite	0.0115	45	0.047	21	2	0.25				250(10)535	540	0.87	535, 565
30s6l	norite	0.0052	67	0.0205	33	2.02	0.254	471	5.34	1.006	170(5)540	540	0.95	550?580
32v53	bronz	0.0285	31	0.164	15	2.01	0.17	4623	3.6	1.43	330(8)530	290(10)530	1.28	545, 570
33s6u	norite	0.0276	32	0.158	14	2.2	0.18	1456	3.9	1.09	160(13)540	540	0.9	545, 570, >600
35v46	norite	0.051	22	0.41	9	2.34	0.13	3083	4.98	1.25	525	525	1.06	545
39pc14	norite	0.0094	32	0.032	15	2.09	0.3	392	6	1.026	530	530	1.2	530, 555
40v34	bronz	0.0074	46	0.049	24	1.93	0.15	412	5.39	1.01	545	540	1.07	530, 550
42pc30	norite	0.022	28	0.205	11	2.56	0.11	2692	3.54	1.12	540	525	1.04	530, 550
43spl3	norite	0.038	31	0.248	14	2.19	0.15	2040	4.64	1.08	535	530	0.99	520, 535
44spl1	norite	0.018	33	0.089	16	1.99	0.2	1008	5.55	1.048	535	540	0.97	520, 535
46pv1	norite	0.0136	47	0.122	22	2.15	0.11				250(9?)540	540	1.14	520, 535
47spm0	bronz	0.0064	108	0.016	74	1.46	0.4	251	25.9	1.008	525	530	1.08	525, 560
50v35	norite	0.004	203	0.017	85	2.39	0.235	273	10.7	1.004	540	540	1.06	550
51v38	norite	0.037	46	0.165	23	1.97	0.22	1129	4.05	1.007	170(10)540	540	0.8	575, 610
53v41	norite	0.0013	50	0.008	24	2.03	0.163	222	2.73	1.009	170(13)540	540. 580	0.94	550, 580, 605
56pt15	norite	0.0069	38	0.0314	19	1.8	0.22	765	3.8	1.03	540	540	1.06	555
61t50	norite	0.0128	33	0.095	12	2.83	0.14	1228	2.78	1.026	535	540	1.18	555
63pt32	gabn	0.0231	51	0.125	22	2.37	0.18	1413	5.3	1.15	150(10)540	540	0.9	555
64t44?	gabn	0.034	28	0.206	13	2.14	0.16	255	3.1	1.012	200(12)550	550	0.87	570
67t53	gabn	0.0089	95	0.0285	48	1.99	0.31	315	4.16	1.032	540	550	1.34	555
68t58	gabn	0.029	68	0.091	33	2.05	0.32	857	9.25	1.065	425(23)540	440(15)540	0.93	490, 555
70t61	gabn	0.066	45	0.499	14	3.18	0.13	3730	15.7	1.041	160(9)550	550	0.95	560, 660

Note: no. – sample number, paleomagnetic unreliable samples are excluded from the table; rock-bronz – bronsitite, gabn – gabbro-norite, harzb – harzburgite; J_{rs} – saturated remanent magnetization, A m^{-1}; H_{cr} – remanent coercive force, mT; J_s – saturation magnetization, A m^{-1}; H_c – coercive force, mT; paramagnetic part along magnetic curve is excluded from values of J_s and H_c; κ – magnetic susceptibility, 10^{-6} SI units; $Q_n = J_n/40\kappa$; $A_\kappa = \kappa_{\max}/\kappa_{\min}$; Tc_1 and Tc_2 – Curie points after the first and second heating of the sample, magnetic phase portion is given in parenthesis; J_{rst} – saturation remanent magnetization after the samples is heated up to 600°C; T_d – unblocking temperature of the high-temperature NRM component.

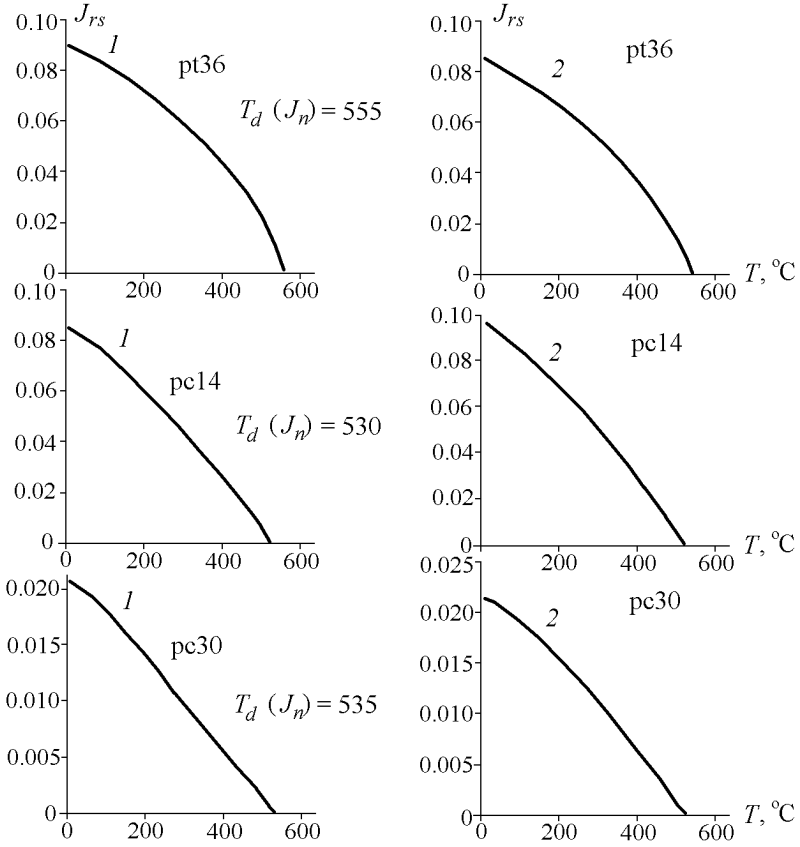

Figure 6. Typical examples of curves of thermal destruction of the saturation remanent magnetization. Kivakka. 1 – first heating, 2 – second heating. pt36, pc14, and pc30 – sample numbers.

in the interval of 150–425°C. Around 5–30% of J_{rs} fell on this phase. This phase is usually absent on curves $J_{rs}(T)$ of the second heating, i.e. more likely it is associated with maghemite or/and with internal stresses. Disappearance of both during heating causes reduction of the remanent magnetization, which is observed in many cases (Table 3). The magnetic phase does not disappear only in two samples during second heating (samples 32v53 and 68t58, Table 3). Probably this is hemoilmenite. It is confirmed by the following fact: sample 32v53 T_c = 330°C, and it falls down to 290°C during second heating and magnetization in this case rises, which is an inherent feature for hemoilmenite. The magnetic phase examined between 150°C and 300°C is of no importance for us as we study the paleomagnetic record above 500°C, where these phases are not present. It is a very rare case when the samples contain a minute amount of magnetite; on curve $J_{rs}(T)$ it is found only in one sample, judging by $J_n(T)$, approximately 50% of the investigated samples contain "tails" of magnetite with the minimal percentage of magnetization. Titanohematite with T_c = 605–660°C has been observed in 6 samples during the thermal demagnetization and its concentration is minute. It is not recorded on the $J_{rs}(T)$ curves because of its low concentration.

Thus, titanomagnetite with T_c = 525–560°C, which is close to magnetite is the main NRM carrier, that defines the paleomagnetic record above 400°C.

Let us consider now the magnetic state of this mineral group. As is seen from the value of H_{cr} = 22–200 mT (Table 3) a magnetic hard material prevails in the samples. Values of Q_n = 3–31 and J_{rs}/J_s = 0.1–0.4 (<0.3 prevail) are relatively not high (Table 3). This obviously speaks about an appreciable portion of the multidomain grains with internal stresses and pseudosingle-domain grains and their deciding contribution into the NRM. The majority of points on the $H_{cr}/H_c - J_{rs}/J_s$ diagram (Figure 7) are near the line separating multidomain and pseudosingle-domain grains [*Day et al.,* 1977] and they are along the theoretical curves for ∼50% mix of the multidomain and single-domain grains [*Dunlop,* 2002]. Consequently, an appreciable portion in the NRM falls on the single-domain and pseudosingle-domain magnetic grains, in the investigated rocks of the Kivakka intrusion. This is at a room temperature, but at temperatures nearing their Curie points, the majority of these grains will behave as single-domain grains.

The majority of the investigated samples of the Kivakka intrusion are magnetically isotropic (Table 3). Anisotropy of magnetic susceptibility exceeds 10% only in 12 samples. Usually these are relatively magnetic samples,

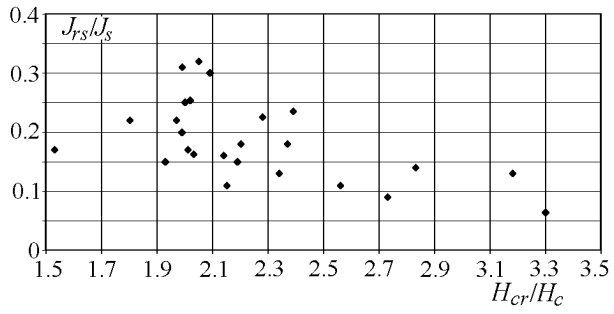

Figure 7. Experimantal values of H_{cr}/H_c and J_{rs}/J_s. Kivakka.

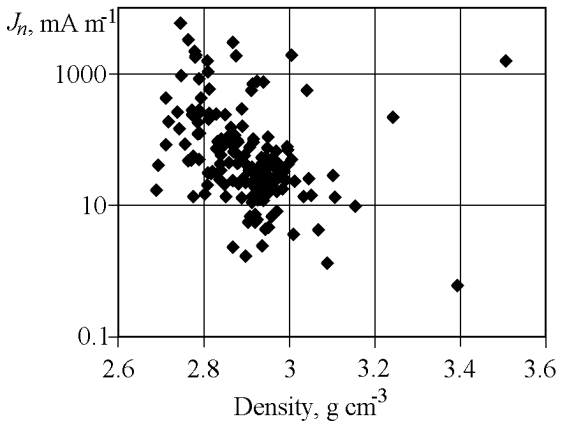

Figure 9. Bushveld intrusion natural remanent magnetization of samples versus their density.

i.e. their anisotropy is determined first of all by distribution and fabric of magnetic minerals. Rocks, whose anisotropy is determined by paramagnetic minerals (weakly magnetic rocks containing less than 0.1% of magnetite) have usually anisotropy of magnetic susceptibility less than 5%. Anisotropic samples have a foliation fabric ($E = \kappa_{\rm in}\kappa_{\rm in}/\kappa_{\rm min}\kappa_{\rm max} = 1.08$–$1.3$, $E_{\rm mean} = 1.17$), which confirms the solid phase conditions of crystallization of the magnetic minerals, probably, under directional pressures (deformations) and/or as a result of crystallization along slice planes of silicates during their exsolution.

Composition, concentration of magnetic minerals, their magnetic fabric (anisotropy of magnetic susceptibility) and magnetic state do not depend on the petrological and mineralogical characteristics of rocks.

C. **The Bushveld intrusion.** The magnetic susceptibility in the investigated part of the intrusion section varies from units up to 1825×10^{-5} SI units and in the main group of samples it is in the range of 20–60×10^{-5} SI units and correlates clearly with the petrological composition of rocks

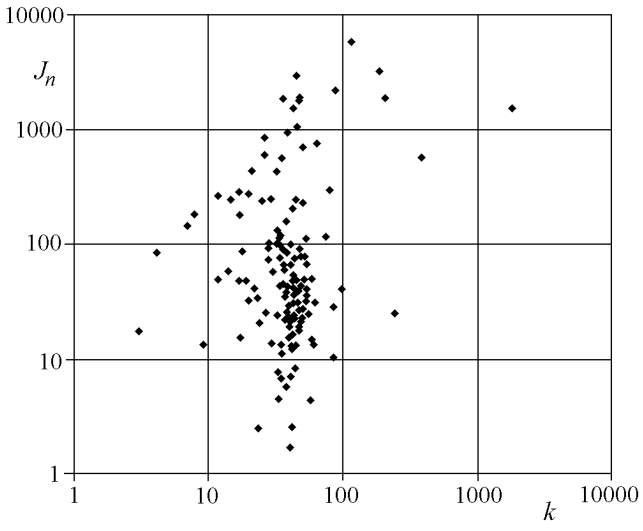

Figure 8. Values of magnetic susceptibility ($k, 10^{-5}$ SI units) and of natural remanent magnetization (J_n, mA m^{-1}). Bushveld. Logarithmic scale.

(Table 4). The latter is connected with a paramagnetic component prevailing in samples with $\kappa < 10^{-4}$ SI units. If to draw lines, which restrict the swarm of points at the top and bottom on Figure 8, they will cross the abscissa axis at points $\kappa = 0.5\times10^{-5}$ and 3×10^{-5} SI units. This, evidently, is the portion of paramagnetic susceptibility in samples under investigation, from anorthosites, where and appreciable portion of the negative diamagnetic susceptibility is likely to be present, to pyroxenites, when concentration of iron in the rock is maximum and this concentration determines the paramagnetic susceptibility. If we consider the NRM versus rock density dependence, which is unambiguously governed by the rock composition, a tendency of growth of the NRM value with reduction of density, i.e. from pyroxenites (density exceeds 3 g cm^{-3}) to anorthosites (density is less than 2.8 g cm^{-3}) (Figure 9). A group of narrow horizons with a relatively high NRM stands out. These belong, as a rule, to anorthosites (Table 4). But this does not mean that all anorthosite samples have a high NRM: only 20% have NRM>1000 mA m^{-1}, and 40% of samples have NRM<100 mA m^{-1}. This ratio is much less in the case of norites and pyroxenites: less than 4% of samples have NRM>1000 mA m^{-1} and more than 80% have NRM<100 mA m^{-1}. Consequently, the bulk of magnetic minerals, close to magnetite, is concentrated in plagioclases of anorthosites.

As it is impossible to perform the thermomagnetic analysis on the Bushveld intrusion samples, we estimate composition of the magnetic minerals according to data of the thermal demagnetization. It is possible to identify four major unblocking temperatures, which are, evidently, the Curie points: 1) an abrupt drop of magnetization near 300–350°C (6 samples), which is, probably, associated with pyrrhotite [*Hattingh,* 1986a], does not participate in the paleomagnetic analysis as the main attention is paid to magnetite and titanomagnetite; 2) an abrupt drop of magnetization between 553°C and 556°C, from 20–30% up to more than 90% of NRM, the Curie point of 556°C has been adopted; judging by data from [*Hattingh,* 1986a], this is a low-titanium titanomagnetite – the exsolution product, mainly, of plagio-

Table 4. Magnetic properties of samples from the Bushveld intrusion

no.	m	rock	$J_{no}/J_{n\,max}$	κ	dT_{in}	I_{in}	pol	dT_{hi}	I_{hi}	pol	dNR	T_d	I_{556}	I_{580}
1	30.81	norite	109	53	450–520	−29.4		555–600	78.3	N		556, 580,TH	77.8	78.1
2v	32.73	anorth	120	76				555–580	72.3	N		556, 580	55	74.2
3v	34.36	norite	180	17				20–580	68.9	N		556, 580	77	78.9
4	35.96	norite	16.2/20.2	38	200–520	−48.9	R	520–580	74.2	N	27	556, 580	75.5	75.9
5	40.34	norite	494/562	35				520–580	72.7	N		556, 580	73.2	71.8
6	44.8	anorth	634/690	51	400–520	−49.8	R	520–620	78.1	N	31	556, 580,TH	78.5	79.6
7v	46.28	anorth	5906	115				540–620	80.6	N		556, 570,TH	80.5	80.7
8v	53.6	anorth	2957	44				20–620	77	N		556, 580,TH	85	83.4
9v	59.58	anorth	3257/3290	187				450–620	86	N		556, 580,TH	87.6	
10	62.22	norite	55.8/57.4	34				20–520	46.7	N		580?		
11v	65.4	anorth	185	8				540–570	67.4	N		556, 580	70.6	74.4
12	68.64	norite	29.6/36.6	43				450–580	59.2	N		556, 580	64	70.2
13	74.63	norite	37.8/49.6	58				350–580	50.4	N		556, 580	62.3	53.5
14v	80.51	norite	66.6	53				400–580	71.4	N		556?575?	64.8	57.6
15v	87.94	norite	7.5/24.1	57	400–520	−51.7	R	520–580	64.8	N	13	556, 572	76.7	84.6
16	93.93	norite	35.6/32.6	54	500–520?	−39.3	R	540–580	72.7	N	37	556, 580	75.3	69.6
17	101.38	norite	34/49.2	51	500–540	−45.1	CN?	555–580	71.3	N	64	556, 580	73.6	59.9
18	107.22	norite	14.4/41.4	52	500–540	−53.8	R	540–580	63.5	N	20	556, 580	71.5	68.8
19	117.39	norite	23/24.8	46				555–580	70.4	N		556, 580	68.1	78.6
21	132.35	norite	19	47				300–580	54	N		556, 570	53.8	64
22	136.62	norite	31/40.4	46	450–520	−76.6	R?	520–580	55.5	N	43	556, 580	54.7	70.1
23	147.08	pyrox	44.2/41.2	36	350–450	−44.5	R	450–580	54.8	N	11	556, 570	57.3	62.5
24	151.55	norite	31.4/31.6	46	500–540	−65.1	R	540–580	60.3	N	9	556, 580	51.1	73.4
25	160.39	norite	26.5/30.8	42	350–450	−46.1	R	540–580	62.1	N	19	556, 580	60.9	72.6
26	167.48	norite	21.3/21.1	40	450–520	−74.7	R	540–580	56.4	N	23	556, 580	62.6	57.7
27	169.43	anorth	82.2	4				520–580	73.5	N		556, 580	72	71.5
28	171.14	anorth	4.2/3.2	59	450–540	−52.6	R	540–565	60.8	N	49	556?, 570	57.4	66.5
29v	171.72	anorth	20.8/20.1	24	500–540	−43.5	R	555–580	73.2	N	31	556, 575	74.7	76.1
30	174.7	anorth	30.8/26.4	41	450–520	−47.3	R	520–580	63.6	N	21	556, 570	68.5	66.2
31	176.57	norite	31/38	44	200–540	−57.8	CN?	540–580	72.7	N	20	556, 580	75.2	70.5
33	187.91	pyrox	20.6/44.2	48	500–540	−63.8	R	540–580	66.8	N	4	556, 580	65.2	74.5
34	190.85	norite	16/27.2	48	500–520	−40.9	R	540–580	53.9	N	36	556, 570?	69.8	
35	195.3	pyrox	21.2/29.2	43	450–540	−54.7	R	540–580	58.2	N	5	556, 580	57.5	63.4
36v	198.15	norite	21.6/21.8	43	450–540	−36.9	R	540–570	60.4	N	25	556, 573	68.2	75.7
37v	206.82	norite	15.5/12	40	450–540	−37.4	R	540–580	59.9	N	24	556?, 580	62.3	77.9
38	213.28	norite	11.3/27.1	51	350–540	−71.8	R	540–580	54.1	N	19	556, 580	56.1	55.4
39	221.87	norite	22.4/41.6	42	500–520	−37.2	R?	520–570	68	N	32	556, 575	67.8	
40	229.34	norite	16.8/44.4	45	500–540	−40.3	R?	540–570	70.4	N	34	556, 570	60	84.6
41	236.86	norite	52.8/49.6	42	450–520	−37.8	R?	520–580	67.9	N	64	556, 580	61.8	70.7
42	241.32	norite	56/74.2	43	500–520	−35.8	R?	540–580	70.5	N	35	556, 580	60.7	73.4
43	251.77	norite	30.8/48.8	46	500–540	−76.8	R?	540–580	54.8	N	22	556, 570	55.1	64.5
44	255.64	norite	18.8/30.5	42	520–540	−38.3	R?	555–580	56.1	N	19	556, 570	53.4	62.7
45	265.32	norite	36.6/48.6	43	450–520	−59.2	R	540–580	63.8	N	8	556?, 580	45.3	85.2
46	272.77	norite	17.7/23.5	43	450–540	−68	R?	540–580	54.5	N	46	556, 580	50.3	68.2
47	280.24	norite	26.6/24.3	49	450–520	−47.9	R?	555–580	64.2	N?	35	556, 580	61.1	81
48	286.24	norite	15/16	42	450–520	−45.5	R?	540–580	60.9	N	16	556. 580	54	66.7
49v	295.2	norite	16.7/23.5	45	500–540	−50.4	R	540–580	58.1	N	9	556, 578	60.6	72.7
50	302.31	norite	9.6/14.9	40	500–540	−53.3	R	540–580	75.3	N	24	556, 580	74.9	75.8
51	309.76	norite	15.7/19	41	500–540	−50.3	R	540–580	69.3	N	20	556, 580	65.6	76.8
52	317.23	norite	53	42	450–520	−75	R	555–580	73.6	N	7	556, 580	72	76.6
53	324.49	norite	19.1/23.6	40	450–520	−49.4	R?	540–580	66.7	N?	19	556, 580	65.2	81.5
54	328.56	norite	34.8/32.2	37	450–520	−47.8	R?	540–580	74.5	N	30	556, 580	72.5	77.2
56	335.15	norite	102	41	400–540	−32.2	R?	565–580	70.3	N	38	556, 580		70.3
57v	340.32	norite	44.6/68.8	41	450–540	−30	R?	540–580	73.2	N	43	556, 580	72	81
58	344.86	norite	61.8/65.2	36	500–520	−28.6	CN?	540–580	76.6	N	50	556, 580	76.6	87.6
59	356.13	norite	158	38	400–540	−36.5	R	540–580	62.7	N	26	556, 580,TH	58.1	74.5

Table 4. Continued

no.	m	rock	$J_{no}/J_{n\,max}$	κ	dT_{in}	I_{in}	pol	dT_{hi}	I_{hi}	pol	dNR	T_d	I_{556}	I_{580}
60v	359.82	norite	35.6/36	42	450–540	-38.2	CN?	540–580	65	N	29	556, 580	76.6	72.4
61	368.75	norite	16.9/42.9	36	450–540	−53.2	R	540–580	66.9	N	15	556, 580	76.1	72.7
62	372.65	norite	36.2/43.9	34	300–520	−64.8	CN?	520–620	67.4	N	38	556, 580,TH	51.6	74.6
63v	376.23	norite	1858	36	300–500	−38.4	R	540–580	67	N	30	556, 580	50.4	79
64v	376.79	anorth	1911	47				555–600	59.1	N		556?, 570,TH	48.2	62
65	385.17	anorth	82.4/90.8	35	520–540	−49.1	R	540–580	54	N	5	556, 580	54.5	72.5
66	393.66	norite	56.2/51.4	37	350–520	−76	R??	555–580	66.7	N	28	556, 580	66	61.2
67	395.14	pyrox	13.1/12.2	62	450–540	−39.5	R	540–570	43.4	N	10	556, 565	53.9	
68v	398.75	norite	75/116	35	500–520	−38.9	R?	555–580	73.7	N	35	556, 580	82.3	75.4
69	404.56	norite	125/150	38	500–520	−46.9	CN?	520–580	69.7	N	25	556, 580	74.3	77.8
70v	409	norite	88.6/91.9	28	450–520	−36.2	R	540–580	74.9	N	40	556, 580	80.7	84.4
71	414.58	pyrox	8.6/14.1	59	200–500	−65.1	CN?	520–570	54.6	N	26	556, 570	54.2	57.4
72v	418.76	norite	236/214	51	500–540	−38.6	R	540–580	72.2	N	34	556, 582	66.2	78.1
73v	429.61	norite	61/90	48	500–520	−38.1	CN?	555–580	73.2	N	35	556, 577, 585	72.8	77.5
74	435.73	norite	12.3/30	47	500–540	−54.6	R	540–580	79.3	N	28	556, 580,TH?	75.1	77.2
76	444.51	norite	4.1/12.2	42	200–450	−51.6	CN?	520–570	56.4	N?	19	550, 570	63.4	60.3
77	448.85	norite	33.6	37	350–540	−36.4	CN?	540–580	51	N	19	556, 580	40.1	70.7
78	449.92	norite	13.4/12.8	35	400–520	−35.7	R?	520–580	53	N	26	556, 580	53.6	55.4
79	453.91	norite	10.6/32	20	400–520	−46.3	R	540–580	53.3	N	15	556, 580	54.5	58
80	455.3	anorth	11.3/23.2	51	350–540	−42.6	R	555–580	69.7	N	27	556, 580	67.1	74.9
81	455.78	norite	25.8/34	23	500–540	−21.3	CN?	565–580	69.9	N	56	556, 580	58.9	69.9
82	456.17	norite	8/12.9	41	500–540	−46.8	R	565–580	52.6	N	10	556, 580	56.4	52.6
83	457.74	anorth	27.1/42.3	39	300–540	−45.2	R	555–580	70.1	N	30	556, 580	58.3	70.1
84-1v	463.06	anorth	237	25	500–520	−35	CN?	520–580	71.3	N	46	556, 582	57.9	87.4
85	465.32	norite	20.2/22.8	47	500–540	−32.5	R?	540–600	49.5	N	19	556, 580,TH	52.6	45.4
86	474.22	anorth	13.2/24.9	27	350–540	−43.4	R	540–570	63.9	N	25	556, 570	59.9	64.9
87	475.47	anorth	6.8	41				555–570	39	N?		556?, 570	32	39
89	483.33	norite	10.1/21.9	37	520–540	−68.9	CN?	540–580	67	N	32	556, 580	64	65.9
90	489.29	norite	28.7/42.7	36	400–540	−21.3	R	540–580	65.7	N	45	556, 580	61.2	72.6
91	491.56	norite	5.6/11.9	41	500–540	−38	R?	540–580	58.1	N	23	556, 580	61.8	65.3
92	493.18	anorth	24.3/25	38				555–580	52.2	N		556, 580	50.3	53.4
95	507.84	norite	55.7/77.2	52	200–350	−68	R??	555–580	74.9	N?	26	556, 580	78	63.6
96	511.65	nprite	4.6/8	44	450–540	−58.3	R	555–570	54.7	N	7	556, 570	52.8	61.7
97	520.41	anorth	424	33				520–580	79	N		556, 580,TH?	77.9	79
98	523.1	anorth	13.6	29	500–520	−23.1	CN?	540–570	52.7	N	51	556, 570	53.2	48
100v	529.29	pyrox	110	34				20–580	74	N!		556?, 580	67.8	75.7
101	533.96	pyrox	17.6	47	20–540	−81						580?		515
102v	535.14	anorth	16.8	3				555–580	75.5	N		556, 580	69.4	78.9
103v	537.16	anorth	934	39				555–580	78.4	N		556, 570,TH	71.2	75.6
104	539.07	norite	13.5/11.6	61	500–540	−31.3	CN?	555–580	44.3	N?	22	556, 580,TH?	43.6	45
105	542.65	anorth	23.9	33										
106v	548.7	anorth	84.4/101	28	200–520	−71.4	R?	555–580	71.2	N	5	556, 580	69.8	75.1
107v	550.14	norite	26.7/32.6	53	500–540	−47.4	CN?	565–580	74.8	N	43	556, 580	80.8	79.4
108v	554.56	anorth	586	26				520–580	75.4	N		556, 580	66.1	81.3
109	556.34	anorth	70.6/85.6	37	500–540	−47.5	R?	555–580	72	N	27	556, 580	73.8	
110	563.5	norite	20.9	48				555–580	63.6	N		556, 570	64	63.6
111	567.4	anorth	44.2/40	35	500–540	−57.5	R	540–580	55.1	N	6	556?, 580	58.1	69
112v	572.19	anorth	228/246	29	200–520	−35.5	R	520–580	70.8	N	36	556, 570,TH	71.4	76.1
113v	576.78	anorth	831	26	500–520	−20.2	R?	540–620	76.4	N	56	556,TH	77.7	78.1
114	582.65	anorth	982/1071	45				555–620	78.6	N		556, 580,TH	78.8	63.1
115	587.84	anorth	1398/1564	42	200–520	−34.2	R	540–630	66.4	N	35	556, 580,TH	68.1	64.4
116v	592.2	anorth	741/762	65				555–580	69.5	N		580,TH		
117v	596.58	anorth	1788	47				555–630	75.8	N		556, 580,TH?	68.8	65.6
118v	601.1	anorth	246	15				540–600	70.5	N		556, 575,TH?	80.4	75
119v	606.33	anorth	279	17				540–600	76.4	N		556, 570,TH	69.5	75.1

Table 4. Continued

no.	m	rock	$J_{no}/J_{n\,max}$	κ	dT_{in}	I_{in}	pol	dT_{hi}	I_{hi}	pol	dNR	T_d	I_{556}	I_{580}
120v	611.76	anorth	427	21				540–600	66.7	N		580?,TH?		49.4
121v	616.6	norite	40/49	19	300–520	−49.6	R?	555–580	55.2	N	6	556?, 585	42.9	67.6
122	621.38	norite	4.3	34	520–540	−63.4	R?	555–580	60	N	6	556, 570	44.6	59
123v	625.69	norite	96.8	33				520–580	61	N!		556, 580	62.8	67.4
124	627.75	norite	27.3/28.3	85	520–540	−34.9	CN?	555–580	51.1	N?	85	556?, 570?	51.1	
125	632.68	norite	37.8	38	500–540	−46	R?	555–580	49.8	N?	9	556?, 580?	54.4	
127v	643.08	anorth	132/145	7				540–580	70.7	N		556, 580	71.9	77.1
128	645.52	anorth	154/278	20	200–300	−56	CN?	540–580	70.3	N	19	556, 580,TH	70.5	76.4
129v	647.75	anorth	203/118	42	200–400	−54.8	R??	500–580	68.4	N?	48	556, 568, 578,TH	64	65.5
130	648.6	norite	1890	206			R??							
131	649.1	norite	289	80	500–?	−35.5	R?					300, 570	−24.2	
132	650.95	anorth	31	61	520–555	−14	CN?	555–580	69	N?	57	556, 580	67.8	68.3
133v	653.05	anorth	158/260	12	200–300	−62.5	R?	540–600	75.4	N	24	556, 580,TH	78.3	78.6
134	657.46	anorth	6.6/13.4	9	450–540	−32	CN?	540–580	54.7	N?	24	556?, 570	40.5	66.2
135v	659.3	anorth	125	32				200–580	70.3	N!		556, 580	67.9	72.2
136	661.39	norite	10.1/14.8	17	500–540	−67.2	R	540–580	60.9	N	16	556, 580	59.7	62.3
137	664.6	norite	2.3	24	350–520	−50	CN?					?		
138	670.23	norite	7.2	33	400–540	−66.5	CN?					560		
139	675.72	norite	5.5	38	500–540	−35	CN?					545		
140	680.92	norite	42.3	98	450–550	−47.8	R					556	−51.8	
141	683.28	norite	6.7	35	500–540	−55	R	540–565	45.5	N?	12	556?	51.3	
142	690.22	norite	1.7	40	300–500	−61.1	CN?					?		
143	692.78	norite	2.4	43	500–540	−45	CN?					540?		
145	702.39	norite	13.3	44	200–350	−58.8	R?						745	
147	711.7	norite	11	36	500–540	−47.2	CN?					545?		
148	718.17	norite	13	36	520–540	−47.4	R?	540–570	78.7	N?	37	570		78.7
149	721.16	norite	23.3	47	450–540	−55.7						540		765
150	726.56	norite	76.2	49				520–565	−60.9	R?		560?		
151	730.34	norite	57.7	36	520–540	−76.1	R	540–570	66.3	N	12	556, 570	78.6	62
152	734.96	norite	40.7	22	200–350	−61.8	R?					350		785
153	739.51	norite	57.4	30	200–300	−85.5	CN?					300		795
154v	745.15	norite	17.7/55.8	14	400–540	−39	CN?	540–580	56.8	N	20	556, 572,TH	55.6	69.8
155v	749.43	anorth	2178	87	200–400	−67.2	R	540–570	75.9	N	24	556, 580,TH	59.8	70.5
156	755.21	norite	241	45	500–555	−35.3	CN?	570–580	57.7	N?	79	350, 580		57.7
157	759.79	norite	30	40	500–540	−51.6	R	555–580	47	N	7	556?, 580	26.4	69.7
158	764.66	norite	77	50	520–555	−67.9	R	555–580	50.7	N?	34	575?		59.7
160	773.31	anorth	72	28	200–540	−65.1	R	555–580	61.3	N	7	556, 570	52.4	63.3
161	779.6	anorth	100	33	520–555	−37.7	R?	555–570	51.9	N?	24	350, 556?, 570?	51.9	
162	783.8	anorth	15/48	12	500–540	−45.2	R	555–580	57.8	N	14	556, 580	53.1	61
163v	788.09	anorth	7/84.8	18	350–540	−29.1	CN?	540–580	29.9	N	8	556?, 580	53.5	72.5
164v	794.54	anorth	35.8/47.6	17				555–580	69	N?		556, 580	54.8	58.8
167	802.42	pyrox	1547	182 5				500–520	−32.6	R		580?,TH	−38.1	
168	802.42	chrom		106										
169	803.45	pyrox	9.7/7.6	88	450–520	82	N?	520–540	−66.3	R?	19	540	−66.3	
172	809.39	norite	25	245	400–500	−55		520–550	−72	R		560	−72	
173	814.15	norite	554	387	450–520	−85	CR	520–540	−41.4	R		580?	−41.4	

Note: no. – sample number, letter "v" is used to mark samples, which were used for analysis of the field variations in the course of cooling of the intrusion at the sampling point; m – sampling level in meters; rock – anorth – anorthosite, pyrox – pyroxenite; κ – magnetic susceptibility, 10^{-5} SI units (data from B. N. Pisakin, 2003); $J_{no}/J_{n\,max}$ – initial and maximum natural remanent magnetization NRM of the sample in the course of thermal demagnetization, respectively, mA m^{-1}; dT_{in} – temperature of isolation of intermediate-temperature NRM component, I_{in} – inclination of intermediate-temperature NRM component; pol – polarity of this component; dT_{hi} – temperature of isolation of high-temperature component; I_{hi} – inclination of high-temperature NRM component; N – normal polarity, R – reversal polarity, C – direction close to the recent field; dNR – difference of directions of the intermediate-temperature and high-temperature components of each sample; T_d – main unblocking temperatures of high-temperature components (Curie points); I_{556} and I_{580} – inclinations of high-temperature NRM components near their Curie points.

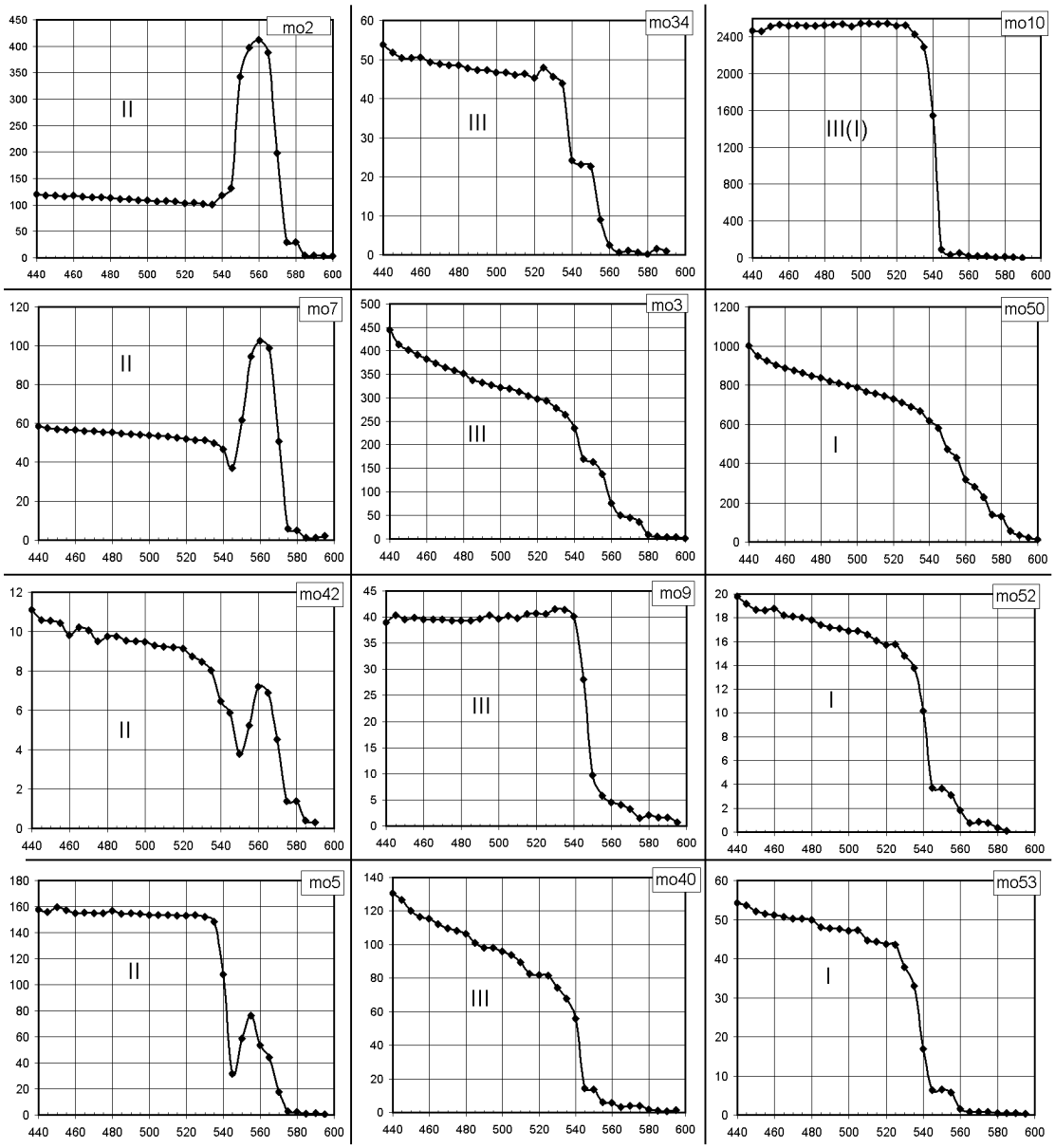

Figure 10. Examples of $J_n(T)$ I, II and III type dependences (see text). A smooth transition from type II to type I. Temperature, °C – everywhere along the horizontal axis, magnetization mA m^{-1} – along the vertical axis. moXX – sample numbers.

clase, more rare of pyroxene (see above). Since this Curie point remains constant throughout the section this speaks in favor of a "one action" formation of this magnetic mineral, which occurred at the phase of a high-temperature exsolution of silicates, the secondary alterations would have definitely caused dispersion of composition of such minerals; 3) after being heated to 580°C and most rare to 570°C the NRM in majority of samples becomes less than 0.1 mA m^{-1} and this is the Curie point of magnetite (Table 4); 4) an appreciable magnetization is recorded in 27 samples (20 of them are anorthosites, 6 are norites and 1 is pyroxenite) at a temperature above 580°C which last to 600–660°C according to data from [*Hattingh,* 1986a]. These are lamellas of titanohematite in the ilmenite grains, the paleomagnetic directions associated with this mineral are very close to "magnetite" directions. The titanohematites fall approximately on the horizons enriched by magnetite and titanomagnetite, i.e. having a high magnetization (Table 4).

Results of Thermal Demagnetization and of Component Analysis

A. **The Monchegorsk intrusion.** According to the magnetization behavior in the process of thermal demagnetization, the curves $J_n(T)$ can be divided into three types (Figure 10):

I) a parabolic curve of the Q type or has a tablelike shape; its T_d value varies from 550°C to 585°C, and one to three phases with different T_d values are present in a number of samples;

II) J_n sharply increases beginning from 545–555°C, and its peak varying in height is observed at 550–560°C.

III) The peak degenerates into a step in the curve $J_n(T)$. A smooth continuous transition exists between types II and III on one side and between III and I (Figure 10); therefore, they are of the same or a similar origin. Type III is intermediate between types I and II. The division of samples into three types in accordance with the shape of the curve $J_n(T)$ does not depend on the susceptibility, NRM and its unblocking temperature (Table 2), Q_n, magnetic anisotropy, and the over-printing amount (the last factor has an effect mainly at temperatures below 520–540°C). In all samples of types II and III, the curves $J_{rs}(T)$ and $J_{rt}(T)$ have the shape typical of magnetite and similar to the Q type [*Pechersky et al.,* 2002]; i.e., peaks in the curves $J_n(T)$ of type II, a tablelike shape of the curves of type I, and steps in the curves of type III are unrelated to the com-position and structural properties of magnetite grains. However, their dependence on the magnetic polarity is evident. Thus, the thermal demagnetization reveals a single magnetic polarity in samples of type I, mostly normal (N) samples 32, 38, 40, 41 and 45–53 and more rarely reversed (R) samples 9–11 and 13. Both polarities are fixed in samples of type III, and this is their main distinction from samples of type I. Finally, 10 samples of type II have the N and R polarities, one sample has the R polarity, and none of the samples has the N polarity. Along the section, samples are located quite regularly: samples of type II obviously prevail in its lower part (the lower ∼250 m), where two magnetic zones of the normal (580–550°C) and reversed (below 550°C) polarities are clearly identified, whereas samples of type I prevail in the upper part of the section (the upper ∼150 m), where the normal polarity alone is observed.

Such behavior of $J_n(T)$ can be interpreted as follows. Two J_n components of opposite polarities exist in samples of type II. One of these polarities (usually reversed) has lower unblocking temperatures (below 550°C), and/or its carriers were formed below 550°C, whereas normal polarity grains formed at a higher temperature and have higher values of T_d and T_c. The relative contributions of these two components are different. The aforesaid explains the appearance of the curves $J_n(T)$ of type II and the smooth transition between type II and type I through type III. This interpretation is valid if the overwhelming majority of magnetite grains are in the single-domain state in the interval 500–580°C. Considering that $J_n/J_{rt} \approx 1$ (Table 2), the crystallization remanent magnetization (CRM) prevails in one-third of the samples studied, and some of them have a primary paleomagnetic direction similar to that of the samples having thermoremanent magnetization coeval with the intrusion cooling (see below). This does not contradict the fact that such samples were magnetized at the stage of the intrusion cooling. If magnetite grains formed at 450–500°C (i.e., below the Curie point of magnetite), they acquired the crystallization magnetization. In this case, their unblocking temperature during the thermal demagnetization, considering the cooling rate of the intrusion (see below), is 500–540°C (Figure 5). Evidently, such a process also took place later, at 2–1.9 Ga, during intense tectonic movements accompanied by heating to ∼400°C (the greenstone metamorphism observed near faults), which corresponds to an ∼500°C unblocking temperature of the thermal demagnetization (Figure 5). This interpretation is supported by the prevalence of the magnetization of this type near the fault crossing the sampling profile (samples 37–46, Table 2). Magnetic grains with the KRM or chemical remanent magnetization (CRM) have lower values of Q_{nf} (Table 2).

The thermal demagnetization results distinguish three ancient NRM components: 1) a conventionally low-temperature component is distinguished in a number of samples below 500°C (frequently below 400°C), 2) a middle-temperature component is detected usually between 500°C and 540°C, 3) a high-temperature component is detected above 540°C (Figure 11a). The middle-temperature and high-temperature NRM components have opposite polarity (Table 5) and they are frequently fixed in one sample. The single-component, two-component and three-component samples according to NRM do not differ by $J_{rt}(T)$, $J_{rs}(T)$, $J_s(T)$ – all of them are single-component [*Pechersky et al.,* 2002], i.e. presence of components of opposite polarity is not a result of self-reversal. Absence of any secondary changes in the intrusion rocks, independence of magnetic polarity from composition of the rocks (peridotites, pyroxenites), content and composition of magnetic minerals (magnetite, phyrrotite), from the domain state of magnetic grains (H_{cr}), it is possible to suppose that opposite polarity of the NRM components is the result of variation of the geomagnetic field polarity in the process of cooling of the intrusion.

As seen from Table 5 the reversal test is performed within α_{95} for the intrusion rocks. The pole coordinates which belong to the Early Proterozoic layered intrusions and mafic dikes of the eastern part of the Baltic shield (Karelia, Finland and the Kola Peninsula), whose age is 2.4–2.45 Ga, have a great scattering: latitude is 11–41°S, longitude is 245–305°E, average coordinates 23°S and 273°E differ from our results. Contradiction can be removed, if the block with the Monchegorsk intrusion to rotate counterclockwise and to tilt in the NW direction at 15°–20°, the Monchegorsk intrusion pole (for example, lines 4 and 5, Table 5) will occupy a place, within α_{95}, in the group of the paleomagnetic poles of Karelia and the Kola Peninsula, whose average age is 2.45 Ga and the average coordinates of this pole will be 23°S, 273°E (Table 5) [*Pechersky et al.,* 2002]. It is very likely that a great scattering of the Early Paleo Proterozoic poles is caused by a neglect of local tectonic movements.

A secondary NRM component associated with both magnetite and pyrrhotite (Table 5) is identified in a wide range of demagnetization temperatures up to the Curie point of magnetite (typically, below 520°C) in many samples of the intrusion and host rocks. Comparison of the pole position calculated from this component with the APWP of the Baltic Shield shows that the age of this component is ∼1.9–2 Ga [*Pechersky et al.,* 2002, 2004]. An intense tectonic reorganization of the region is dated at this time (see Brief geological description). A certain scatter in the pole coordinates and the presence of normal (predominantly) and reversed (occa-

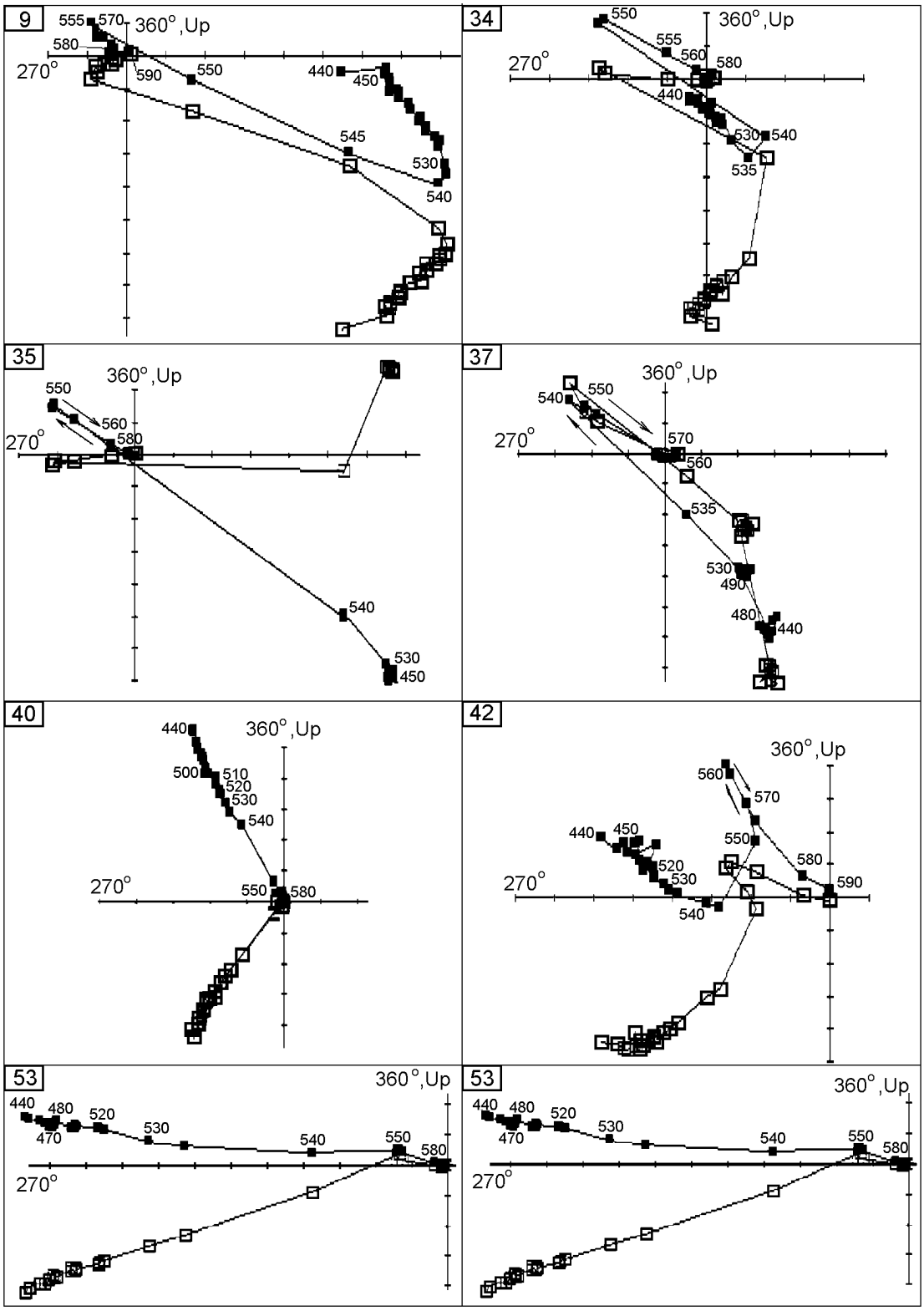

Figure 11. Examples of the orthogonal projections in the process of thermal demagnetization of the natural remanent magnetization (Zijderveld diagrams). Filled signs – horizontal plane, open signs – vertical plane. **A** (this page). Monchegorsk intrusion: sample 9, the primary reverse polarity KRM is detected in the 480–515°C range, the secondary normal polarity KRM – between 540°C and 555°C, the primary reverse polarity KRM – between 555°C and 580°C; sample 34, the secondary normal polarity NRM is detected below 540°C, the primary reverse polarity component – between 540°C and 550°C and

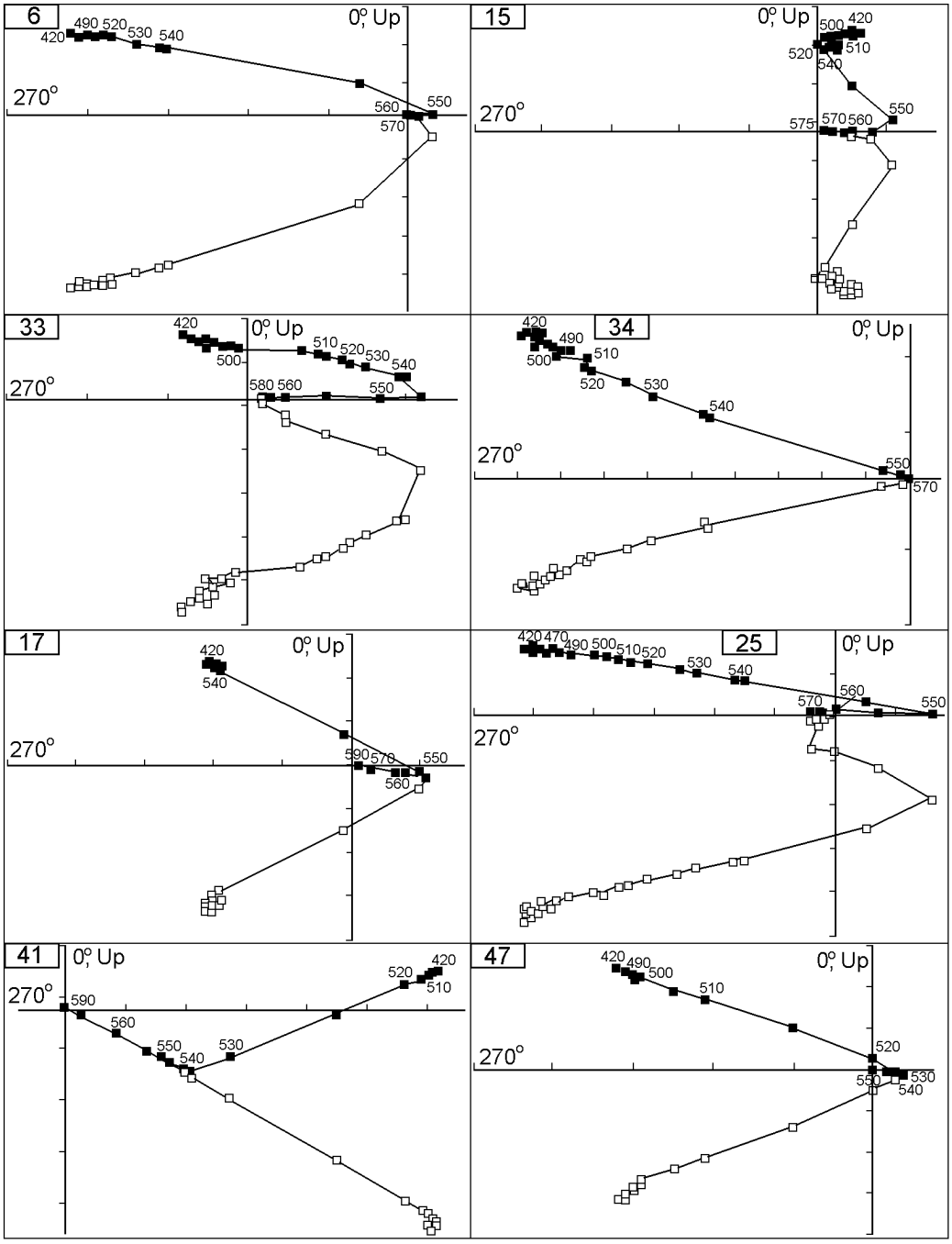

the primary normal polarity component – between 550°C and 570°C; sample 35, the secondary reverse polarity component is distinguished below 515°C, the primary reverse polarity component is detected from 540°C to 550°C, the primary normal polarity component is detected from 555°C to 580°C; sample 37, the secondary reverse polarity component is detected from 20°C to 500°C, the primary reverse polarity KRM is fixed from 500°C to 540°C, the primary normal polarity component is fixed from 540°C to 565°C; sample 40, the secondary normal polarity component is fixed up to the magnetite Curie point, this is most likely a chemical magnetization; sample 42 – example of a complicated behavior of NRM near the fault, this is predominantly the KRM, up to 545°C this is the secondary normal polarity component, between 550°C and 560°C – primary reverse polarity component, above 560°C – primary normal polarity component; sample 47, from 20°C to 580°C the primary normal polarity NRM (TRM) component is fixed; sample 53, up to 550°C the secondary normal polarity component is detected, above up to 575°C – the primary normal polarity component is detected.

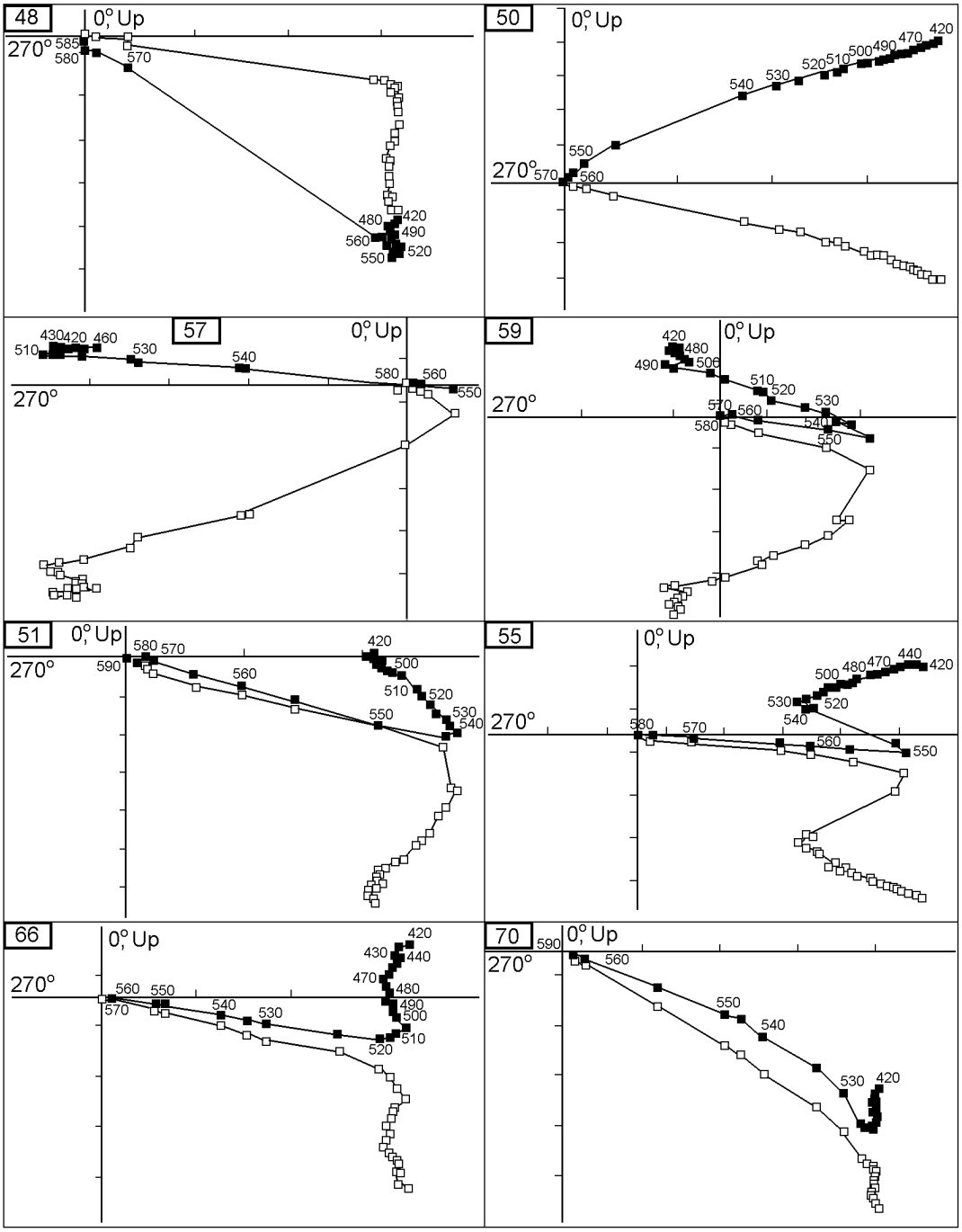

Figure 11. Continued. **B** (on pages 411 and 412). Kivakka: sample 6 – component B prevails, above 550°C component A_2 is detected; samples 15, 17 and 47 – component A_1 is detected above 535–550°C, component B – between 420–520°C and 550°C, between 420°C and 520°C – a component close to the recent; sample 25 – component A_2 is detected from 550°C, component B – between 450°C and 550°C, below a component close to the recent is fixed; sample 33 – up to 545°C component B prevails, above – component A_1; sample 34 – component B; sample 41 – component A_1 (A_2) is detected from 535°C, the sum of components A_1+B with similar spectra of unblocking temperatures is fixed between 420°C and 535°C, a component, evidently, close to the recent is present up to 500°C; sample 48 – component A_2 is detected above 540°C, below the sum of components A_2+B is fixed; sample 50 – the sum of components A+B with similar spectra of unblocking temperatures; samples 51, 55, 57, 59 and 66 – component A_1 is detected above 520–550°C, below the component B is fixed or B+A and a component close to the recent (below 500°C); sample 70 – components A_1 and A_2 are detected from 520°C to 660°C (smooth transition), below is the sum of components A_2+B.

Table 5. Average paleomagnetic directions and pole coordinates of the Monchegorsk intrusion and of the neighboring regions

Number of samples and magnetization age	Polarity	D	I	K	α_{95}	Pole	
						longitude	latitude
1) 27, primary	N	305	−15	19.7	6.1	267.6 E	5.2 N
2) 23, primary	R	127	30	10.4	9	263.2 E	4.7 S
3) Difference between 1 and 2	N+R	306	−23	57.6	13	265.3 E	1.3 N
4) D-50	N+R	256	−23			310 E	16 S
5) D-30, I+17	N+R	276	−40			289 E	19.7 S
6) 19, secondary	N+R	334	33	12.5	9.1	244.6 E	37.3 N
7) 13, pyrrhotite, primary	N+R	328	−33	5.8	16.1	255.3 E	2 S
8) 14, pyrrhotite, secondary	N+R	316	46	12.3	10.7	282.7 E	37.4 N
9) Dikes of the Main Range	N					251.1 E	7.9 N
10) Diabases, Voche-Lambina	N+R					247.6 E	5.7 N
11) Average on 9 poles	N+R				12.2	273 E	23 S

Note: The polarity column presents polarities of the high-temperature NRM component (N – normal, R – reversed) that were determined after [*Elming et al.,* 1993; *Khramov et al.,* 1997]; D and I are, respectively, the declination and inclination of this component; K is the precision parameter; α_{95} – is the confidence angle; pole – coordinates are determined from the directions of the high-temperature primary and secondary NRM components. Poles 9 and 10 [*Khramov et al.,* 1997] were derived from structures similar in location and age to the Monchegorsk intrusion. Pole 11 – average pole of 9 determinations for Kola Peninsula and Karelia, its average age 2448 Ma [*Ein and Sokolov,* 2000; *Elming et al.,* 1993; *Khramov et al.,* 1997; *Krasnova and Gooskova,* 1995; *Mertanen,* 1995; *Mertanen et. al.,* 1989, 1999].

sionally) polarities in the secondary component indicate that the process of its acquisition was long. The preservation of the primary NRM component in several pyrrhotite-bearing samples (Table 5) indicates an irregularity of this process. The secondary component exhibits properties of the TRM, KRM and CRM (Table 2), indicating its association with a later (1.9–2 Ga) heating to very high temperatures and a possible formation of new magnetic minerals under these conditions; this resulted in the acquisition of the crystallization magnetization (see above). As seen from position of the pole associated with the secondary NRM component with respect to the APWP of the Baltic Shield, the tectonic movements are likely to have preceded the acquisition of the ancient secondary NRM component. It is conceivable that the northward displacement of the Monchegorsk intrusion pole toward the poles of remagnetization (1.9–2 Ga) is related to an incomplete destruction of the high-temperature remagnetization at 1.9–2 Ga, because the range of T_d values in newly formed magnetite grains is close to that of grains formed at the stage of the intrusion cooling. This must adversely affect quality of the paleovariation record.

B. **The Kivakka intrusion.** Two NRM components are identified in the process of thermal demagnetization (Figure 11b): a high-temperature component A has a re-

Table 6. Paleomagnetic directions and coordinates of poles of the NRM components of the Kivakka intrusion

NRM Component	no.	Dg/s	Ig/s	K	α_{95}	Polar	Pole	
							Latitude	Longitude
A_{1g}	17	134°	20°	11.6	10°	R	5.9°N	258.4°E
A_{1s}	17	138.7°	55.6°	11.6	10°	R	17.8°S	247°
A_{1s}(D-30)	17	108.7°	55.6°			R	26.2°S	271.5°
A_{2g}	10	130.3°	60.9	26.3	7.3°	R	25.3°S	249.9°E
B_g	47	340°	45°	20.6	4.5°	N	47.7°N	240.1°E
Sum of mean (A_1+B)g	2	88.5°	57°					
Sum of mean (A_2+B)g	2	22.2	78°					
Mean pole	9				12.2	N	23°S	273°E

Note: NRM component – high-temperature component, A_1 – high-temperature, primary, prefolded; A_2 – high-temperature, afterfolded or synfolded, its indication temperature is usually slightly below A_1 component; B – secondary component, result of the second heating of the intrusion approximately 1.9 Ga ago, maximum temperature at which it is identified varies from 500°C to 580°C; no. – number of samples; D, I – paleomagnetic declination and inclination, respectively; g, s – geographic and stratigraphic coordinates; K – precision parameter; α_{95} – confidence angle; Polar – magnetic polarity; N – normal; R – reversed; Pole – coordinates of the north paleomagnetic pole; Mean pole – mean coordinates of the north paleomagnetic pole of the Kola Peninsula, Karelia and Finland (mean for 9 definitions of different authors, average age 2448 Ma), [*Pechersky et al.,* 2002].

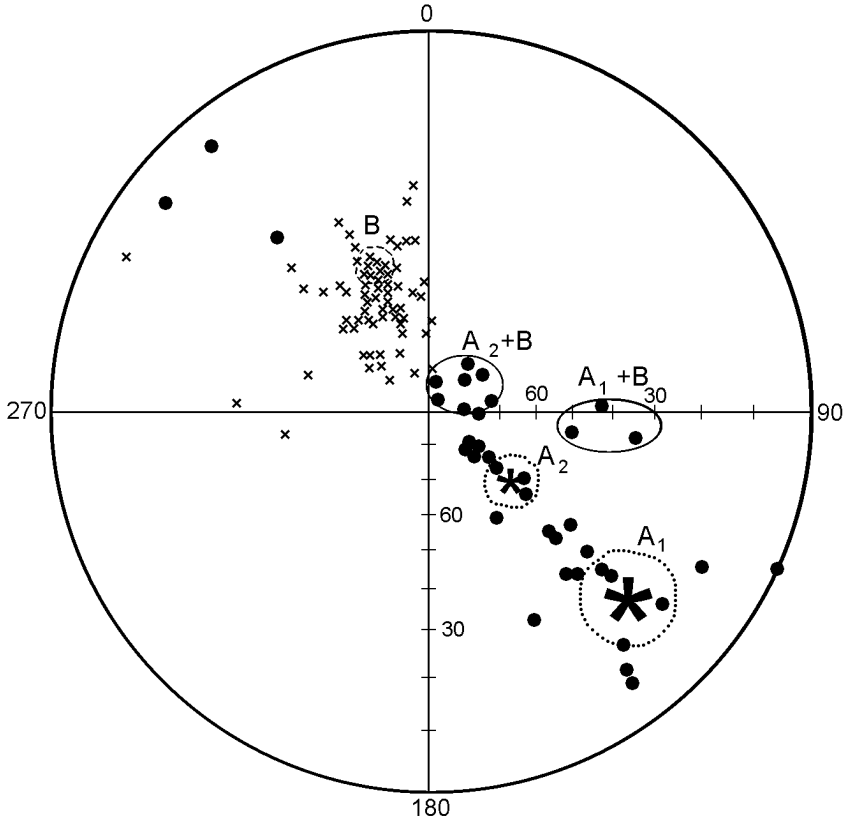

Figure 12. Kivakka. Stereogram of paleomagnetic directions of NRM components detected during the thermal demagnetization and a component analysis in the geographic coordinates. Circles show components A (the second quadrant and low inclinations – component A_1, high inclinations – component A_2, acquired after tilting of the Kivakka block), crosses show component B. Circles in the 4 quadrant are high-temperature components, possibly normal polarity A, a typical component B is distinguished in these samples, two of these points are included in calculation of the mean direction of A_1, for which purpose their polarity was changed for a reversal. "Jumped off" crosses refer to component B as an ordinary high-temperature reverse polarity component A is detected in the same samples. The dotted line show areas of points where components A and B are not separated.

versed polarity (declination in the second quadrant, a positive inclination, polarity is adopted according to [*Elming et al.,* 1993; *Khramov et al.,* 1997]); the component B has a normal polarity (declination in the fourth quadrant, a positive inclination). Components A and B on the stereogram (Figure 12) in the geographic coordinates form a swarm of points where three groups can be distinguished: 1) the second quadrant, positive and occasionally negative low and intermediate inclinations (circles on Figure 12), here are only high-temperature NRM components of the reverse polarity, a component A_1; 2) the second quadrant, high positive inclinations, a high-temperature component A_2; 3) the fourth quadrant, high and intermediate positive inclinations (crosses on Figure 12), a component B, in samples containing both components A and B, the latter is isolated at temperatures below temperature that indicates component A, but only one component B is quite often is recorded at a temperature up to 580°C (Figure 11b).

Average paleomagnetic directions and coordinates of poles are defined for three mentioned above groups (Table 6). If elements of the layered intrusion bedding are taken into consideration, i.e. to adopt its original bedding as horizontal, coordinates of the Kivakka paleomagnetic pole (component A_1) in the stratigraphic coordinates are close to mean coordinates of the pole of a similar average age (Table 6, Figure 13). If the Kivakka block is turned around the vertical axis through 30°, they will coincide (Table 6, Figure 13). This is the evidence, first of all, in favor of a close to the time of cooling of the Kivakka intrusion component A_1, and second, of the tectonic origin of divergence of the Kivakka pole and the mean pole of the region of the same age. The next important fact is the practical coincidence of the paleomagnetic directions and, consequently, of the paleomagnetic poles of the A_1 component *in the stratigraphic coordinates* and of A_2 component *in the geographic coordinates*. According to the geological data the Kivakka block was tilted prior to intrusion of the dolerite dikes, which are dated to the same magmatic phase to which the Kivakka intrusion

belongs. Thus, tilting of the Kivakka intrusion occurred at the stage of its cooling at temperatures close and/or exceeding 500°C. The paleomagnetic fixing of this event is also evidence about acquisition of A_1 component and about variation of its direction at the stage of cooling of the Kivakka intrusion, i.e. the A_1 component from the paleomagnetic point of view is primary. The block turned around the vertical axis after the A_2 component has been acquired (as it coincides with the A_1 component).

The paleomagnetic pole of the B component almost falls on APWP of Baltic shield close to 1.9 Ga (Figure 13). Most probably, occurrence of the B component is associated with the secondary heating of the block during the Svecofennian tectonomagmatic activation. No appreciable secondary alterations in the Kivakka intrusion rocks in the area in question are found; samples where component A or B prevails do now show any peculiarity. Therefore, it would be more logical to assume a pure effect of heating approximately to 400–500°C, when a part of the single-domain and pseudosingle-domain magnetic grains with the blocking temperatures below 500°C, which were formed, mainly, at the stage of the primary cooling of the intrusion, would acquire a new magnetization. The unblocking temperatures of such magnetization will be 500–550°C respectively (Figure 5). As this is practically the same ensemble of magnetic grains, it is impossible to fully divide components A and B by the thermal demagnetization and, depending on such division the component B or A and their indivisible sum with similar unblocking temperatures will prevail in the sample (Figure 11b). Thus, in case of the sum of components A_1+B declination is towards E-N-E and inclination is higher than for A_1 or B, in case of the sum of components A_2+B declination becomes more northern and inclination is close to a vertical (Figure 11b and 12, Table 6).

The components A_1 and A_2 are detected, as a rule, above 500°C, and frequently above 540–550°C (Figure 11b). Some samples are completely remagnetized and this is in agreement with heating of a portion of minerals up to the Curie points (quite often T_c = 525–540°C, see Table 3). Thus, for example, intervals between 358 m and 370 m, between 421 m and 500 m, between 665 m and 746 m, between 1030 m and 1132 m were remagnetized completely (Figure 14a,b).

C. **The Bushveld intrusion.** According to behavior of the NRM during of thermal demagnetization all samples can be divided into 4 types: 1) tablelike shape, up to $T \geq$550°C the NRM intensity does not change practically and afterwards it drops abruptly (21 samples), 2) parabolic Q-type (11 samples), 3) linear decrease, L-type (8 samples), 4) majority of samples show increase of magnetization during of thermal demagnetization; this increase is smooth (P-type of thermal demagnetization curve show (30 samples) and/or sharp (45 samples), which is connected with presence of two NRM components of a normal and reversed polarity. The NRM component with a negative inclination is identified in 119 samples; temperature of its detection is always below the NRM component with a positive inclination, the latter is found in majority of samples (142), the samples with pyrrhotite (6) and low-magnetic samples (16). Declination was restored for both components according to a viscous magnetization. Due to reasons indicated in the "Methods"

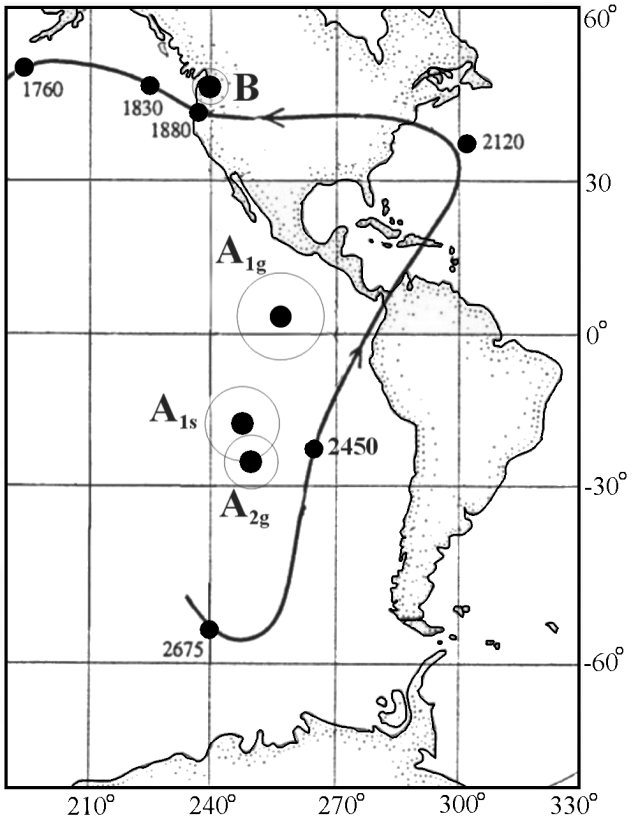

Figure 13. Position of the paleomagnetic poles of components A_1, A_2 (before and after tilting of the Kivakka block) and B relative to APWP of Fennoscandia [*Elming et al.,* 1993].

section a great scatter of the unit paleomagnetic directions occur (Figure 15). The average direction, however, does not differ practically from that obtained for samples selected from the natural outcrops in the western and northern parts of the Bushveld intrusion [*Hattingh,* 1986a; *Hattingh and Pauls,* 1994], both in the geographic and in the stratigraphic coordinates (Table 7).

The average bedding of the intrusion lamination in the region of well WP-16 with the dip azimuth 20°, dip angle 13.5°, was calculated according to data taken from [*Hattingh,* 1986a].

An ever greater scatter of directions is observed in the case of a intermediate-temperature component of the reverse polarity; its mean direction differs appreciably by inclination from the high-temperature component with the normal polarity in one system of coordinates (Table 7). It is possible to state that this is not a remagnetization affected by the field, which is close to the the present day field direction first, the inclination is notably more steep, second, and, more important – the mean declination is opposite to declination of the recent field. It should be noted that the paleomagnetic direction of the high-temperature component in the stratigraphic coordinates, and, consequently, coordinates of

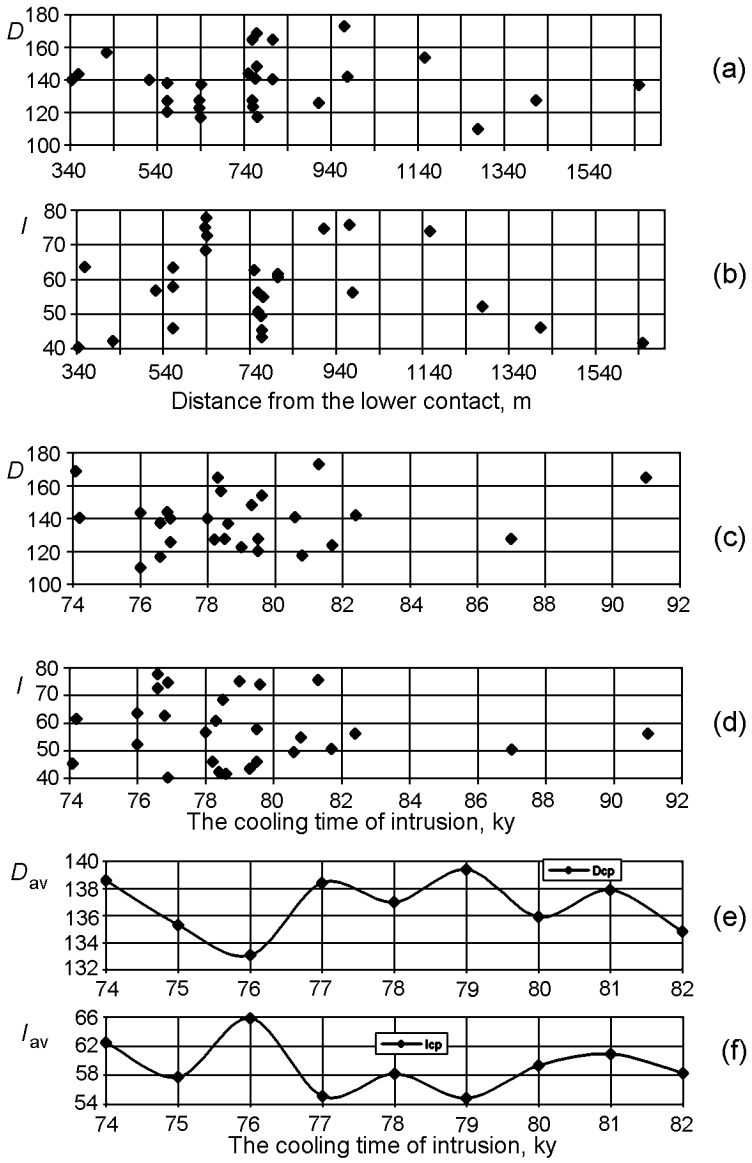

Figure 14. Kivakka. Distribution of declination and inclination of components A_1 and A_2 over the section (a, b) and in time (c, d). a, b – data of the component analysis, the range close to the Curie point of the main magnetic mineral in the sample. c, d – direction of NRM close to Curie point. e, f – averaged data, averaging interval is 3 thousand years, averaging step is 1 thousand years. Time is given from the moment of emplacement of intrusion. Direction of component A_1 is in the stratigraphic coordinates; A_2 is in the geographic coordinates.

the paleomagnetic pole do not differ practically from the paleomagnetic direction and coordinates of the pole of the intermediate-temperature component in the geographic coordinates (Table 7). It is likely that the tectonic tilting has occurred at the stage of cooling of the intrusion and, consequently, the normal polarity component was acquired before tilting, and the reverse polarity component was acquired after the intrusion was tilted. The situation is similar to that of the Kivakka intrusion (see above).

Following [*Hattingh,* 1986a, 1986b, 1989] we adopt a normal polarity for the NRM high-temperature component and the fact that this component is associated with thin inclusions of titanomagnetite-magnetite in plagioclases and pyroxenes, formed during their exsolution, and was acquired at the time of cooling of the Bushveld intrusion from the temperature exceeding the magnetite Curie point.

Table 7. Paleomagnetic directions and the pole of the Bushveld intrusion

NRM	no.	D	I	K	α_{95}	paleopole	
						Latitude	Longitude
A_{Ng}	101	2°	81°	10.1	4.4°	8.1°S	21.1°E
A_{Ns}	101	12.5°	68.3°	10.1	4.4°	12°N	35.4°E
A_{Rg}	58	182°	−66°	5	8.2°	16°N	28.9°E
A_{Rs}	58	188°	−52.9°	5	8.2°	30.3°N	35.2°E
A	32	336.1°	82°	58	3.4°	11.2°S	28.1°E
B	32	357.8°	70.9°	80	2.8°	9.2°N	27.3°E
North	12				15	1.6°N	22.3°E

Note: NRM — natural remanent magnetization component, A_N – normal polarity high-temperature component, A_R – reverse polarity intermediate-temperature component, our results; g – geographic coordinates, s – stratigraphic coordinates; A, B, and North – a stable NRM component, identified in samples from outcrops of the Main Zone in the western (A, B) and in the northern part of the Bushveld intrusion as a result of an an AF demagnetization, in the geographic (A, North) and stratigraphic (B) coordinates [*Hattingh,* 1986a; *Hattingh and Pauls,* 1994].

Thermal Physical Estimation of the Cooling Process of Intrusions

In order to analyze variations of the geomagnetic field, recorded in the cooling process of the intrusion, it is necessary to determine the cooling time within the range of blocking temperatures and the total duration of cooling. To model the dynamics of temperature variation after the emplacement of the intrusive body and estimate these time intervals, we examined the nonstationary problem of heat conduction (with regard for crystallization of the intruded melt).

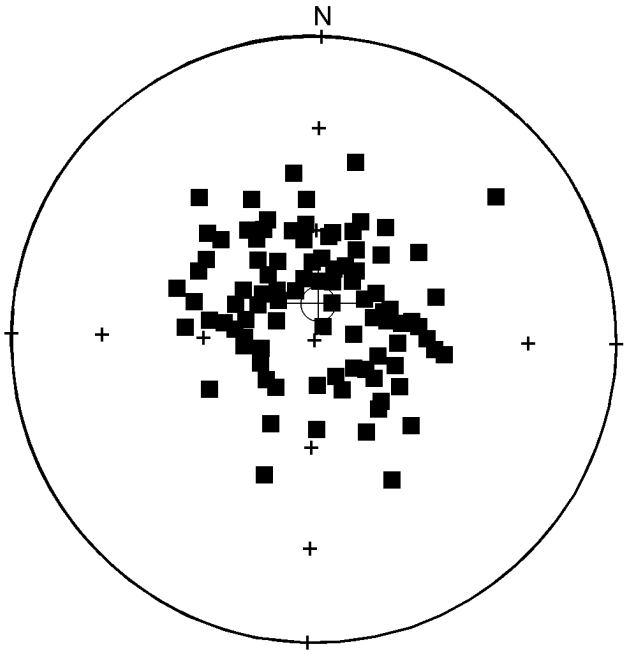

Figure 15. Stereogram of directions of the high-temperature NRM component of the specimens from the core of well WP-16. Bushweld. Declinations were determined with aid of the viscous remanent magnetization (difference vector $J_{n20} - J_{n200,300}$).

We assume that the emplacement of the intrusive body was relatively rapid (as compared with the characteristic time of cooling). Then, the heat exchange during the emplacement can be neglected, and the temperature of the surrounding rocks at the initial time can be assumed to be the same at the upper and lower boundaries of the intrusion (this temperature is defined by the undisturbed geotherm). The temperature of surrounding rocks at the time of emplacement of the intrusion has to be estimated. The resent geothermal gradient in the region of the Kola ultradeep borehole which is about 20° km^{-1} is known. The steady (balanced) geothermal gradient is determined by thermophysical properties of the environment and, accordingly, must not differ notably from the recent gradient. According to [*Berk et al.,* 1980], it is unlikely that the ancient continental crust was affected exclusively by high geothermal gradients (except for a rather narrow accretion belts). Based on similarity of behavior of the ancient continental fragments with the regime of more recent epochs, these authors come to a conclusion that the equilibrium geothermal gradients in the Archean time did not exceed, usually, 25° km^{-1}. According to E. V. Koptev-Dvornikov (verbal information, 2003), the best agreement (on energy- and mass exchange) of the model results with those observed, during modeling the Kivakka intrusion crystallization, can be obtained if temperature of the surrounding rocks at the depth of emplacement of the intrusion is adopted to be about 200°C. In accordance with the above and considering the depth of emplacement of this intrusion about 10 km, the geothermal gradient becomes equal to 20° km^{-1}. This gradient was adopted for all intrusions under study.

The problem of cooling of the intrusion can be divided into two stages. First, we estimated the cooling time of the intruded melt at the time of emplacement of the intrusion (about 1400°C) to the solidus temperature (about 1200°C) and obtained the temperature distribution in the intrusion and surrounding rocks at the time of complete solidification. To do this, we solved the Stefan problem. Two phases were discussed and in each phase the temperature satisfies the

heat conduction equation:

$$\rho C_s(T)\frac{\partial T}{\partial t} = \sum_{p=1}^{N}\frac{\partial}{\partial t}\left(k_s\frac{\partial T}{\partial x_p}\right) , \qquad (1)$$

where T – is the temperature; t – is the time; x_p – is the coordinate, p takes the values from 1 to N (dimension of the problem); ρ – is the density, C – is the thermal capacity at a constant pressure, k – is the coefficient of thermal conductivity, $s = 1$ (solid phase), $s = 2$ (melt). The temperature is constant $T = T^*$ (crystallization temperature) at the phase interface, the heat flows are discontinuous and their difference is equal to $\lambda\mathbf{v}$, where λ – is the melting heat, $\mathbf{v}$ – is the velocity vector of the phase interface.

It is rather difficult to follow the movement of the phase interface for a three-dimensional case. Aside of this, the task of this work is to model the cooling within the range of temperatures which is much lower than the solidus temperature (below 600°C). Therefore, to solve the Stefan problem we use the approach of [*Dudarev et al.,* 1972; *Tikhonov and Samarsky,* 1966], which being relatively simple, allows with an adequate accuracy for our purpose to describe the thermal exchange during crystallization. We write equation (1) as follows:

$$\rho(C(T) + \lambda\delta(T - T^*))\frac{\partial T}{\partial t} = \sum_{p=1}^{3}\frac{\partial}{\partial t}\left(k_s\frac{\partial T}{\partial x_p}\right) , \qquad (2)$$

where $\delta(T - T^*)$ denotes δ-function, the thermal capacity function $C(T)$ is given by:

$$C(T) = \begin{cases} C_1, T < T^* \\ C_2, T > T^* \end{cases} ,$$

in a similar way it is possible to write down also for the coefficient of thermal conductivity. Further, a function of effective thermal capacity is introduced

$$C_{eff}(T) = C(T) + \lambda\delta(T - T^*) ,$$

Then we have the following equation for T

$$\rho C_{eff}(T)\frac{\partial T}{\partial t} = \sum_{p=1}^{3}\frac{\partial}{\partial t}\left(k_s\frac{\partial T}{\partial x_p}\right) . \qquad (2^*)$$

When all the points of the system have cooled below the crystallization temperature T^*, equation (2) becomes an ordinary equation of the thermal conductivity for an inhomogeneous medium.

The finite difference method was used to solve the equation. With the computational solution the δ-function is substituted in the rough for the function $\delta(T - T^*, \Delta)$, which differs from the 0 only in the interval $(T^* - \Delta, T^* + \Delta)$ and satisfies the normality condition of 1.

Calculations were made for different values of the thermal physical parameters, geometric characteristics and dimensions of bodies, depth of their formation, which are given in the geological section.

Below we give the calculation results for every intrusive body.

A. **The Monchegorsk intrusion.** The geometry of the intrusive body (length is ≈10 km, thickness is ≈3 km) allows examining a one-dimensional problem (depending on the depth only) for the sampling area 375 m thick. Values of the thermal and physical parameters were taken from [*Dudarev et al.,* 1972; *Thermal field of Europe,* 1982; *Turcotte and Schubert,* 1985]. The thermal conductivity for surrounding rocks is $k = 3.05$ W m^{-1} K^{-1}, thermal capacity is $C = 1150$ J kg^{-1} K^{-1}, density is $\rho = 2.75$ kg m^{-3}. The melting heat for the intrusion rocks is $\lambda = 350$ kJ kg^{-1}, the thermal conductivity is $k = 4.35$ W m^{-1} K^{-1}, the thermal capacity is $C = 1005$ J kg^{-1} K^{-1}, density is $\rho = 3.31$ kg m^{-3}. With the computational solution the step in spatial coordinate was 100 m, and the step in time was 100 years.

According to these calculations it takes approximately 25000 years for the melt to solidify completely. As is evident from the temperature versus time curve (Figure 16) the initial difference in temperature between parts of the section under study (about 150°) rapidly disappears. Thus, the difference between the times at which the upper and lower parts of the section attain the Curie point of magnetite (580°C) is ≈12,000 years. The entire section attains a blocking temperature of 480°C almost simultaneously as is indicated by the coinciding curves $T(t)$ (Figure 16). The period between the times when the section assumes temperatures of 580°C and 480°C, is about 160,000 years. During further cooling, the curves once again diverge; the direction of the temperature gradient becomes normal (to the surface) and tends with time to the undisturbed direction. The time of cooling of the lower part of the intrusion to the undisturbed temperature (250°C) is estimated as 15–20 Myr.

It is seen from calculations that the surrounding rocks are heated; those adjacent to the intrusion are heated up to 550–650°C, and those which are 2 km below the intrusion foot are heated up to 450°C.

The cooling velocity changes appreciably: at 580°C it varies from 1100°/Myr at the contact to 1170°/Myr at a distance of 400 m from the contact, at 480°C it varies from 400°/Myr at the contact to 450°/Myr at a distance of 400 m from the contact (Figure 17).

B. **The Kivakka intrusion.** A tapered shape of this intrusion has required a solution of a three-dimensional problem. On the basis of data presented by E. V. Koptev-Dvornikov and colleagues the following thermal physical characteristics were adopted for modeling. The surrounding rocks: the thermal conductivity $k = 2.51$ W m^{-1} K^{-1}, the thermal capacity $C = 1050$ J kg^{-1} K^{-1}, the density $\rho = 2.65$ kg m^{-3}. The thermal and physical properties of the intrusion proper were determined on the basis of data about its composition, assuming the additive model. The average weighted composition of the Kivakka intrusion is as follows (mole fractions): plagioclase – 31.9%, clinopyroxene – 11.7%, orthopyroxene 23.2%, olivine – 32.6%, ilmenite 0.6%. Data on the thermal conductivity, thermal capacity and melting heat of minerals of the were presented by S. V. Bolikhovskaya (verbal presentation, 2003). Finally the following values of parameters were adopted for our model: $k = 3.52$ W m^{-1} K^{-1}, the thermal capacity $C = 1110$ J kg^{-1} K^{-1}, the density $\rho = 3.22$ kg m^{-3}, the melting heat $\lambda = 550$ kJ kg^{-1}.

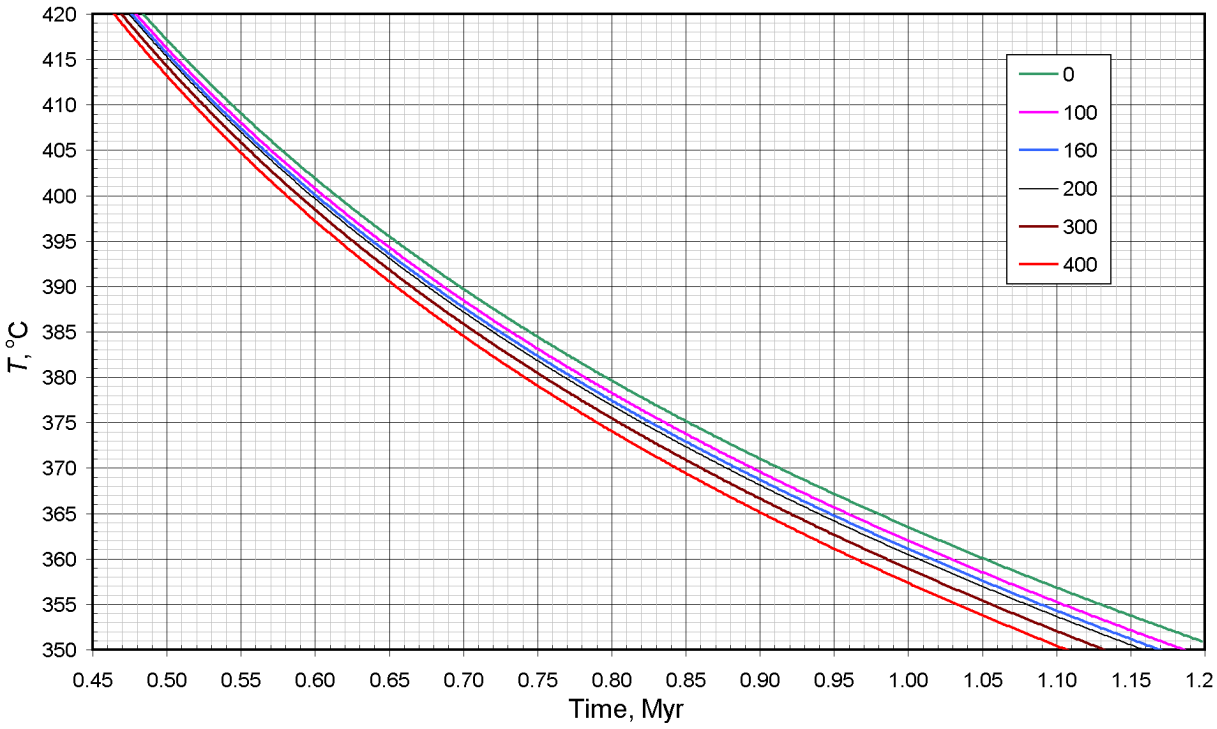

Figure 16. Temperature (T) versus Monchegorsk intrusion cooling time at different parts of the section (at the contact, 160, 200 and 400 m from the contact). a, b, c – different time ranges.

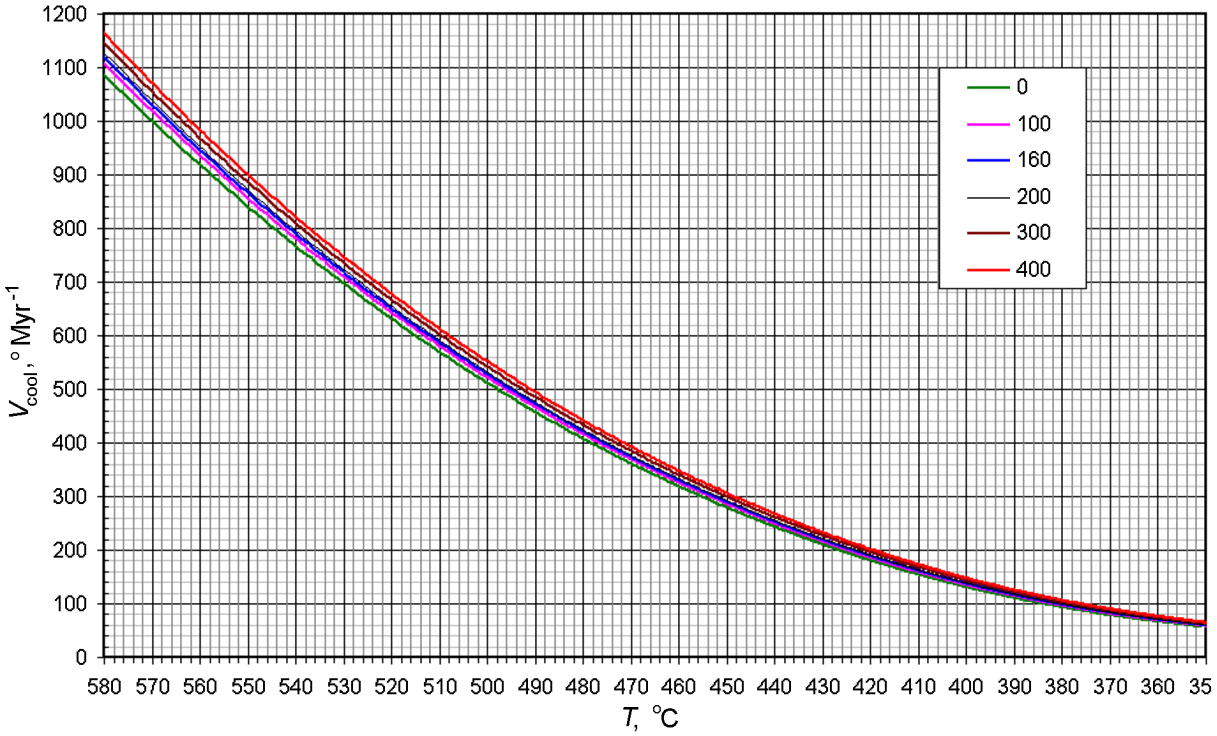

Figure 17. Calculated velocity of cooling of Monchegorsk intrusion versus temperature. Symbols are the same as in Figure 16.

As is evident from Figure 18, cooling of the intrusion lasted for about 25,000 years within the temperature range from 580°C to 500°C. As the intrusion approached the upper contact it cooled rapidly as seen by the shift of the $T(t)$ isolines to the left, beginning approximately from 1200 m (Figure 18). The cooling velocity of intrusion at different points of the section and at different temperatures changes within a relatively narrow range: from 4.5° to 5° in one thousand years at 575°C and from 3° to 3.5° in one thousand years at 515°C (Figure 19).

C. **The Bushveld intrusion.** Since dimensions of the intrusion are quite large (approximately 480×80 km), and WP-16 well is located near the side boundary, it is reasonable to examine a two-dimensional model of cooling, i.e. a vertical section crossing the well region. The shape of the intrusion is a flat-laying truncated ellipsis with the overlying rocks and whose maximum dip angle on the lateral contact is 20°.

When selecting values of the thermal physical parameters for the model of cooling we were based on information about structure and rocks of the intrusion and the host rocks offered by [*Eales and Cawthorn,* 1996; *Sharkov,* 1980; *Wager and Brown,* 1970] and the reference data. We adopted the following thermal physical characteristics for modeling. For the host rocks: the thermal conductivity $k = 2.1$ W m^{-1} K^{-1}, the thermal capacity $C = 880$ J kg^{-1} K^{-1}, the melting heat $\lambda = 285$ kJ kg^{-1} – for the overlying rocks which were submelting, the density $\rho = 2.6$ kg m^{-3}. The thermal physical properties for the intrusion proper were determined on the basis of data about its composition and the additive model. The average weighted composition of the Bushveld intrusion was adopted as follows on the basis of data taken from the literature mentioned above: plagioclase – 47%, clinopyroxene – 53% (mole fractions). As a result the following values of parameters were adopted: the thermal conductivity $k = 3.19$ W m^{-1} K^{-1}, the thermal capacity $C = 1117$ J kg^{-1}K^{-1}, the melting heat $\lambda = 472$ kJ kg^{-1}. The value for density $\rho = 2.9$ kg m^{-3} was adopted on the basis of averaging data on the core from WP-16 well (data of B. N. Pisakin, 2003).

According to the geological and experimental data (see Brief geological description), the intrusion roof at the time of emplacement was at a depth of about 3 km. The temperature of the intruded melt has bee adopted about 1400°C, the crystallization temperature has been taken as 1200°C. We have taken into consideration the fact when modeling that the roof over the intrusion was rising at the time of emplacement (the value of 800 m was adopted as no precise data is available) and afterwards this uplift eroded. Though there are evidences that the intrusion could have taken place in several stages (see Brief geological description) we considered a single-act intrusion in a simplified way as no specific information about the number of these stages, their sequence and volume is available, and we are mostly interested in the stage of cooling of the intrusion at a temperature 600°C.

It follows from modeling of cooling of the intrusion in the zone corresponding to the well (Figures 20, 21) that the higher the sampling points are in the bore hole, the lower their temperature at the similar times is (Figure 20). This result needs a certain explanation as at a glance an inverse dependence must be observed; points from lower levels are most close to the inner layers of the intrusion and, consequently, they must cool slowly. In fact, first lower points of the well (which are closer to the lower boundary of the intrusion) cool rapidly, whereas the temperature gradient here has a reverse direction (with regards to the normal). Then, after some time (which depends on properties of the system) of the beginning of cooling, the temperature alonge the well-section equalizes practically and at a further cooling the curves again diverge and direction of the gradient becomes normal, and with time it tends to the undisturbed direction. In this case the reason of a rather rapid (approximately 0.5 Myr) overturn of the gradient is the influence of a relatively close located cold upper boundary – the day surface where temperature is adopted to be constant and equal to 0°C. As a result by the time the system has cooled to 580°C, i.e. to the beginning of the paleomagnetic record, a temperature rise with depth is observed everywhere in the area under study (in intrusion and in the host rocks).

The cooling velocity (Figure 21) varies from 580°C to 480°C, accordingly, from 290–330°/Myr to 200–230°/Myr, i.e. the velocity changes insignificantly along the section.

Paleomagnetic Record of Variations of the Geomagnetic Field During Cooling of Intrusions, Wavelet Analysis Results

Let us examine two variants of the record of variations described in the introduction: 1) record for the time the Curie point is "running" along the section and 2) record in every sample from the result of the detailed thermal demagnetization.

Because of finite intervals of the thermal demagnetization step (3°–5°) in the first and second variants we do not obtain a continuous record of the field, but we obtain difference magnetization vectors between adjacent temperatures. We obtain a certain averaged pattern of behavior of the remanent magnetization vector. In the first variant of the paleomagnetic record we adopted the magnetization density to be constant in the three-degree intervals, though the spectrum of blocking temperatures of the remanent magnetization may be non-homogeneous and quite narrow.

In order to tie the obtained paleomagnetic results to the time in the second variant of the record it is necessary first to go from unblocking temperatures to the NRM blocking temperatures in the process of cooling of intrusions. To convert unblocking temperatures during of thermal demagnetization into the intrusion cooling temperature, we assume, that the magnetic grain state is sufficiently close to the single-domain state, in the temperature range under study, then blocking temperatures of the magnetic minerals will correspond to the intrusion cooling temperature at the sampling point. Should the multidomain grains play an appreciable role, their magnetization will take place near the Curie point. The NRM carriers behave as the single-domain and pseudosingle-domain particles at $T_d > 530°$ C, as it was shown above.

The cooling velocity V_{cool}, was determined for every unblocking temperature, obtained in the course of thermal de-

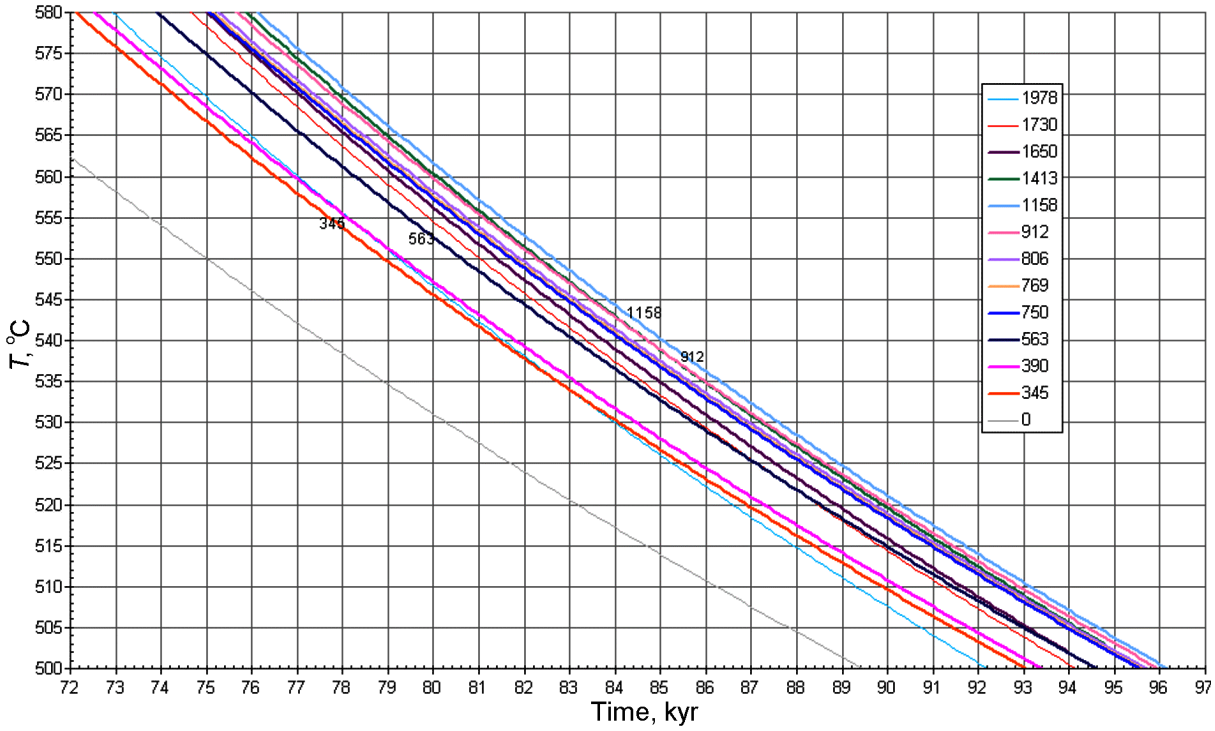

Figure 18. Temperature at different points of the section versus time of cooling of the Kivakka intrusion. Time is given from the moment of magma intrusion. Numbers in the figure show thickness in meters from the lower contact to the given point of the section.

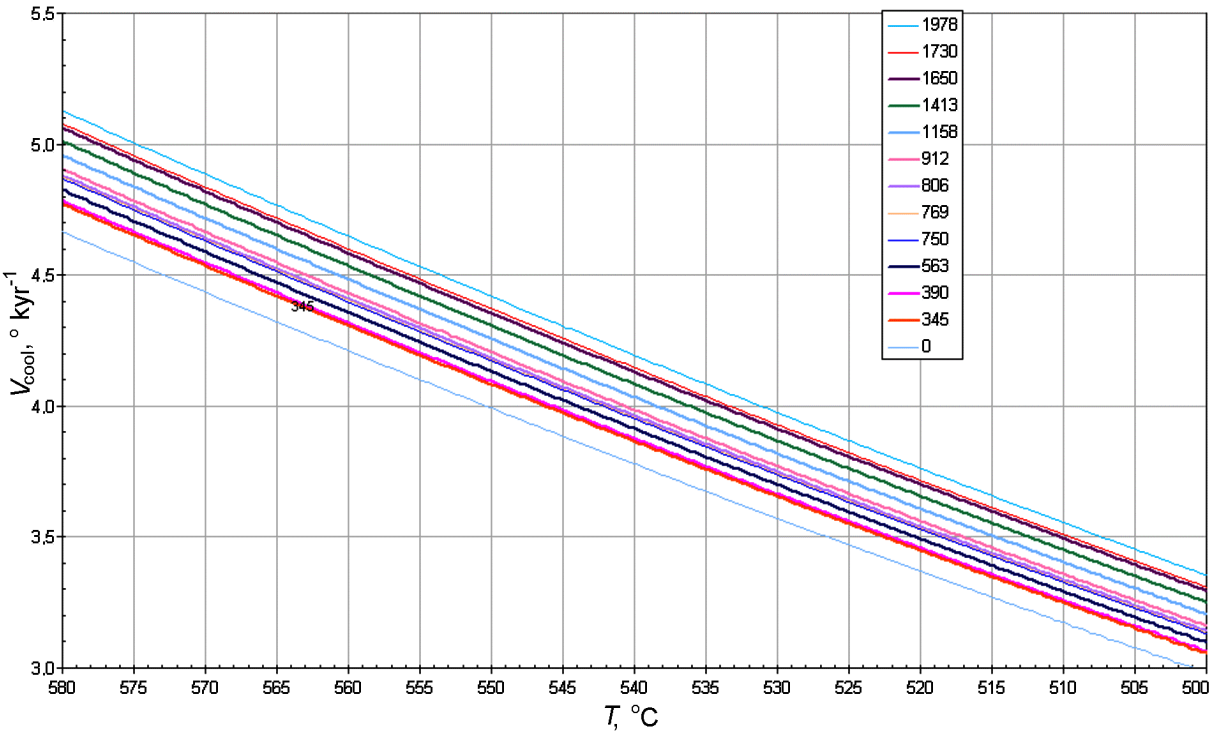

Figure 19. Velocity of cooling of the Kivakka intrusion versus temperature. Symbols are the same as in Figure 18.

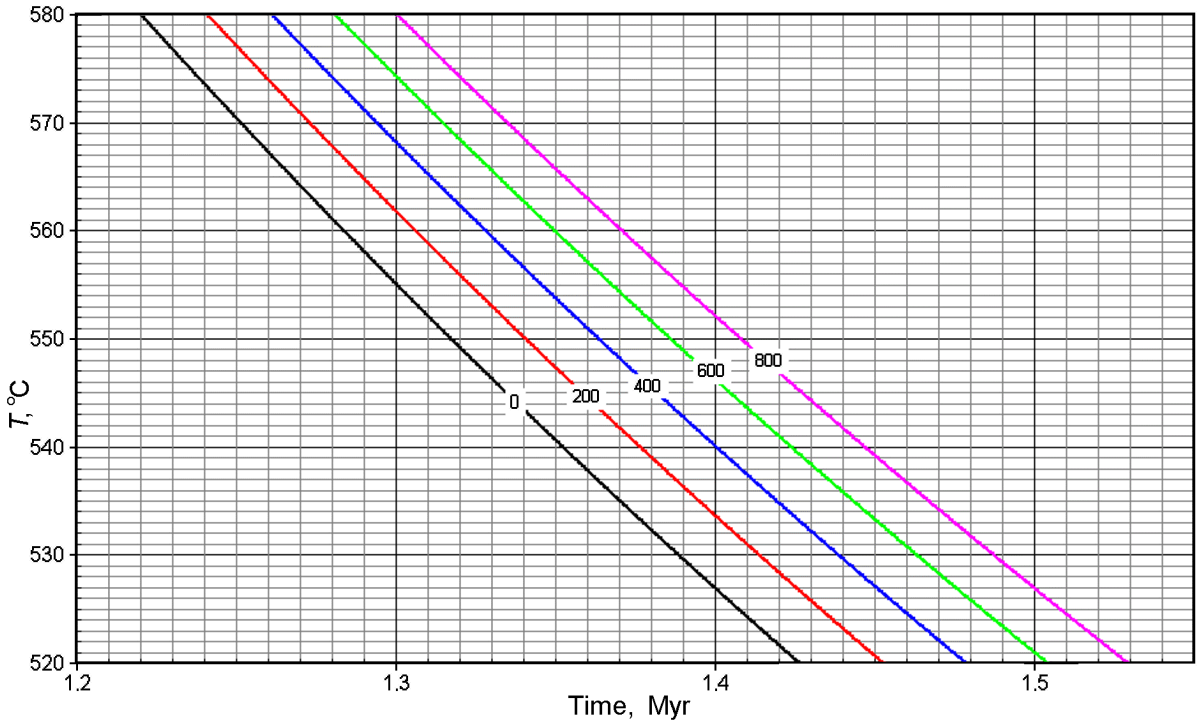

Figure 20. Calculated temperature versus time of cooling of the Bushveld intrusion. Numbers near the lines indicate depth in meters from the well mouth (0) top-down.

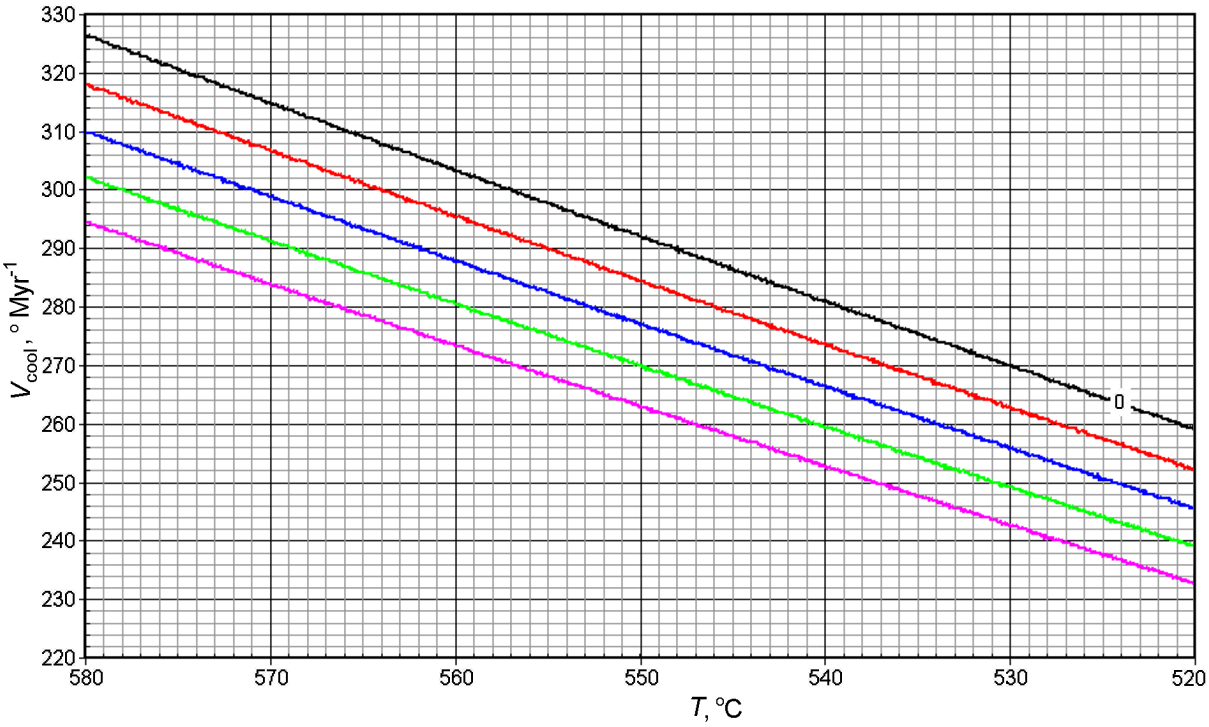

Figure 21. Velocity of cooling of the Bushveld intrusion versus temperature. Symbols are the same as in Figure 20.

magnetization, according to data of Figure 17, 19, 21, and, afterwards the NRM blocking temperature T_b in the course of cooling of the intrusion was found with the help of a transparency $T_b(T_d, V_{\text{cool}})$ (Figure 5). The Curie points of the samples under study vary appreciably from 525°C to 580°C (see petromagnetic section). For such cases Figure 5b is used, where relative values of T_d/T_c and T_b/T_c, are given which can help to define T_b easily.

The next step is the transition from temperatures to the cooling time for which purpose the $T(t)$ dependences are used for various points of the section (Figure 16, 18, 20).

Thus, we obtain a pattern of behavior of the NRM direction (D, I) for every sample, for each five-degree and/or three-degree range depending on the unblocking temperature (heating in the laboratory) calculated blocking temperature and the estimated relative cooling time. To conduct a further analysis, the samples were selected where we can judge with a greater confidence about the record of behavior of the geomagnetic field direction. The main criterion is proximity of the NRM components detected in a certain temperature range to the average paleomagnetic direction throughout the section, which is isolated above 540°C.

In the first variant of the paleomagnetic record conversion of T_d into T_b becomes simple as $T_b = T_d$ near the Curie point. However, errors in estimation of the Curie point, cooling time have a more appreciable effect, and, consequently, the scatter of determinations increases (see below); besides, the cooling time is by three degrees comparable with the Curie temperature "running" along the section, for example, in the case of a detailed sampling in the Monchegorsk intrusion (see below).

Time series wavelet analysis. The initial or basic data are a sequence of couples of numbers $\{t_j, z_j, \}$, $J = 1, \ldots,$ N where the first are the time marks, the second is the angle of orientation of the paleomagnetic field component. The times marks t_j form a nonuniform mesh of values, characterized by presence of the closeness intervals (a very frequent measurement), and by sufficiently long intervals of absence of data. The measured values of z_j are characterized by a high noise of measurements; this can be judged by large amplitude of their variations in the intervals of concentration the time marks. To proceed with the analysis of data it is necessary to pass to a uniform time step, for which purpose the initial (nonuniform) data about each time point is to be smoothed. First of all a quantization time interval must be specified. A nuclear averaging method of Nadaray-Watson [*Hardle,* 1989] was employed to obtain values of the uniformly numbered signal $x(\tau)$:

$$x(\tau) = W_1(\tau|H)/W_0(\tau|H) \tag{3}$$

where:

$$\begin{aligned} W_1(\tau|H) &= \sum_{j=1}^{N} z_j \cdot \varphi\big((t_j - \tau)/H\big), \\ W_0(\tau|H) &= \sum_{j=1}^{N} \varphi\big((t_j - \tau)/H\big) \ , \end{aligned} \tag{4}$$

where, in its turn:

$$\varphi(s) = \exp(-s^2) \tag{5}$$

– is the Gaussian averaging kernel, and, $H > 0$ – is the parameter of the averaging kernel width. By implication of formulas (3) and (4), the initial measurements (t_j, z_j) for which the time marks satisfy the condition $|\ t_j - \tau| \le H$, make the main contribution into the average value $x(\tau)$. The choice of the parameter H follows herefrom; it must be equal to a half of the selected time step. While implementing this method of transition to the uniformly numbered signal a situation may occur when a direct use of formula (3) will lead to an uncertain type of zero division (in the case when the point τ is inside a sufficiently long period when measurements are not available). In this case it is necessary to increase the averaging parameter H so that the averaging kernel would be able to reach from the point τ the nearest time marks t_j. The averaging program envisages this possibility and begins to increase H gradually in the case if $|W_0(\tau|H)| \le 10^{-6}$ – till this inequality does not change for a reverse and, thereby, the zero division situation is eliminated.

For a further application of the wavelet analysis, removal of the low-frequency trends is a useful operation to avoid the fringe effects, which occur in case of sufficiently strong low-frequency variations of the signal. After a number of trials, we have selected a polynomial of the 3-rd order. Further we have taken a difference between the base curve and the smoothing result and a wavelet diagram was drawn for this difference. The smaller radius of the sliding time slot of the polynomial smoothing is the boldly small-scale (high-frequency) peculiarities of the signal behavior seen.

Let $x(t)$ – is the times series being analyzed. We are interested in its time-and-frequency structure. A continuous wavelet analysis is the most sensitive tool for the purpose [*Chui,* 1992; *Daubechies,* 1992; *Mallat,* 1998]. Let $\psi(t)$ – is a certain function satisfying the admissibility condition: $\int_{-\infty}^{+\infty} \psi(t)dt = 0$ and the normality condition: $\int_{-\infty}^{+\infty} |\psi(t)|^2 dt = 1$. A value which depends on two parameters (t, a), $a > 0$ is called a continuous wavelet transform:

$$\begin{aligned} Wx(t,a) &= \frac{1}{\sqrt{a}} \int_{-\infty}^{+\infty} x(s) \cdot \psi\left(\frac{s-t}{a}\right) ds \\ &= \sqrt{a} \int_{-\infty}^{+\infty} x(t + av) \cdot \psi(v) dv \ . \end{aligned} \tag{6}$$

Here t – is the time point, $a > 0$ – is the scale parameter, which we will further give a more usual term as "period" or "rhythm". The value (6) reflects behavior of the signal under study about a point t with a typical period of variations a. It is reasonable that the value (6) depends greatly on the choice of the function $\psi(t)$. Further we will use the so-called Morlet wavelet or a complex-valued modulated Gaussian:

$$\psi(t) = \frac{1}{\pi^{1/4}} \exp(-t^2/2 - i\pi t) \ . \quad (7)$$

This wavelet is adapted best of all for distinguishing short-lived harmonic peaks (trains) and has certain optimality properties in the search of a compromise between the frequency and time resolution (yielding the so-called Heisenberg bound). Our primary aim is to construct a two-dimensional map of the module of value (6) ($|Wx(t,a)|$), which gives a pictorial presentation of the dynamics of the onset, evolution and disappearance of typical periods of the harmonic peaks of the signal under study.

A. **Monchegorsk intrusion.** Taking into consideration the above statements (see sections Petromagnetic measurements and Thermal demagnetization results), it is reasonable to examine variations of the field direction at temperatures above 530–540°C. We tried to reveal the long-period variations by the thermal demagnetization from 400°C to 580°C with the five-degree steps [*Pechersky et al.,* 2002, 2004]. Here we will discuss the results of the wavelet analysis data of demagnetization with the five-degree steps above 530°C along the 375 m section (samples were taken every 10 m at the average), and of a more detailed thermal demagnetization with the three degrees steps from 540°C to 580°C in the 100–161 m range of the section (samples were taken every 1–2 m). Both in the first and in the second variant of the record the amplitude of variations of declination reaches ±20°, and that of the inclination usually does not exceed ±10°.

The first variant of the record of paleovariations. Let us examine data of the component analysis and behavior of the direction at unblocking temperatures near the Curie points (Tables 8, 9). As has been stated above, two NRM composites of the opposite polarity are distinguished according to data of the component analysis (Table 5). Directions of the medium-temperature (R), and high-temperature (N) NRM components vary within the range usual for variations as is evident from the standard deviations, D=134.7°±14.2° and 297°±11.9°, I=23.2°±11.6° and −8.8°±6° respectively. Appreciable deviations from the average refer, first of all, to several samples with a relatively high magnetic susceptibility (evidently, due to an incomplete demagnetization of partially remagnetized multi-domain magnetic grains) and second, a paleomagnetic anomaly (excursion) with a complete change o the polarity (Table 9 and Figure 22) is fixed in the interval from 150 m and 157 m of the section in the direction of the high-temperature component; the NRM vector circumscribes a complicated, close to a circle movement during the excursions (Figure 23).

Data of the component analysis are no good for conversion of temperature into time as direction of the NRM components distinguished is averaged from a large temperature range (Table 8). Therefore, to convert temperatures into time the unblocking temperatures close to the Curie points were used (Table 9). These are temperatures of an appreciable sharp drop (more than 50%) of the NRM value in a three-to-five degrees step in the process of the thermal demagnetization. However, even in this case difference between the adjacent three-degrees points amounts to 3–4 thousand years, i.e. a certain smoothing takes place all the same. We refer the value of D, I to the point one degree above the Curie point and the smoothing interval will be less than two degrees.

As seen from Table 9, the NRM high-temperature component has only a normal polarity during its movement along the 375 m section, whereas in a more detailed case during the movement along the 61 m section the excursion is fixed between ∼128 and 130 thousand years. Its absence in the record of a long section is explained by the fact that the time intervals between the observation points are approximately 5 thousand years and our excursion of about 2 thousand years falls in one of these gaps.

The number of field direction points over a "long" section are insufficient for the wavelet analysis and therefore, only a "short" section, where an excursion is cut off, is analyzed. The record analyzed covers the time period from 116 to 155 thousand years from emplacement of the intrusion.

The time marks obtained for a nonuniform mesh of values and the values D, I proper are characterized by a high noise (Table 9, Figure 24). This is mainly due to inaccurate determination of the Curie points and the relevant temperatures and time. Therefore, a transition is made to a uniform time step, smoothing has been made and the trend has been extracted (Figure 24a,b). After these operations are made the wavelet diagram shows distinctly a 7–9 thousand years rhythm in declination and in inclination (Table 10); it can be traced over the entire record and reduces slightly with time. Aside of this, a series of splashes ranging from 4.5 to 1.7 thousand years, forming the chains, is fixed in the entire record (Figure 24b,f).

In the *second variant* let us examine only those samples where the record of behavior of the field direction is clearly seen (Table 11). A short section of record of the reverse polarity (Table 11) is insufficient for an independent analysis, therefore, its polarity was changed for a normal polarity and it was combined with the remaining record (Figure 25). It should be noted that the reverse polarity interval takes time between 160 kyr and 220 kyr from emplacement of the intrusion (Table 11, see also Introduction and Figure 1). Since there is no reverse polarity behind the fault (Figure 1, Table 11), the shift in time between the sections before and after the fault is approximately 100 kyr and these two sections differ in the paleomagnetic declination, their average values are: mo-1-42 – D=302.4° and mo-45-53 – D=290.3°. It is quite likely, that aside of the interval in time the upper block has turned counterclockwise relative to the lower block. The time for the upper part of the section is estimated from a single curve of the intrusion cooling (Figure 16) and then was increased by 100 kyr.

The excursion of the reverse magnetic polarity registered in the first variant of the record has not been fixed in the given variant of the record in none of the samples in the process of their detailed thermal demagnetization. It will be recalled that the thermal demagnetization step is three degrees that equals to 3–4 thousand years when converted into time. The excursion at such an interval of the thermal demagnetization (three degrees) is simply omitted, whereas less than 100 years pass between adjacent samples of the "short" section (the first variant of the record) near the Curie point.

Table 8. Some magnetic properties and paleomagnetic data. Monchegorsk intrusion

no.	M	J_{nt}	κ	Q_{ntf}	T_d	D	I	T_d	D	I
ch46	161	3.61	522	0.74	530–540	126.2	21.9	540–543	280.4	−14.6
ch45	160	7.06	485	2.09	530–543	134.3	19.1	543–552	303.8	−9
ch44	159	12.9	500	3.24	540–546	119.2	24.1	546–555	285.2	−12.7
ch43	158	11.9	415	19.9	500–540	129.5	15.7	540–558	286.8	1.8
ch42	157	54.8	1261	1.6	500–530	159.5	45.1	543–558	299.4	−17.6
ch41	156	86.1	1046	3.35	500–552	132.3	−16.2	561–579	102.6	−22.1
ch40	155	6.06	460	2.54	530–543	129.5	20.1	555–579	87.2	40.5
ch38	153	561	715	44.7	520–561	156.3	29	567–579	165.6	35.4
ch37	152	593	707	48.5	500–549	143	31.9	552–579	150.1	39.6
ch36	151	128	490	35.7				564–579	321.1	−52
ch35	150	166	820	9.93				540–579	268.6	−7.4
ch34	149	22.4	407	80.4?	540–543	140	14.6	549–558	297.1	−13.9
ch32	147	14.07	451	6.94	540–549	117.2	24.4	552–558	310.6	−20.5
ch31	146	6.08	426	5.87				543–549	293.7	−16.4
ch30	145	121	1335	3.25	543–546	145.3	34.2	555–576	306.6	−10.5
ch29	144	20.3	771	1.37	500–530	142.1	26.4	543–564	320.4	−6.3
ch28	142	14	400	100?	500–530	75.8	18.3	530–576	244	−9
ch27	141	60.6	615	7.08	540–543	120.7	19.7	543–576	296.6	−7.2
ch26	140	36.9	540	6.62	520–543	133.3	19.2	543–570	314.6	−9.1
ch25	139	14.7	490	4.1	530–540	124.4	34.1	549–561	297.9	−12.4
ch24	138	0.73	353	100?	530–543	123.7	18.7	543–546	303.7	−10.4
ch23	137	105	790	6.76	530–546	127.4	21.9	549–567	302.6	−8.1
ch22	136	93.3	664	8.9	520–530	104	40.8	540–573	323.7	−3.8
ch21	135	117	723	9.1	530–543	133.9	15.1	549–570	307.3	−6.5
ch20	134	22.8	422	26	520–540	142.4	43.4	540–570	286.4	−6.7
ch19	133	3.04	432	2.39	530–546	161.4	26.5	543–555	284	−13.2
ch18	132	41.4	1387	1.05	540–549	153.9	62.6	552–573	304.6	0.3
ch17b	130.5	316	5030	1.71	540–564	157.3	6.9			
ch16	128.5	82.5	640	8.63	520–546	126.7	21.3	552–567	300.6	−19.3
ch15	126.5	186.6	934	8.8	530–546	125.3	23.5	555–567	294.1	−12.5
ch14	124.5	138.1	459	58.8	540–579	153.7	6.5			
ch12	120.5	43.8			500–543	112.4	4.8	552–570	292.2	−2.7
ch11	118.5	65.5	690	5.67	520–540	129.4	8	543–570	303.8	0.6
ch10	116.5	120	673	11	520–540	123.9	4.1	546–567	298.7	−2.7
ch9	114.5	87.2	860	4.76	520–546	144.3	10	546–576	275.5	−2.6
ch8	112.5	177.6	4380	1.11	530–540	208.3	46.3	540–567	292.3	−3.4
ch7	111	101	2760	1.08	540–546	130.6	24.8	546–567	293.2	−12.5
ch6a	109	75.6	861	4.12	530–543	130.4	25.6	546–579	292.7	−12
ch5	107.5	61.5	720	4.83	530–543	132.7	30.8	555–573	293.8	−13.6
ch4	105.5	42.2	873	2.24	540–543	121.3	19	543–576	302.5	−7.3
ch3	103.5	21.7	540	3.9	530–552	110.8	4.9	552–567	309	−20.9
ch2a	101.5	25.5	517	5.37	540–549	142.4	18.5	549–567	299.4	−5
ch1	100	98.5	1047	3.82	540–543	151.1	48.8	558–570	279.7	−7.9

Note: no. – sample number; m – thickness in meters; J_{nt} – NRM value in the process of thermal demagnetization, mA m^{-1}; κ – magnetic susceptibility, 10^{-5} SI units; $Q_{ntf} = J_{nt}/\kappa$-400; T_d – NRM component identification interval; D, I – declination and inclination of the identified component, respectively.

An irregular distribution of the points in time and an appreciable noise is noted in the case of the first variant of the record. Because of it a transition was required to a uniform time step and smoothing of the observation data (Figures 25, 26).

A wavelet analysis has been performed to make a quantitative assessment of the spectral components of the field oscillations. The pattern of variations is complicated (Figures 25, 26). Rhythms that are stably traced during the record obtained are distinguished, as well as rhythms that change with time and individual splashes (Table 10). In general, the spectrum of rhythms of variations of the geomagnetic field direction covers the periods from 1 thousand years to 30–40 thousand years (Table 10 and Figures 25, 26). In case of a "short" section (Table 10, Figure 25) the most distinct and clear, with the maximum amplitudes

Table 9. Paleomagnetris directions for the high temperature (near T_c NRM component. Monchegorsk intrusion

no.	meters	T_d	time	D	I	no.	meters	T_d	time	D	I
mo2	34	570	120	311.6	−17.4	ch1	100	558	134.5	301.1	7.1
mo3	40	570	120.3	307.4	−8.3	ch2A	101.5	551	142.4	300.5	−7.9
mo4	49	570	120.5	336.6	−17.1		101.5	569	123.3	284.5	10.3
mo5	64	570	121	302.6	−6.4	ch3	103.5	556	137	302.3	−14.3
mo6	74	570	121.3	310.4	−10.2		103.5	566	126.2	312.8	−24.8
mo7	83	570	121.6	315.7	−10.1	ch4	105.5	567	125.2	299	−8.8
mo8	92	570	121.8	311.6	8.7		105.5	577	116	278	2.3
mo10	108	570	122.5	329.9	−12.1		105.5	545	149.8	302.6	−6.9
mo11	109	575	117.8	288	−7.7	ch5	107.5	560	132.5	296.1	−16
mo12	109	545	149.8	317	−5.7		107.5	572	120.2	296.8	−11.8
	110	555	138	320	1	ch6b	109	562	130.4	298.7	−12.8
mo30	138	560	133.4	318	−2.7	ch6a	109	554	139.2	287.5	−12.8
mo32	148	555	138.8	282.2	−16.5		109	569	123.4	304.2	−1.4
	148	575	118.8	270.2	−12.8	ch7	111	566	126.2	299.3	−0.7
mo33	158	560	134	313	−9.6	ch8	112.5	566	126.5	296.1	−4.2
mo34	168	550	145	304.6	−3.1	ch9	114.5	554	139.3	284.2	−2.7
mo35	170	560	134.2	298.9	0.2	ch10	116.5	566	126.4	300.4	1.9
mo37	193	555	140	304.5	−25.8	ch11	118.5	548	146.5	302.5	0.7
mo41	232	570	125.7	292.3	−28.3	ch12	120.5	566	126.5	291.1	−7.8
mo42	246	575	121.2	312.4	−5.2	ch15	126.5	566	126.8	294	−9.3
mo43	257	570	126.2	297.9	−23.3	ch16	128.5	554	139.5	300.1	−19
mo47	302	540	259.7	275.9	−17.3		128.5	566	126.8	287.5	2.5
mo51	356	575	223.6	280.5	−5.1	ch19	133	549	145.5	276.5	−21.7
mo52	367	545	254.6	277.8	−13.4	ch20	134	570	123	289.5	−2.1
	367	560	238.3	282.4	−12.6		134	551	143	288.4	−6.1
	367	575	224	279.5	−5.3	ch21	135	557	136.5	306.3	−5.6
mo53	375	555	243.7	288.4	−8.8		135	566	127	308.5	−9.1
						ch22	136	547	147.8	323.6	−6.6
							136	560	133	317.1	0.5
							136	569	124.2	336.6	5.4
						ch23	137	553	141	303.8	2.4
							137	567	125.8	300.5	−4
						ch24	138	545	150.2	303.7	−10.4
						ch25	139	559	134.5	302.5	−17
						ch26	140	560	133.3	315.6	−6.4
							140	570	123.3	309.2	−4.2
						ch27	141	560	133.2	314.8	−14
							141	569	124	301.6	−0.7
						ch29	144	570	123	291.1	−14.6
						ch30	145	569	124.2	317.1	−8.3
							145	566	127.1	305.3	−11.7
						ch31	146	548	146.7	293.7	−16.4
						ch32	147	557	136.8	310.7	−20.4
						ch34	149	554	140	294.2	−11.2
						ch35	150	563	130.2	275	−5.6
						ch36	151	566	127.2	320.8	−50.5
						ch37	152	566	127.5	150.2	34.7
						ch38	153	564	129.2	173.6	27.7
						ch40	155	551	143.5	312.9	−8.4
						ch41	156	564	129.6	102.2	−15.8
						ch42	157	557	137	298.6	−18.4
						ch43	158	557	137	256.8	6.5
						ch44	159	554	140.3	276.9	−0.6
						ch45	160	551	143.8	303.8	−3.2
						ch46	161	542	154.8	280.4	−14.6

Note: no. – sample number, mo – 375-meter section, ch – 61-meter section; T_d – unblocking temperature close to the Curie point, °C; time in kyr converted, from Figures 16 and 17; D, I – NRM declination and inclination at T_d.

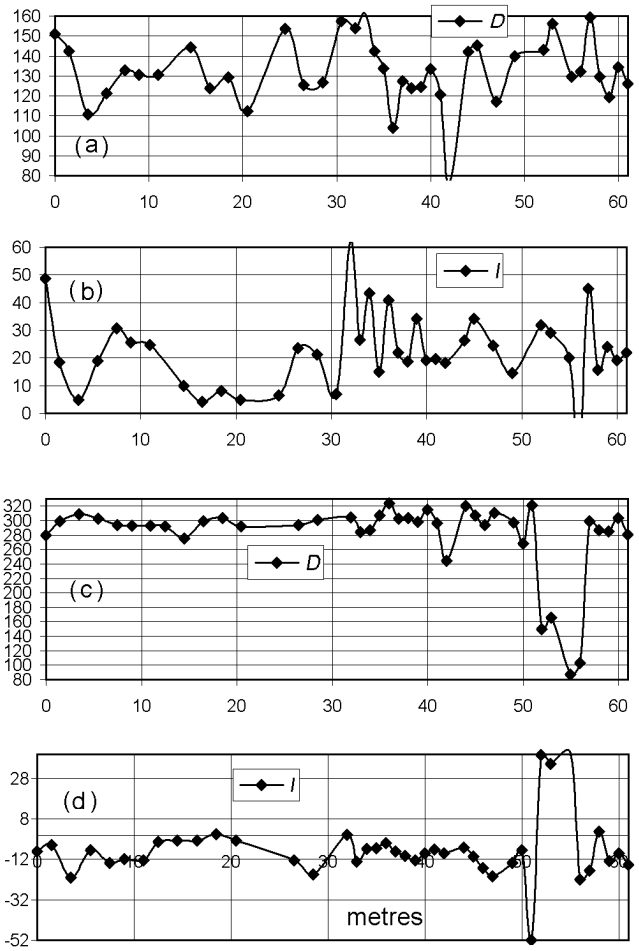

Figure 22. Variations of the geomagnetic field direction obtained as a result of the component analysis of the NRM thermal demagnetization of samples along the section: a) declination D, b) inclination I, obtained in the 500–540°C range; c) declination D, d) inclination I, obtained in the 540–576°C range. Monchegorsk intrusion.

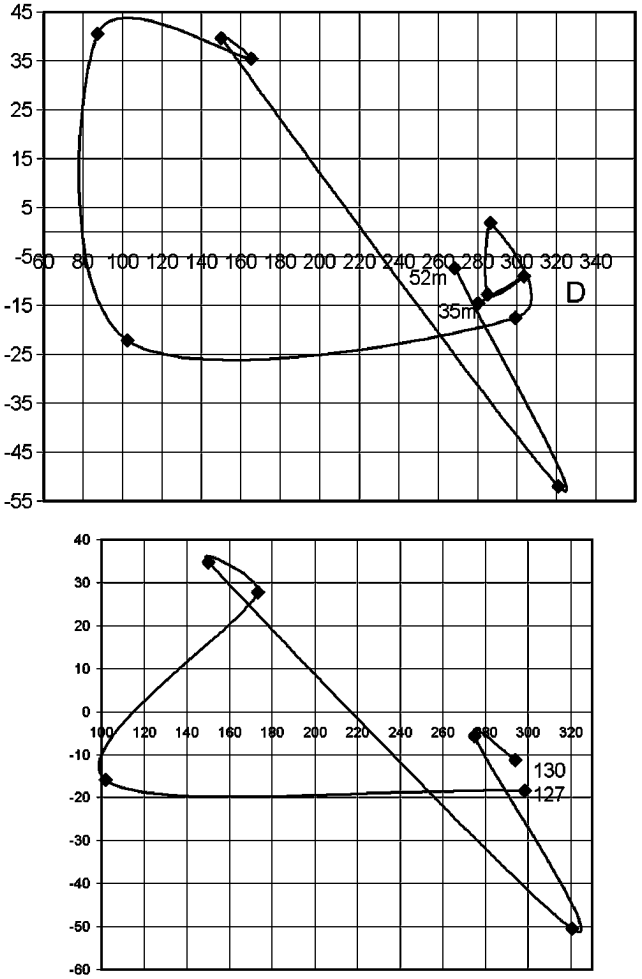

Figure 23. Behavior of direction of the high-temperature NRM component during the excursion. a – results of the component analysis, record along the section, between 35 m and 52 m; b – record during time interval between 127 kyr and 130 kyr Monchegorsk intrusion.

long-lived declination rhythms are: 30–40, 16, 11.5 and 9 thousand years, the inclination rhythms are: 40–36, 27, 16 and 8–10 thousand years; in case of a "short" section (Table 10, Figure 26) – the declination rhythms are 11–9, 7.6–5.5, and 4–6 thousand years, the inclination rhythms are 14–10, 9–6.5 and 3–4 thousand years.

Attention is attracted by a similarity of the wavelet diagrams in the time interval of 110–150 thousand years in the first and second variant of the record (see Figures 24, 25, 26), that counts in favor of objectivity of the results obtained.

B. **Kivakka intrusion.** The time distribution of the observation points is nonuniform therefore, the declination and inclination versus time curves were plotted from which values of D, I were obtained with the equal intervals (every 0.5 thousand years) by means of a linear interpolation.

For the first variant of the analysis of behavior of the geomagnetic field direction, directions of the A_1 component (inclinations no more than 40°) are converted into the stratigraphic system of coordinates and directions of the A_2 component (inclinations more than 40°) are retained in the geographic system of coordinates (Table 12). Such simplification of the situation (an momentary tilting of a body) caused scattering of data. As has been stated above, the wide intervals in the section of the intrusion were remagnetized in the direction of component B, and thus, the pattern has large interruptions (Figure 14a,b). Despite the interruptions it is evident that during cooling of the intrusion the geomagnetic field had predominantly one reverse polarity. The declination and inclination at a temperature which is standing no more than 3° from T_c are written out in the samples where it becomes possible to detect the A component (Table 13). A relative time of acquisition of component A has been determined from temperature and position in the section according to Figure 18. Thus, behavior of the paleomagnetic direction over the section in time was obtained (Figure 14c,d). A great scatter of data should be noted that, first of all, is as-

Table 10. Wavelet analysis results. Monhegorsk intrustion

D, I	Rhythm	"length"	Standard	Note
A. First variant of record. The 60 m section, sampling every 1–2 m (ch). Figure 24				
D and I	∼15?	115–145		Unclear and weak
I	9.1–7.6	115–155	±1.3	Intensive, clear
I	5.6?	115–125?		Weak
I	3–3.4–3	115–147	±1.3	Chain of splashes or a single rhythm with varying amplitude
I	1.9	144–147	±1.1	Splash
D	8–8.3–7.2	115–155	±1.2	Intensive, clear
D	4.5	115–125	±1.1	Splash
D	3.3–2.5	124–145	±1.1	Chain of splashes or a single rhythm, decreasing with time
D	2	146	±1.1	Splash
D	1.7	125	±1	Splash
D	1	143 and 147		Splashes
B. Second variant of record. The 375 m section, sampling every 10 m (mo). Figure 25				
D	30–40	135–260	±1.2	Intensive
D	20	140–180?	±1.2	?
D	15.8	195–230	±1.2	Intensive
D	11.5	160–190?	±1.2	Intensive
D	9.1	180?–230	±1.1	Nonuniform amplitude
D	8.1	140	±1.1	Weak splash
D	5.2	180–190	±1.1	Splash
D	4.5	160	±1	Weak splash
D	2.7	116	±1	Weak splash
I	40–36	155–200	?	Weak
I	26.9	190–260	±1.5	Intensive
I	15.8	140–245	±1.2	Intensive
I	10–9–8–10	125–270	±1.2	Intensive, amplitude varies
I	7.2	135	±1.1	Splash
I	5.4	155–170	±1.1	Intensive splash
I	5.4	220–240?	±1.3	Most likely two splashes
I	4.7	255	±1.1	Splash
I	4.5	196	±1	Weak splash
I	4.4	117	±1.1	Splash
I	3.7	139 and 239	±1.1	Splashes
C. Second variant of record. The 61 m section, sampling every 1–2 m (ch). Figure 26				
D	18	115–150?		Runs into intensive rhythm 11–9
D	11.2–9	115?–185	±1.3	Intensive, fades away in the middle of the interval
D	7.6	115?–165?		Weak
D	7.6–5.5	115–145	±1.2	Intensive
D	4–5.8	160–185	±1.2	Intensive
D	5–2.4	115–130	±1.1	Chain
D	2.8	130–145	±1.1	
D	3.7	182	±1.2	Intensive splash
D	2.4	170	±1.1	Intensive splash
D	2.1	181	±1.1	Intensive splash
D	1.7	141		Weak splash
D	1.5	161	±1	Splash
D	1.3	135	±1	Splash
D	1	141 and 155		Splashes
I	14–10	130–180	±1.2	Amplitude increases sharply with time
I	9.1–7.2–6.5	125–185	±1.2	Rhythm fades away in the middle of the interval, then, amplitude increases sharply

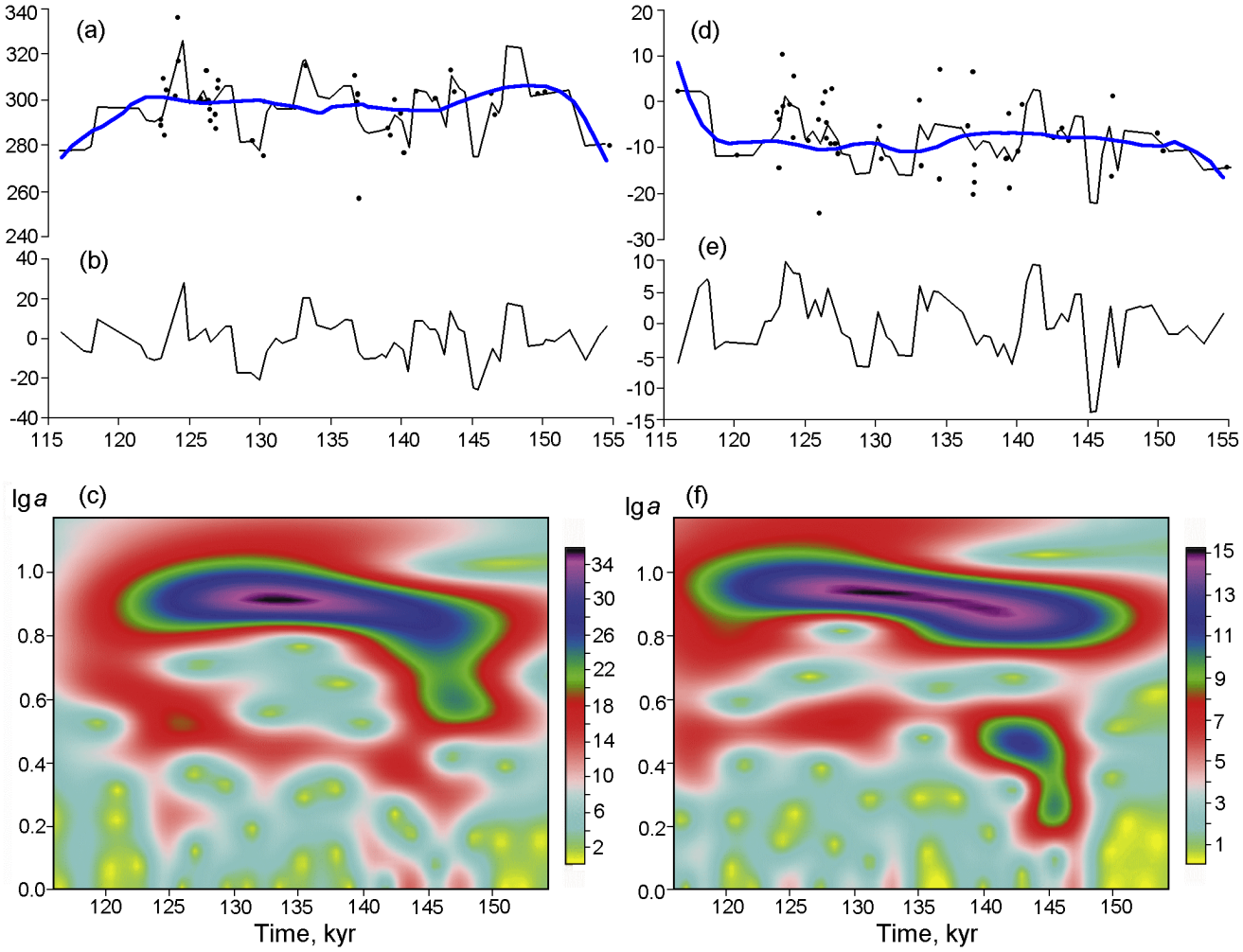

Figure 24. The first variant of recording the behavior of the geomagnetic field declination and inclination. Monchegorsk intrusion; 61m section, sampling every 1–2 m (ch). Points – initial data; line – averaging result (H=0.25) and transition to a uniform step in time ($\Delta t = 0.5$); thick blue line – assessment of the adaptive trend with the help of a local-polynomial smoothing by the 3rd order polynomial in a running window of a radius of 20 counts (10 kyr). Time row D, b) result of subtraction of the trend (D), c) wavelet diagram of the remainder after subtraction of the trend (D); d) time row I; e) result of subtraction of the trend (I); f) wavelet diagram of the remainder after subtraction of the trend (I). Lga – logarithm of the time scale (period).

Table 10. Continued

C. Second variant of record. The 61 m section, sampling every 1–2 m (ch). Figure 26

D, I	Rhythm	"length"	Standard	Note
I	6.5	180	±1.2	Intensive splash
I	3.8–4.7–4.3–3.2	126–185	±1.2	Rhythm fades away in the middle of the interval, then, amplitude increases sharply
I	2.8–3.3	150–160	±1	
I	2.8 and 2.7	126 and 166	±1	Splashes
I	2	157 and 174	±1	Splashes
I	1.7	127	±1	Splash

Note: D, I – paleomagnetic declination and inclination accordingly; rhythm – the limiting values are given, if the rhythm changes with time; standard – standard deviation of rhythm (±); "length" – duration of oscillation of the given rhythm. All data are given in kyr.

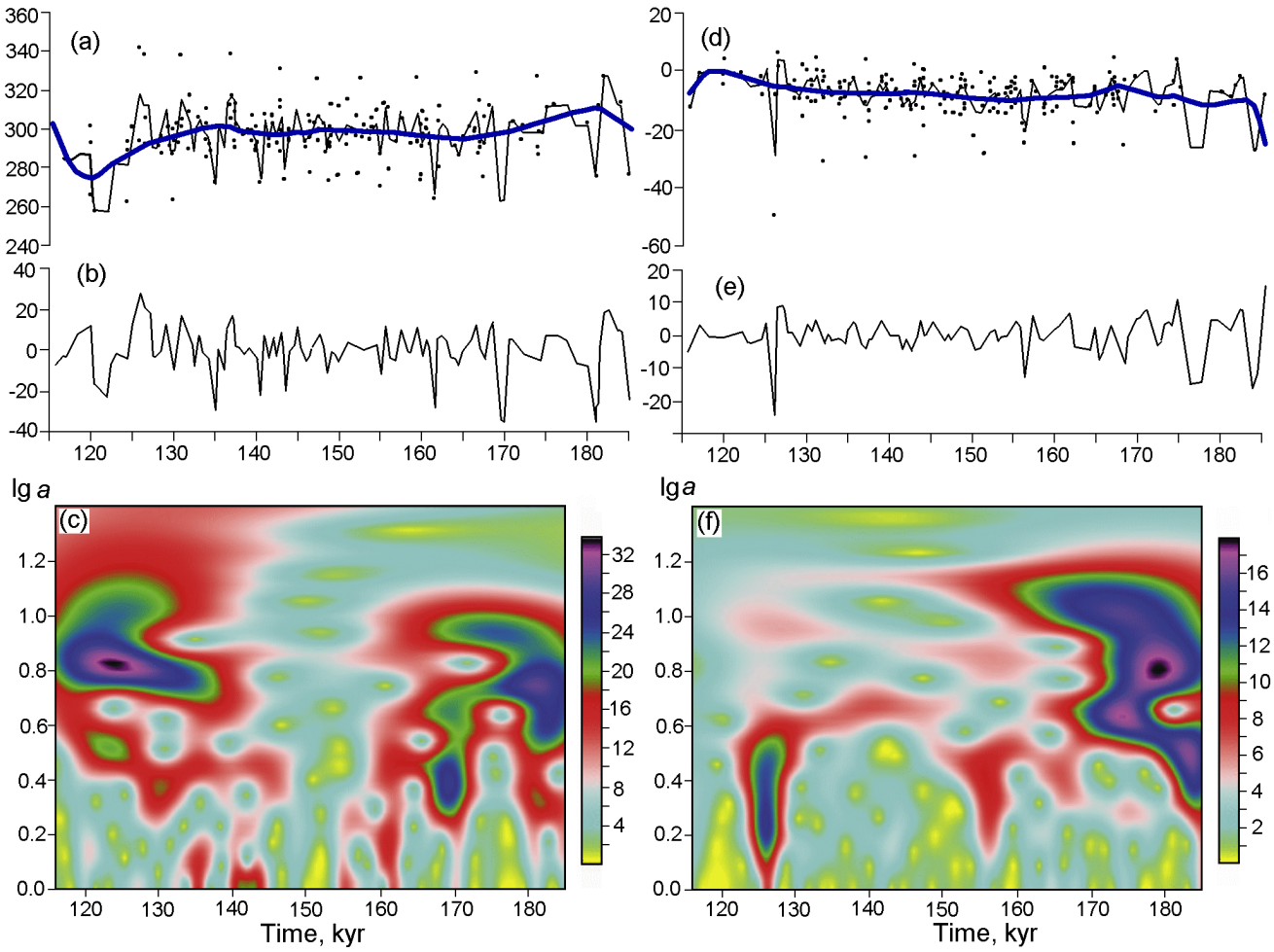

Figure 25. The second variant of recording the behavior of the geomagnetic field declination (a–c) and inclination (d–f). Monchegorsk intrusion; 375 m section, sampling every 10 m (mo). Symbols are the same as in Figure 24, radius of smoothing – 40 counts (20 kyr).

sociated with impossibility to divide completely components A_1 and A_2, in the process of the thermal demagnetization, and inaccuracy in assessment of the Curie points and, consequently, of the time of acquisition of components A_1 and A_2 had a certain effect. As a result of averaging data in the interval of 74–82 thousand years (Figure 14e,f) rhythmic oscillations of D and I are seen in the antiphase, and the rhythm is equal to 2 thousand years.

The second variant of the record we shall examine only for those samples, where components A_1 and A_2 are separated from B most reliably as a result of the detailed thermal demagnetization (Figure 27, Table 12). The pattern of variation of the field direction is "smearing" especially in the case of inclination because of a tilt of the intrusion. Therefore, and also because of the short time series of every sample we shall examine behavior of declination and inclination averaged from records for 9 samples (Figures 28a, 29a). After extraction of the trend it is evident that variations exist on its background, where rhythm is observed even visually (Figures 28b, 29b). Oscillations of D and I in the left part of the record are synphasal, amplitudes are different, the rhythm is equal to approximately 10 thousand years; oscillations of D and I in the right part of the record are antiphase and their rhythm "extends" up to 12–20 kyr. The complexity of the situation is reflected in a complicated process of oscillations of the field vector: the DI diagram (Figure 30) shows that the vector performs complicated oscillations, forming frequently incomplete loops of 2.5–9 thousand years, the vector in the loops rotates anticlockwise and counterclockwise (Figure 30). The loops with the rhythm of ∼10 kyr are seen best of all.

An appreciable change of the rhythm pattern and of D, and I falls on the period of 85 thousand years from the moment of emplacement of intrusion, a sharp deflection of the vector occurs during this interval (Figure 30). This is, evidently, associated with the beginning of tilting of the intrusion which disturbed cooling condition of the body. A pattern of the trend for the tilting counts in favor of this association: just from 85 thousand years there is a linear increase of I from values typical for the A_1 component (in the

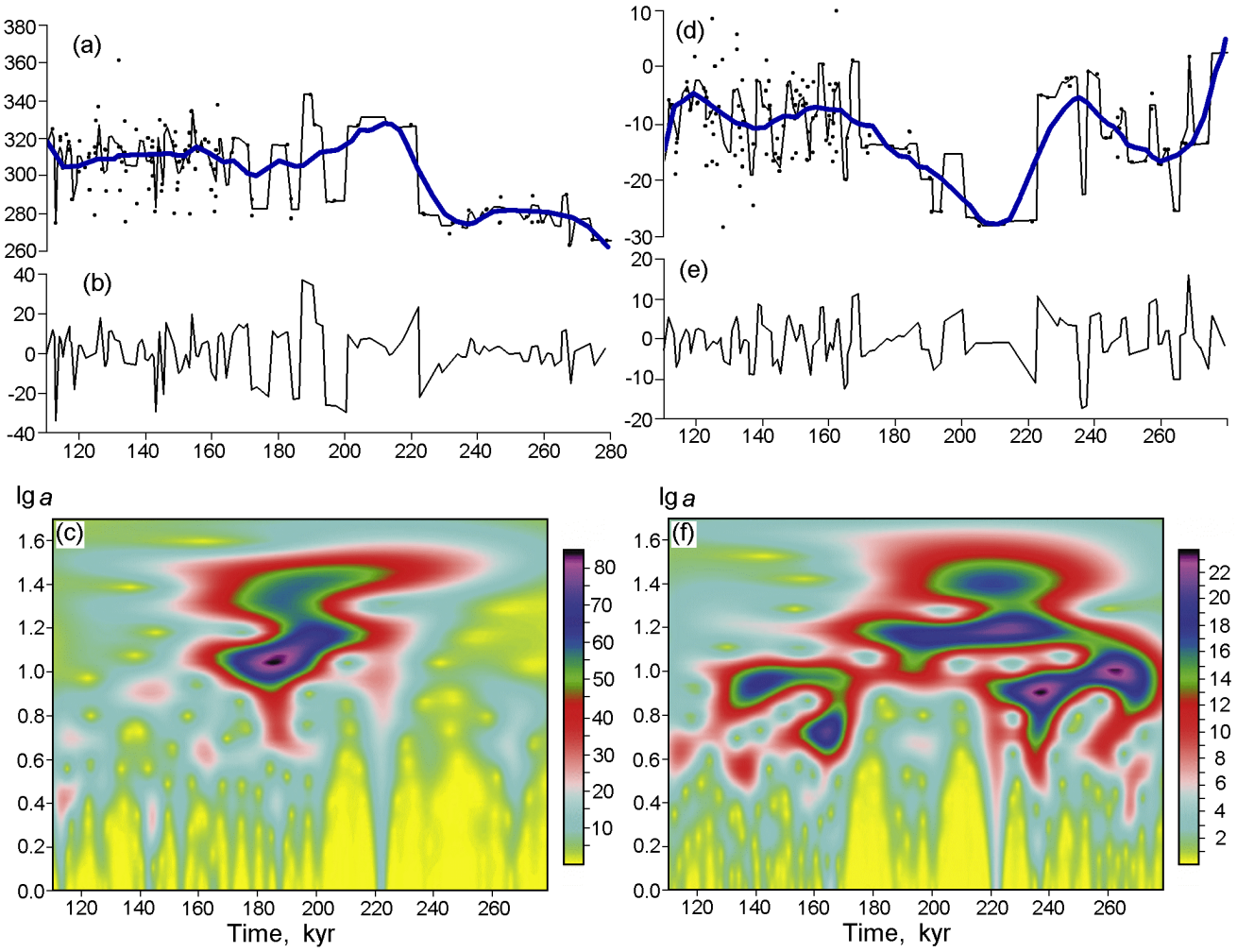

Figure 26. The second variant of recording the behavior of the geomagnetic field declination (a–c) and inclination (d–f). Monchegorsk intrusion; 61 m section, sampling every 1-2 m (ch). Symbols are the same as in Figure 24, radius of smoothing – 40 counts (20 kyr).

geographic system of coordinates (Table 6)) to values typical for A_2 to 105–100 thousand years (Figure 29a, Table 6). Thus, it is possible to assume that this linear trend had fixed the process of tilting of the intrusion that lasted for 20–25 thousand years.

A wavelet analysis has been performed to make a quantitative assessment of the spectrum of the field oscillations. The pattern of variations is complicated (Figure 31). In general, the spectrum of rhythms of variations of the geomagnetic field direction covers the period from 1 thousand years to 17 thousand years (Table 14 and Figure 31). Out of these the most distinct and bright, with the maximum amplitudes declination rhythms are 15–17, 10.5–9.5 and 5–6 thousand years (Figure 31a,b), the inclination rhythms are 12, 8–9 and 5 thousand years (Figure 31c,d). It is quite natural that with a greater smoothing window the short rhythms disappear partially or completely.

C. **Bushveld intrusion.** To analyze behavior of the geomagnetic field in the process of cooling of the Bushveld intrusion, meters of the well WP-16 section are converted into time (Table 15). In the *first variant* we have examined three sections of the *T*-Time diagram (Figure 20), corresponding to three NRM components of normal and reverse polarity: 1) a sharp drop of magnetization between 553°C and 556°C; the paleomagnetic direction has been determined from the difference vector between 553°C and 556°C; the inclinations obtained in this way are given in Tables 4 and 15; 2) a sharp drop of magnetization near 580°C, this is the Curie point of magnetite, the paleomagnetic direction has been determined from the difference vector between 577° and 580° (Table 15); 3) temperature of detecting the reverse polarity component in a vector analysis of the detailed thermal demagnetization covers more frequently a 520–540°C interval (Tables 4, 15). The temperature of 530°C has been adopted conventionally, when the end of the record of "running" of temperature 556°C is slightly overlapped and when negative inclinations appear with the beginning of the record of the negative polarity component (Tables 4, 15). As a result a

Table 11. Paleomagnetic data of the Monchegorsk intrusion. The second variant of record

no.	time	D	I	no.	time	D	I
mo1	160	292.7	−3.2	ch3	184	313.7	−27.1
	150	292.8	−4		176	312.5	−25.3
	141	292.6	−4.2		168	312.4	−25
	132	292.6	−4.1		162	312.5	−24.1
	123	292.8	−4.2		156	311.7	−24.4
	114	308.8	−6.6		151	315	−27.6
mo2	160	309.6	−13.6		143	314.6	−28.4
	150	311.6	−15.1		137	312.2	−29
	141	310.9	−15.3		132	317.8	−30.5
	132	310.9	−15.6		126	342	−48.8
	123	311.6	−17.4	ch4	180	302.6	−6.9
	114	321	−19		172	302.4	−7.9
	110	319.9	−19.5		166	301.9	−8.1
mo3	161	304.2	−4.1		160	303.2	−7.9
	151	304.6	−5.1		153	302.2	−8
	142	307.7	−6.7		147	302.4	−7.5
	133	307.2	−6.9		140	301.4	−7.7
	124	307.4	−8.3		134	303.2	−9
	122	304.4	−3.8		129	309.1	−9.1
	115	304	−6.4		125	301.1	−0.5
mo4	162	337.3	−15		120	301.7	−0.7
	154	334	−15.7		116	294.7	−11.8
	144	330.1	−16.6	ch5	164.5	286.8	−5.2
	134	328.8	−17.6		159.5	293.2	−13.5
	126	336.6	−17.1		154	294.5	−14.2
mo5R	183	137	14.5		148.5	295.1	−14.4
	171	136.4	14.1		142.5	293.1	−13
	159	138	12.9		137.5	294.5	−13.2
mo5N	150	297	−6.7		132.5	290.6	−5.6
	142	300.6	−7.5		134.5	292.6	−15.4
	134	302.6	−7.5		130.5	293.6	−9.9
	127	303.1	−7.1		7 126	293.5	−8.1
	120	302.6	−6.4	ch6a	164	291.9	−11.7
mo6	160	305.6	−8.6		158.5	292.9	−11.5
	150	307.9	−9.1		151	292.7	−11.9
	141	310.2	−9.9		146	291.5	−11.1
	132	309.8	−10.1		140	290.3	−9.2
	123	310.4	−10.2		136	291.2	−7.9
	114	319	−15.1		140	293.6	−9.6
	110	316.7	−13.8		134.5	288.8	−8.6
mo7	162	312.3	9.9		128	290.9	−4.3
	152	313.7	−2.4	ch7	166.5	299.1	−0.3
	142	315.3	−10.1		158.5	297.4	1.3
	133	315.2	−10.8		151	297.4	−0.1
	125	315.7	−10.1		144	299.6	0.3
	117	322.4	−2.7		139	299.7	−1.9
	112	325.1	−5.8		125	300.1	0.4
mo8?	162	308.2	−3.3		130	300	0.6
	152	309.2	−6.8	ch8	174	289.7	−2.5
	142	310.4	−2.5		168	295.6	−2.7
	134	309.8	−2.4		161	292.3	−3.9
	125	311.6	8.7		157	293.3	−3.2
mo10R	197	107	15.4		152	296.4	−3.6
	184	107.6	15		146	294.4	−3
	172	108.1	15		140	291.6	−2.3
	161	109.7			134.5	292.6	−3.5

Table 11. Continued

no.	time	D	I	no.	time	D	I
mo10N	153	315.4	−6.5		130.5	296.1	−4.2
	142	319	−9.2	ch9	169.5	263.4	−1.6
	133	308.9	−21		161.5	264.6	−1.5
	125	329.9	−12.1		155	270.3	−2.3
mo11	184	98.3	11.5		148.5	274	−2.6
	172	98.7	12.1		143.5	274.4	−2.2
	161	101.1	12.4	ch10	174	298.9	−3.2
	149	322.9	−1.1		167	300.3	−1.6
	153	323.1	−3.5		160	298.7	−3.6
	142	317	−9.5		155	299.7	−2
	132	311.2	3.2		148.5	299.5	−1.4
	125	279.4	−16.7		144	297.7	−2.1
	118	287.7	−7.7		139.5	299.8	−1.5
	113	275.4	−6.6		134	301.1	−3.6
mo12	161	313.9	−8.2		129.5	300.6	2.4
	149	317.1	−5.7	ch12	174	290.7	−3.5
	149	315.6	−6		167	290.9	−3.9
	141	319.7	1		160	291.5	−4.8
	132	361.6	5.7		155	292.6	−3.9
mo30	167	319.9	1.1		149	291.8	−3.2
	158	319.1	0.3		144	295.2	−5.2
	148	318.4	−3		139.5	294	−4.9
	138	318	−2.7		134	295.1	−11.5
	128	313.7	1.4		129.5	292.4	−15.2
	126	317	0.2	ch15	167	291	−9.2
	120	318.1	1.7		160	293.8	−11.4
mo32	149	280.1	−16		155	293.6	−11
	153	280.5	−16.4		149	293.6	−10.9
	143	282.2	−16.5		144	294.6	−12.6
	134	275.6	−14.8		139.5	293.6	−12.1
mo33R	220.5	146.8	27		134	294.7	−10.9
	204	146.3	26.6		130	293.8	−8.9
	191	146.9	25.4		126.5	292.5	3.4
mo33N	177.5	261.7	34.1	ch16	158.5	298.1	−12.2
	165.5	312.6	−12.5		152.5	298.7	−12.4
	153.5	312.5	−11.7		147.5	300	−13.2
	144	313.1	−12.7		144	299.9	−18.2
	134	313	−9.6		138.5	297.3	−6.9
mo37R	220	151.3	26.4	ch19	162	280.9	−17.2
	205	151.5	27.8		156	279.3	−18
	190	163.5	19.7		150	276.5	−21.7
mo41	165	296.1	−19.7	ch20	174	286.6	−3.4
	155	303.3	−15		167	287	−5.6
	145	292.1	−18.2		160	274.8	−5.1
	137	285.5	−24.5		155	287.5	−6.1
	128	292.3	−28.3		148.5	289.3	−5.4
mo42	155	323.5	−2.7		143	289	−5.2
	146	326.6	−10.5		137.5	290.5	−7
	137	325.9	−13.5		132	289.7	−2.8
	129	320.8	−14.6		134	285.9	−5.3
	123	312.4	−5.2		128.5	288.2	−3
	117	314.3	−4.2		124.5	289.5	−2.1
					120	293	4.3
	fault, gap				117	284.5	−0.3
	∼100 kyr			ch21	171	304.3	−0.2
					162	304.5	−2.4

Table 11. Continued

no.	time	D	I	no.	time	D	I
mo45	260	275.9	−17.3		157.5	308	−6.7
	264	273.8	−25.4		152	306.9	−6.9
	255	278.3	−16.5		146.5	307	−6.8
	247	275.4	−15.9		141	307.2	−6.7
	237	273.3	−22.3		137.5	308.5	−8.3
mo47	279	266	2.4		133	306.8	−8.1
	268	263.9	1.8		129	307.4	−8.9
	257	275.6	−4.9		128.5	296.6	−6.7
	248	283.2	−7.6		124.5	293.3	−8
	240	276.8	−1.4		120	266.2	−4.9
	232	278.3	−2.1	ch22	182	327.1	−1.7
	224	280.5	−5.1		174	326.5	−2.6
mo51	270	277.8	−13.4		166.5	329	−0.4
	261	279.7	−14.3		159.5	326.6	−1.6
	251	282.1	−16.9		152.5	326.1	−1.9
	243	282.4	−12.6		147.5	325.8	−2
	233	275.3	−1.9		143	330.7	2.1
	232	269.3	−3.4		137	339	4.1
	226	279.5	−5.3		131	338.3	4.8
mo52	267	290.7	−13.6		126.5	338.5	6.4
	257	289.6	−7.5	ch23	167	293.9	4.5
	247	288.4	−8.8		160.5	299.9	−3.5
	238	281.6	−1		154	301.5	−5.8
mo53	267	290.7	−13.6		148	302.7	−7.3
	257	289.6	−7.5		142	302.3	−6.7
	247	288.4	−8.8		146.5	303.7	−7.2
	238	281.6	−1		141	303.7	−7.4
					135.5	302.4	−2.2
					130.5	302.5	−2.7
				ch25	174	298.9	−11.5
					167	298.7	−11.4
					160	298.4	−11.6
					154.5	298	−12.2
					149	298.5	−12.6
					143	299.5	−11.7
					137.5	302.5	−17
				ch26	167	314.7	−7.9
					160	309.2	−2.1
					154.5	310.7	−3.5
					149	313.1	−3.8
					143	312.1	−3.5
					137.5	312.1	−4.1
					132	309	−2.1
				ch27	167	296.4	−6.1
					160	297.9	−6.1
					154.5	297.5	−7.2
					149	296.3	−5.7
					143	298.9	−7.4
					137.5	303.2	−4.3
					132	298.3	0
					139.5	294.4	−4.2
					131	301.6	0.5
				ch29	181.5	312.3	−4.9
					175	311.2	−5.7
					168.5	311	−5.8
					162	311.2	−3.3

Table 11. Continued

no.	time	D	I	no.	time	D	I
					155.5	313.4	−6
					150	312.1	−5.4
					145	308.6	−4.1
					139.5	306.9	−6.8
					134	310.9	−4
					128.5	296.7	−8.7
				ch30	174.5	298.5	4
					167.5	306.6	−9.3
					160.5	305	−8.8
					154	306.6	−7.5
					147.5	306	−9.5
					142	307.1	−9.8
					137	304.6	−10
					131	305.4	−10
					126.5	306	1.9
					165	296.4	−13.6
				ch34	158.5	296.5	−12.4
					152	296.6	−13.4
					146.5	296.4	−13.5
					141.5	294.2	−11.2
				ch35	185	277.1	−8
					181	275.4	−8
					167.5	275.9	−6.4
					160	276.8	−8.4
					152.5	277.3	−8.6
					146.5	277.8	−9.2
					140.5	272.6	−6.3
					135	272.4	−4.3
					130	264	0
					124.5	262.8	−4.3
					120.5	258	−0.2
				ch42	172	295	−13.2
					165	295.7	−13.9
					158.5	295.8	−14.5
					153	296.2	−14
					147.5	294.1	−14.2
					141.5	292	−11.6
				ch45	166.5	300.5	−5.5
					160.5	301.7	−6
					154.5	302.6	−5.4
					149	301.3	−5.1

Note: Symbols are the same as in Table 9.

record of variations for ∼270 thousand years was obtained (Figure 32). If to convert the reverse polarity distinguishing temperature component T_d = 520–540°C, into blocking temperatures T_b = 480–515°C then the gap between the end of record of the 556-degree component and beginning of the 530-degree component will be 100 thousand years according to Figure 20. Absence of the reverse polarity at the thermal demagnetization above 540°C, used in the second variant of the record indicates that that this gap exceeds 300 thousand years. An artificial removal of this gap does not change the pattern of the spectrum of variations.

Sign of the reverse geomagnetic polarity interval has been

Table 12. Selected samples of paleomagnetic record of the Kivakka intrusion

no.	m	T_c	Comp.	Interval T_d	Interval T_b	Time, kyr
2pk19	344.6	560	A_1	560–532	560–521	76.9–87.9
17b27	563	580	A_1	580–537	580–516	73.9–89.6
41b31	750	572	A_1	572–530	572–509	76.8–92.7
48pc25	769	580, 562	A_1	577–520	577–500	75.7–95
51v38	806	585, 570	A_2+A_1	585–530	585–510	74.2–92.4
55t52	912	575	A_2	575–537	575–519	76.9–90
66t48	1158	562	A_2	562–530	562–516	79.6–91.4
68t58	1413	565	A_2	565–505	565–470	78.9–111
70t61	1650	562	A_2	562–500	562–464	78.5–109.4

Note: no. – sample number; m – sampling level in the section in meters from the lower contact; T_c – Curie point of the essential mineral, carrier of the magnetic record; Comp. – NRM component (see text) from which the paleomagnetic record is fixed; interval T_d of paleomagnetic record; interval T_b of paleomagnetic record; time – time of cooling of the intrusion in the mentioned interval T_b (according to Figure 18).

changed for a more convenient statistic analysis of the spectrum of variations of the geomagnetic field (Figure 33a). The time marks form a very irregular net of values (Tables 4, 15). The values D, I are characterized by a high noise, which can be judged about by a large amplitude of their variation in the interval of the time mark closeness (Figures 32, 33). Therefore, we have made smoothing and a transit to a uniform time step. The value of 0.5 thousand years has been selected as a step as this value is most typical for an increment. The basic (nonuniform) data about each time point were averaged. A nuclear averaging method was employed to obtain values of the uniformly numbered signal (see above).

The Figures 32 and 33b show a smooth increase of the amplitude of the inclination variations during the recording. A sharp increase of the amplitude, distinguished on the wavelet diagram (Figure 34) is fixed at the end of the normal polarity interval; the reverse polarity interval begins with an appreciable decrease of the amplitude, and further a smooth increase of the amplitude of the inclination variations con-

Table 13. Paleomagnetic data of the Kivakka intrusion

no.	m	T_c	t	D	I	Comp.
2	344.6	560	76.9	140.1	40.3	A_1
3	358.9	560	76	143.4	63.6	A_2
11	423.6	555	78.4	156.7	42.3	A_2
13	523.1	560	78	139.9	56.7	A_2
14	563.3	560	78.2	127	45.9	A_1
15	563.3	555	79.5	120.3	57.9	A_2
17	563.4	580	73.9	137.9	63.4	A_1
25	636.8	560	79	122.7	75.1	A_2
26	637.9	560	78.5	127.5	68.4	A_2
28	640.6	570	76.6	116.7	77.7	A_2
29	641.4	570	76.6	137.1	72.6	A_2
41	750.4	572	76.8	144	62.7	A_1
44	760.3	550	81.7	123.5	50.6	A_2
46	760	515	91	164.8	56.2	A_2
46	760	530	87	127.5	50.4	A_2
47	767.5	555	80.6	140.6	49.4	A_1
48	769.2	560	79.3	148.3	43.4	A_1
48	769.2	585	74.1	168.7	45.4	A_1
49	771	555	80.8	117.4	54.9	A_2
51	806	585	74.2	140.3	61.5	A_1
51	806	570	78.3	164.9	60.7	A_1
55	912	570	76.9	125.8	74.7	A_1
57	971.3	555	81.3	173.1	75.7	A_2
59	978.5	550	82.4	141.8	56.2	A_2
66	1157.6	555	79.6	153.9	73.9	A_1
67	1279	580	76	110	52.2	A_1
68	1413	560	79.5	127.6	46.1	A_2
70	1650.2	560	78.6	136.9	41.7	A_2
70	1650.2	560	78.6	160.9	75.7	A_1

Note: no. – sample serial number; m – distance (thickness) from the lower contact in meters; T_c – Curie point, °C; t – time from the moment of emplacement of intrusion in kyr; D and I – declination and inclination of the NRM component; Comp. – NRM component.

Table 14. Wavelet analysis results. Kivakka

D, I	Rhythm	Standard	"length"	Note
D	15–17	1	35	uniform
D	10.5–9.5	1	>40	
D	5–6	1	>40	
D	4	1	10	
D	3			splash
D	2.5			splash
D	2.2			splash
D	1			splash
I	12	1	>40	
I	8–9	1	>40	Overlapped by splash
I	5	1.5	20	
I	5.5	1	>10	
I	2.5			splash
I	1.3			splash
I	1?			splash

Note: D, I – paleomagnetic declination and inclination accordingly; Rhythm – limiting values are given, if the rhythm varies with time; Standard – standard deviation of rhythm (±); "length" – duration of oscillation of the given rhythm. All data are in kyr.

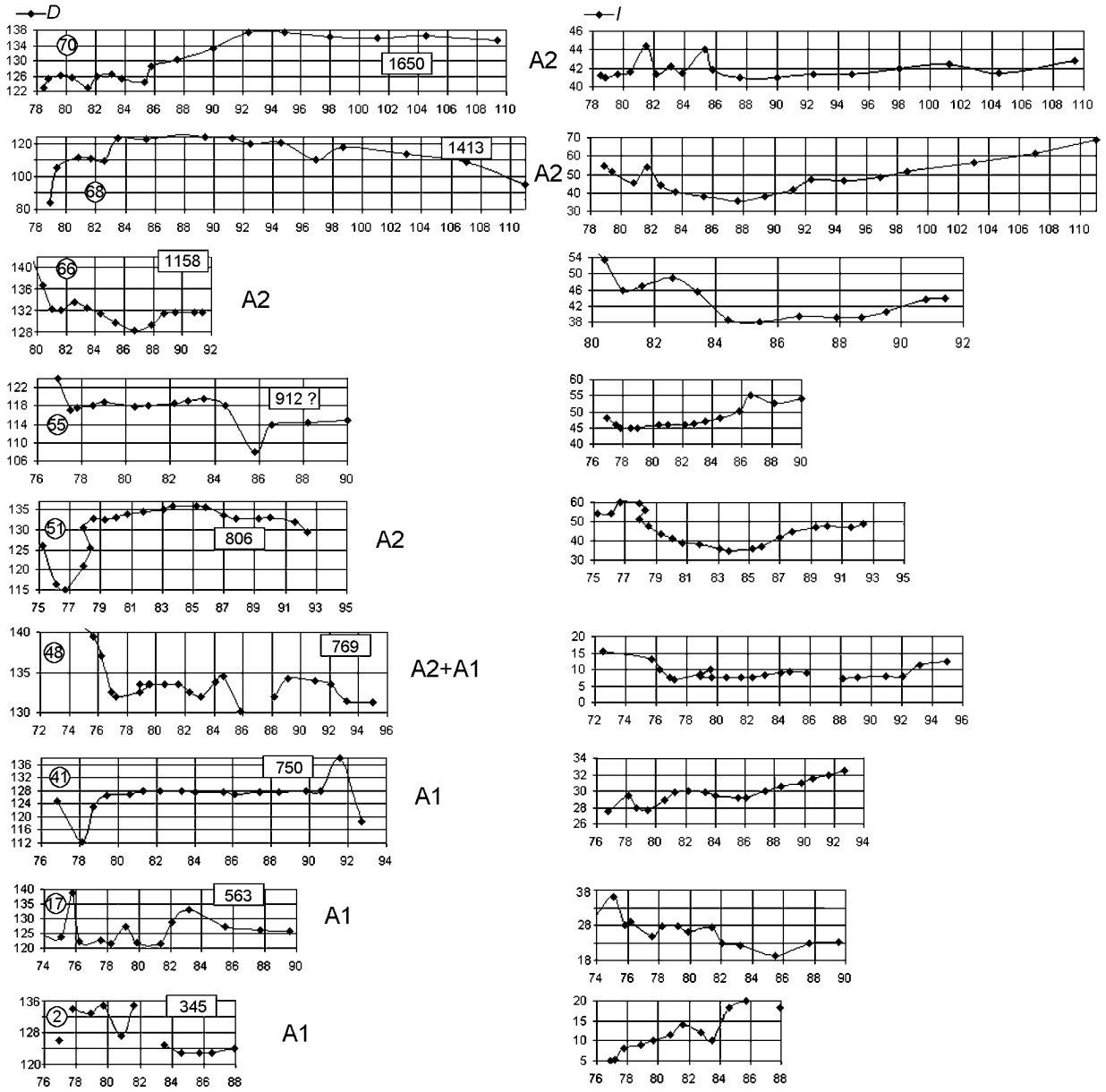

Figure 27. Kivakka. Variations of declination and inclination of components A_1 and A_2 in each sample versus cooling time. Left column – declination, right column – inclination. Numbers in circles – sample numbers, numbers in rectangles – distances from the lower contact vertically in meters.

tinues. The rhythm of oscillations inside the observed strong splash is 7.6±1 thousand years and similar splashes (6) with a similar rhythm but less intensive amplitude are seen almost on the entire interval of the record (Table 16, Figure 34).

In general, a series of oscillations of inclination with the rhythms from 68 to 6.5 thousand years is seen from the data of the wavelet analysis (Table 16, Figure 34). All of them are either not stable or their duration is short (different rhythms have the number of oscillations ranging from 1–2 to 7–9), or the rhythm value changes in time, more frequently it increases with time (Table 16, Figure 34) or oscillations form the chains of short and rapidly fading and appearing again splashes (for example oscillations with the rhythms of 6.5–7.5 and 2.5–4.5 thousand years. Distances between splashes with a close rhythm are uneven (Figure 34).

It will be recalled that the paleomagnetic direction in each case was determined with the use of a three-degrees interval to the Curie point; such temperature interval covers a period of about 10 thousand years. Consequently, with the linear magnetization – temperature and time relationship we obtain a smoothed direction of the field for 10 thousand years. This can be slightly less if the multidomain grains are present in this interval (then the drop of magnetization comes closer to the Curie point). The most reliable are rhythms of no

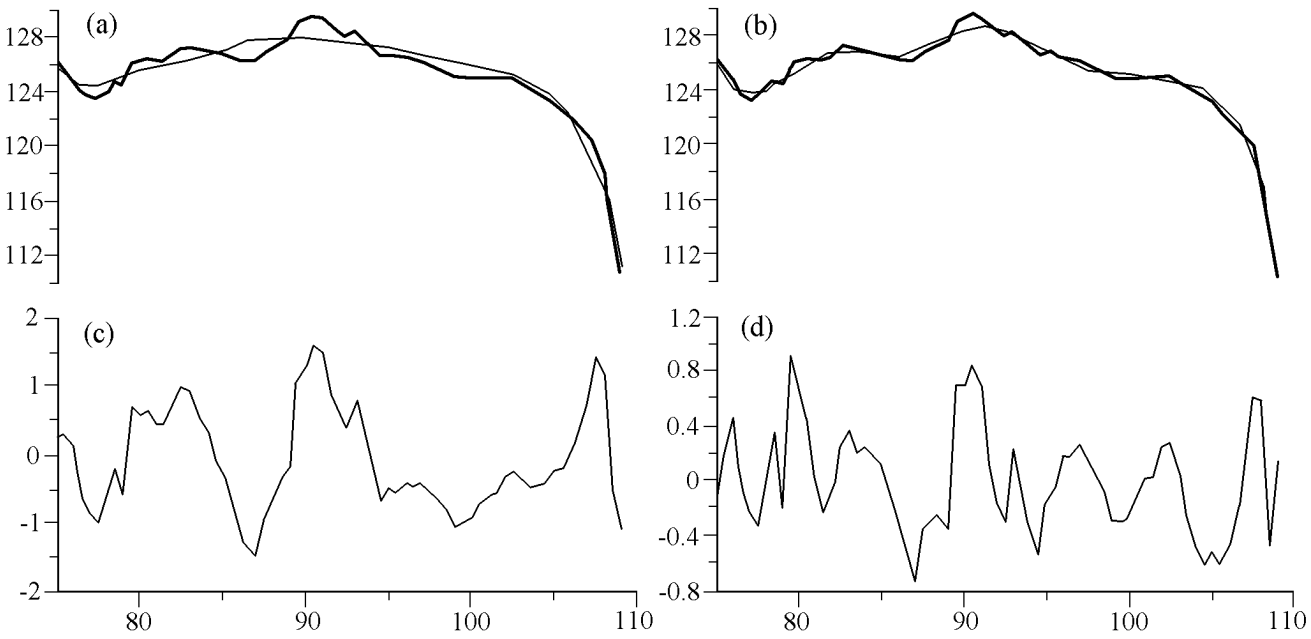

Figure 28. Kivakka. Charts of time series of the mean values of declination D (on 9 samples). The second variant of recording. a – initial data (black line) and averaging by the 3rd order local polynomial in a running window of a radius of 20 counts (10 kyr); b – initial data (black line) and averaging by the 3rd order local polynomial in a running window of a radius of 10 counts (5 kyr); c, and d – difference between initial data and a smoothed curve.

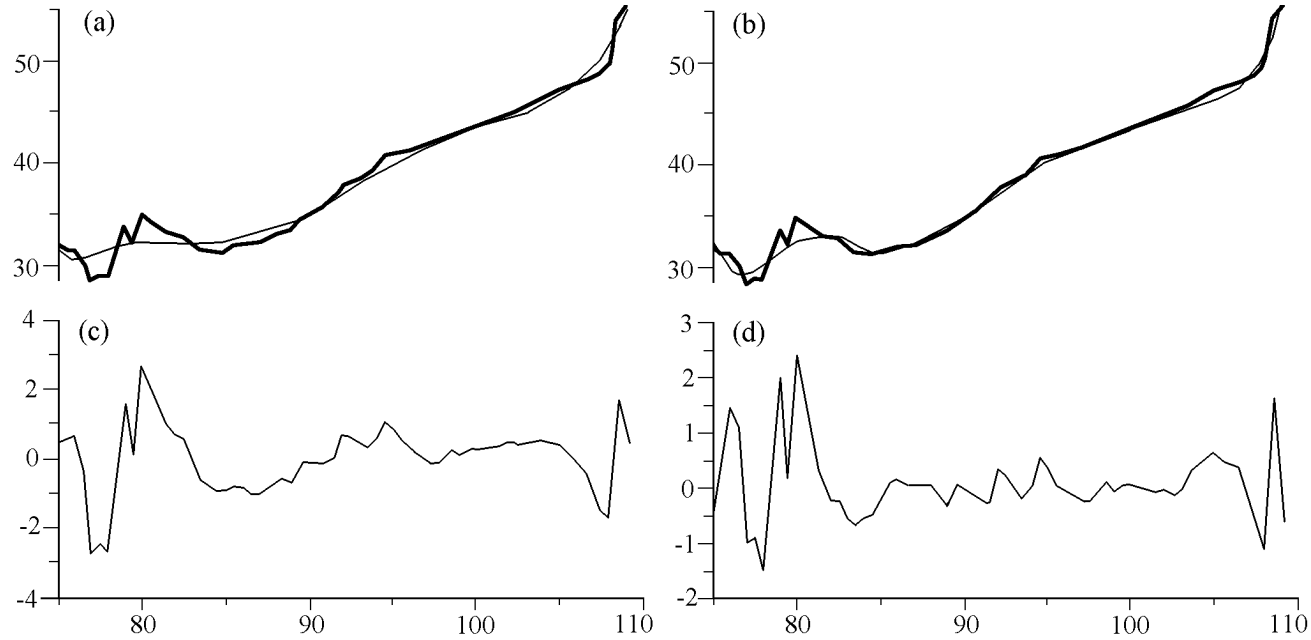

Figure 29. Kivakka. Charts of time rows of the mean values of inclination I (on 9 samples). The second variant of recording. a – initial data (black line)and averaging by the 3rd order local polynomial in a running window of a radius of 20 counts (10 kyr); c – initial data (black line) and averaging by the 3rd order local polynomial in a running window of a radius of 10 counts (5 kyr); c, and d – difference between initial data and a smoothed curve.

Table 15. Paleomagnetic data of the Bushveld intrusion

m	$T_d(R)$	I_{530}	Time, kyr	I_{556}	Time, kyr	I_{580}	Time, kyr
30.81	450–520	−29.4	167.85	77.8	83.4	78.1	3.08
32.73			168	55	83.56	74.2	3.27
34.36				77	83.74	78.9	3.44
35.96	200–520	−48.9	168.5	75.5	83.91	75.9	3.6
40.34				73.2	84.39	71.8	4.03
44.8	400–520	−49.8	169.6	78.5	84.87	79.6	4.48
46.28				80.5	85.03	80.7	4.63
53.6				85	85.83	83.4	5.36
59.58				87.6	86.48		5.96
62.22							
65.4				70.6	87.11	74.4	6.54
68.64				64	87.46	70.2	6.86
74.63				62.3	88.12	53.5	7.46
80.51				64.8	88.76	57.6	8.05
87.94	400–520	−51.7	175	76.7	89.56	84.6	8.79
93.93	500–520	−39.3	165.74	75.3	90.16	69.6	9.39
101.38	500–540	−45.1	176.67	73.6	91.03	59.9	10.14
107.22	500–540	−53.8	177.4	71.5	91.66	68.8	10.72
117.39			178.67	68.1	92.77	78.6	11.74
132.35				53.8	94.39	64	13.24
136.62	450–520	−76.6	181.08	54.7	94.86	70.1	13.66
147.08	350–450	−44.5	182.38	57.3	96	62.5	14.71
151.55	500–540	−65.1	182.94	51.1	96.48	73.4	15.16
160.39	350–450	−46.1	184.05	60.9	97.44	72.6	16.04
167.48	450–520	−74.7	184.94	62.6	98.21	57.7	16.75
169.43				72	98.42	71.5	16.94
171.14	450–540	−52.6	185.39	57.4	98.61	66.5	17.11
171.72	500–540	−43.5	185.47	74.7	98.67	76.1	17.17
174.7	450–520	−47.3	185.84	68.5	99	66.2	17.47
176.57	200–540	−57.8	186.07	75.2	99.2	70.5	17.66
187.91	500–540	−63.8	187.5	65.2	100.44	74.5	18.79
190.85	500–520	−40.9	187.86	69.8	100.75		
195.3	450–540	−54.7	188.41	57.5	101.24	63.4	19.53
198.15	450–540	−36.9	188.78	68.2	101.55	75.7	19.82
206.82	450–540	−37.4	189.85	62.3	102.49	77.9	20.68
213.28	350–540	−71.8	190.66	56.1	103.19	55.4	21.33
221.87	500–520	−37.2	191.73	67.8	104.13		22.19
229.34	500–540	−40.3	192.67	60	104.94	84.6	22.93
236.86	450–520	−37.8	193.6	61.8	105.76	70.7	23.69
241.32	500–520	−35.8	194.17	60.7	106.24	73.4	24.13
251.77	500–540	−76.8	195.47	55.1	107.38	64.5	25.18
255.64	520–540	−38.3	195.96	53.4	107.8	62.7	25.56
265.32	450–520	−59.2	197.17	45.3	108.85	85.2	26.53
272.77	450–540	−68	198.1	50.3	109.66	68.2	27.28
280.24	450–520	−47.9	199.03	61.1	110.48	81	28
286.24	450–520	−45.5	199.78	54	111.13	66.7	28.63
295.2	500–540	−50.4	200.9	60.6	112.1	72.7	29.52
302.31	500–540	−53.3	201.79	74.9	112.88	75.8	30.23
309.76	500–540	−50.3	202.72	65.6	113.69	76.8	30.98
317.23	450–520	−75	203.65	72	114.5	76.6	31.72
324.49	450–520	−49.4	204.56	65.2	115.29	81.5	32.45
328.56	450–520	−47.8	205.07	72.5	115.73	77.2	32.86
335.15	400–540	−32.2	205.89		116.45	70.3	33.52
340.32	450–540	−30	206.54	72	117.01	81	34.03

Table 15. Continued

m	$T_d(R)$	I_{530}	Time, kyr	I_{556}	Time, kyr	I_{580}	Time, kyr
344.86	500–520	−28.6	207.11	76.6	117.5	87.6	34.49
356.13	400–540	−36.5	208.52	58.1	118.73	74.5	35.61
359.82	450–540	−38.2	208.98	76.6	119.13	72.4	36
368.75	450–540	−53.2	210.09	76.1	120.1	72.7	36.9
372.65	300–520	−64.8	210.58	51.6	120.53	74.6	37.27
376.23	300–500	−38.4	211.29	50.4	120.92	79	37.62
376.79				48.2	120.98	62	37.68
385.17	520–540	−49.1	212.15	54.5	121.89	72.5	38.52
393.66	350–520	−76	213.21	66	122.81	61.2	39.37
395.14	450–540	−39.5	213.39	53.9	122.97		39.51
398.75	500–520	−38.9	213.84	82.3	123.36	75.4	39.88
404.56	500–520	−46.9	214.57	74.3	124	77.8	40.45
409	450–520	−36.2	215.13	80.7	124.48	84.4	40.9
414.58	200–500	−65.1	215.82	54.2	125.09	57.4	41.46
418.76	500–540	−38.6	216.35	66.2	125.54	78.1	41.88
429.61	500–520	−38.1	217.7	72.8	126.72	77.5	42.95
435.73	500–540	−54.6	218.47	75.1	127.39	77.2	43.58
444.51	200–450	−51.6	219.56	63.4	128.34	60.3	44.47
448.85	350–540	−36.4	220.11	40.1	128.8	70.7	44.88
449.92	400–520	−35.7	220.24	53.6	128.93	55.4	45
453.91	400–520	−46.3	220.74	54.5	129.36	58	45.39
455.3	350–540	−42.6	220.91	67.1	129.51	74.9	45.53
455.78	500–540	−21.3	220.97	58.9	129.57	69.9	45.57
456.17	500–540	−46.8	221.02	56.4	129.61	52.6	45.62
457.74	300–540	−45.2	221.22	58.3	129.78	70.1	45.77
463.06	500–520	−35	221.88	57.9	130.36	87.4	46.31
465.32	500–540	−32.5	222.16	52.6	130.6	45.4	46.53
474.22	350–540	−43.4	223.28	59.9	131.57	64.9	47.42
475.47				32	131.71	39	47.55
483.33	520–540	−68.9	224.4	64	132.56	65.9	48.33
489.29	400–540	−21.3	225.16	61.2	133.21	72.6	48.93
491.56	500–540	−038	225.45	61.8	133.46	65.3	49.16
493.18				50.3	133.63	53.4	49.32
507.84	200–350	−68	227.48	78	135.23	63.6	50.78
511.65	450–540	−58.3	227.96	52.8	135.64	61.7	51.19
520.41				77.9	136.57	79	52.04
523.1	500–520	−23.1	229.39	53.2	136.89	48	52.31
529.29				67.8	137.56	75.7	52.93
533.96	20–540	−81	230.75				
535.14				69.4	138.2	78.9	53.51
537.16				71.2	138.42	75.6	53.71
539.07	500–540	−31.3	231.38	43.6	138.62	45	53.91
542.65							
548.7	200–520	−71.4	231.59	69.8	139.67	75.1	54.87
550.14	500–540	−47.4	232.77	80.8	139.83	79.4	55.01
554.56				66.1	140.3	81.3	55.46
556.34	500–540	−47.5	233.54	73.8	140.5		55.64
563.5			234.44	64	141.28	63.6	56.35
567.4	500–540	−57.5	234.93	58.1	141.7	69	56.74
572.19	200–520	−35.5	235.52	71.4	142.23	76.1	57.22
576.78	500–520	−20.2	236.1	77.7	142.72	78.1	57.66
582.65				78.8	143.36	63.1	58.26
587.84	200–520	−34.2	237.48	68.1	143.93	64.4	58.78
592.2							

Table 15. Continued

m	$T_d(R)$	I_{530}	Time, kyr	I_{556}	Time, kyr	I_{580}	Time, kyr
596.58				68.8	144.88	65.6	59.67
601.1				80.4	145.37	75	60.13
606.33				69.5	145.94	75.1	60.63
611.76						49.4	61.17
616.6	300–520	−49.6	241.08	42.9	147.06	67.6	61.66
621.38	520–540	−63.4	241.67	44.6	147.58	59	62.14
625.69				62.8	148.04	67.4	62.57
627.75	520–540	−34.9	242.47	51.1	148.27		
632.68	500–540	−46	243.09	54.4	148.8		63.27
643.08				71.9	149.93	77.1	64.31
645.52	200–300	−56	244.69	70.5	150.2	76.4	64.55
647.75	200–400	−54.8	244.97	64	150.44	65.5	64.78
648.6							
649.1	500–?	−35.5	245.14				
650.95	520–555	−14	245.37	67.8	150.79	68.3	65.1
653.05	200–300	−62.5	245.63	78.3	151.02	78.6	65.3
657.46	450–540	−32	246.18	40.5	151.5	66.2	65.75
659.3				67.9	151.7	72.2	65.93
661.39	500–540	−67.2	246.67	59.7	151.93	62.3	66.13
664.6	350–520	−50	247.08				
670.23	400–540	−66.5	247.78				
675.72	500–540	−35	248.47				
680.92	450–550	−47.8	249.12	−51.8	154.05		
683.28	500–540	−55	249.41	51.3	154.31		
690.22	300–500	−61.1	250.28				
692.78	500–540	−45	250.6				
702.39	200–350	−58.8	251.8				
711.7	500–540	−47.2	252.96				
718.17	520–540	−47.4	253.77			78.7	71.82
721.16	450–540	−55.7	254.15				
726.56	520–565	−60.9	254.82			62.9	72.66
730.34	520–540	−76.1	255.29	78.6	159.42	62	73.03
734.96	200–350	−61.8	255.87				
739.51	200–300	−85.5	256.48				
745.15	400–540	−39	257.14	55.6	161.04	69.8	74.52
749.43	200–400	−67.2	257.68	59.8	161.5	70.5	74.94
755.21	500–555	−35.3	258.4			57.7	75.52
759.79	500–540	−51.6	258.97	26.4	162.63	69.7	75.98
764.66	520–555	−67.9	259.58			59.7	76.47
773.31	200–540	−65.1	260.66	52.4	164.1	63.3	77.33
779.6	520–555	−37.7	261.45	51.9	164.78		77.96
783.8	500–540	−45.2	261.98	53.1	165.24	61	78.38
788.09	350–540	−29.1	262.51	53.5	165.7	72.5	78.81
794.54			263.32	54.8	166.41	58.8	79.45
802.42				−38.1	167.27		
803.45	520–540	82	264.43	−66.3	167.38		
809.39	400–500			−72	168.02		
814.15	450–520	−85	265.77	−41.4	168.54		

Note: m – sampling level in meters; $T_d(R)$ – temperature of detecting the intermediate-temperature reverse polarity NRM component, the component analysis result; I_{530} – inclination of the intermediate-temperature NRM component; I_{556} and I_{580} – inclinations of the high-temperature NRM components close to their Curie points.

Table 16. Bushveld intrusion. First variant of record

Rhythm, kyr	Standard	Length, kyr	Number of rhythms	Note
56–67	±7.8–5.8	10–270	4–5	
29.5–40	±3–4.6	10–270	7–9	
20–25	±2	120–220	5	
16	±2.8	60–110	3.2	Chain of trains
15	±2	140–160	1.5	
15.8	±2.8	185–245	4	
11	±1.6	160–170	1	Splash near N-R
6.3	±1	65–70	1	Series of splashes
7.1	±0.6	80–100	3	of close rhythm
7.6	±1.2	140–170	4	Most intensive
7.1	±0.6	195–210	2	
7.4	±1	225–245	3	
8.5	±1	250–270?	2.5	

less than 10 thousand years, considering the above statement, and smaller rhythms should be viewed with caution.

We selected 44 samples with the most reliable results of the thermal demagnetization (Tables 4, 15) for the *second variant* of the field variation record. We can watch the behavior of not only inclination but also declination in each sample (Figure 35). A direct comparison of declinations is impossible, however, due to an arbitrary orientation of the horizontal plane. We are not so interested in the values of declinations as their behavior in time. Therefore, the following operation was made: a mean value of D was calculated for each sample in the process of the thermal demagnetization and a difference value of declination was plotted relative to the mean value. We can compare the difference values of samples and study the record of behavior of direction of a complete vector of the magnetic field. However, due to a sharp tilt in values of declination great mistakes are likely to happen (deviation of the vector by 2°–3° through errors of measurements causes alteration of declination by 10° and more!).

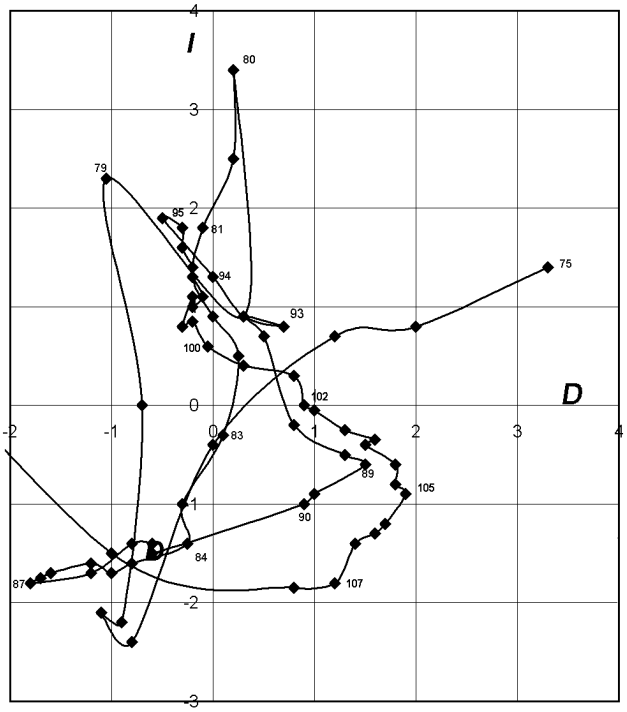

Figure 30. *DI*-diagram of behavior of the geomagnetic field vector in the process of cooling of the Kivakka intrusion. The second variant of recording.

As has been stated above, two magnetic minerals with the Curie points 556°C and 580°C are regularly present in samples of the intrusion. Two types of the record were composed: 1) it is assumed that a sample has *one magnetic phase* with one of the Curie points prevailing (if the NRM intensity drop at 556°C certainly exceeds 70%, the record is analyzed only up to 556°C, if the drop is less than 50% the first Curie point is ignored); 2) both Curie points are taken into consideration. In the first case the record covers ∼0.4 million years. In the second case the magnetic record is shifted relative the titanomagnetite record and the stacked record looks as if it is shorter as compared with the first case by ∼60 thousand years; this portion of ∼60 thousand years is "cut short". We analyze both types of the record.

After the results on all the samples selected for the analysis are averaged and after a transition to a uniform time step, cyclicity becomes apparent in declination and especially in inclination (Figure 36).

A series of the inclination oscillations with the rhythms from 100 to 5 thousand years is seen from the wavelet analysis data as in the first variant of the record (Tables 16, 17, Figure 37). They are usually unstable or their duration is not long (no one of the rhythms does not cover the entire interval of the record, the number of oscillations in different rhythms is from 1–2 to 10–12), or the rhythm value varies in time (Tables 16, 17, Figure 37), or oscillations form chains of rapidly fading and appearing again splashes that are especially appreciable in the zone of no less than 10 thousand years. The pattern of behavior of declination and inclination

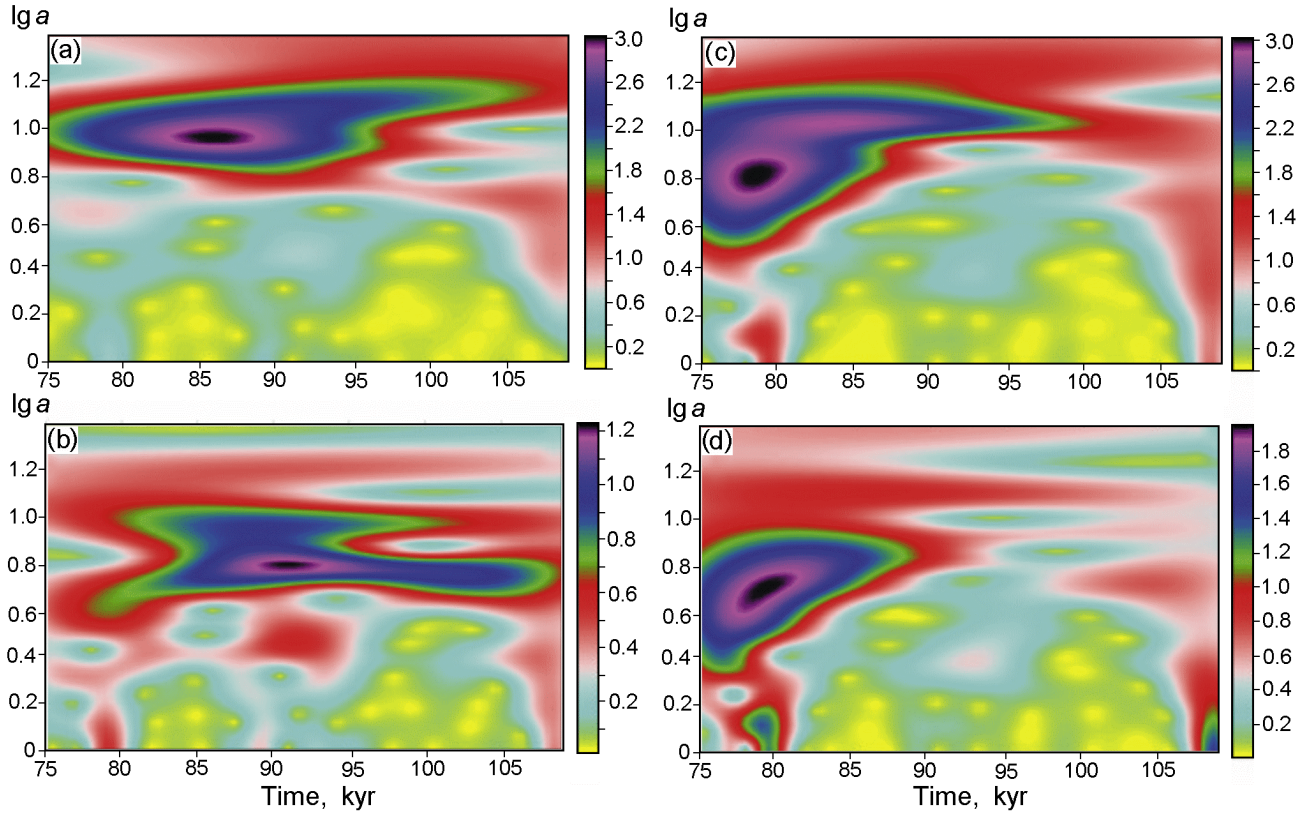

Figure 31. Kivakka. Wavelet diagram of difference between initial data and the mean curve D, a) window of 20 counts (10 kyr, see Figure 28c); b) window of 10 counts (5 kyr see Figure 28d). Wavelet diagram of difference between initial data and the mean curve I, a) window of 20 counts (10 kyr, see Figure 29c); b) window of 10 counts (5 kyr see Figure 29d). Lga – logarithm of the time scale (period).

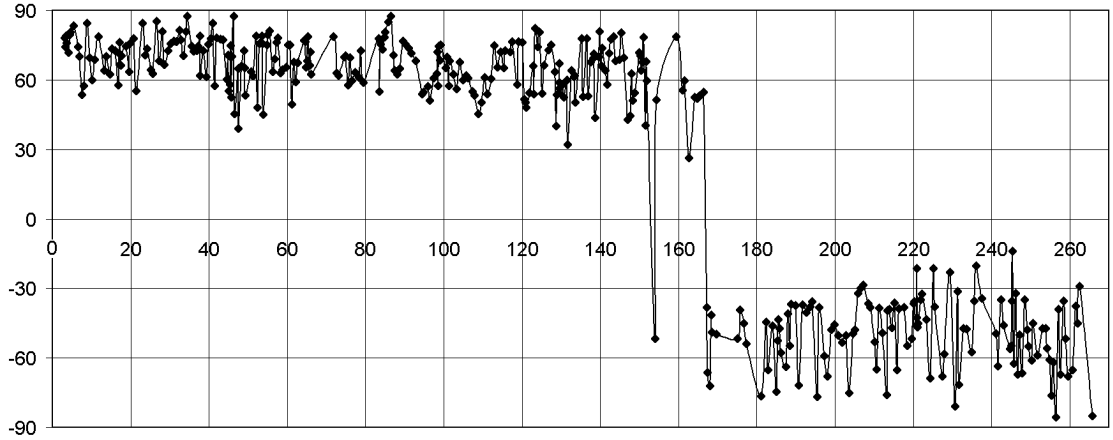

Figure 32. Bushveld. Behavior of inclination of different NRM components during a relative time of "running" of 580°C temperature (0–78 kyr), 556°C (80–168 kyr) and 530°C (more than 168 kyr) along the section uncovered by well WP-16 (Table 15). Meters are converted into time according to Figures 20, 21. The start of the count is the moment when the temperature of 580°C was at the beginning of the well section, cooling was from the top down (see text).

Table 17. Bushveld intrusion. Second variant of record

Rhythm	Standard	"length"	Number of rhythms	Note
A. One Curie point. Declination				
89–100		>400	>4	Very weak
55–63	±2.5	1200–1400	4	bright
55–53	±5	1580–1700	2–3	bright
35–37	±3	1200–1360	4–5	weak
31.5–34	±4	1620–1700	2–3	bright
20–24	±2	1400–1500	4–5	very weak
18	±3	1300–1350	3	Chain of splashes, the first is bright
18	±2	1400–1430	1–2	-*-
19	±2	1500–1540	2	-*-
15	±5	1200–1320	6–10	bright
12	±2	1650	1	Splashes, weak
10	±3	1240	1–2	bright
10	±2	1270	1	
10	±2	1340	1	
7.5		1490	1	
6.6		1290	1–2	
6		1370	1	
6		1410	1	
5.5 and 4.5		1310		2 splashes
B. One Curie point. Inclination				
83–60	±3	1240–1320	1?	weak
63–74	±3	1550–1700	3–4	
55–58	±3	1240–1360	2–3	
24	±5	1640–1720	3	Bright splash
24–19	±3	1530–1640	4–5	
20–17	±5–2	1240–1500	10–12	Series of trains (4), first is bright, last is weak
14	±3	1620		Series of splashes
12	±3	1570		
11	±2	1660		
10	±3	1260		
7.5	±2	1550		bright
7	±2	1630		bright
7	±2	1650		bright
6.5 and 6.3		1450		2 splashes
4.7–5.3		1300–1510		8 splashes
C. Two Curie points, 556°C and 580°C. Declination				
100–87		1360–1660	>3	? very weak
63–50	±4	1560–1660	2	bright
45	±2	1300–1350	1	splash, weak
36–42	±4	1360–1460	3	weak
34–36	±4	1560–1660	>3	bright
21	±2	1240–1300	>3	
18–16	±2	1240–1370	7	bright
17	±2			weak, splash
14–18	±4	1570–1650	5	bright
13	±3	1260–1320	4	bright
9.5	±3	1290		bright, splash
9	±2	1440		splash
10.5		1550		splash, weak
10	±3	1610		splash
9.3	±2	1580		bright, splash
8.5 and 8	±4	1500, 1590		splash
7		1410, 1440		2 splashes
6.6	±2	1340		splash
5.8, 5.4		1310, 1390		splashes

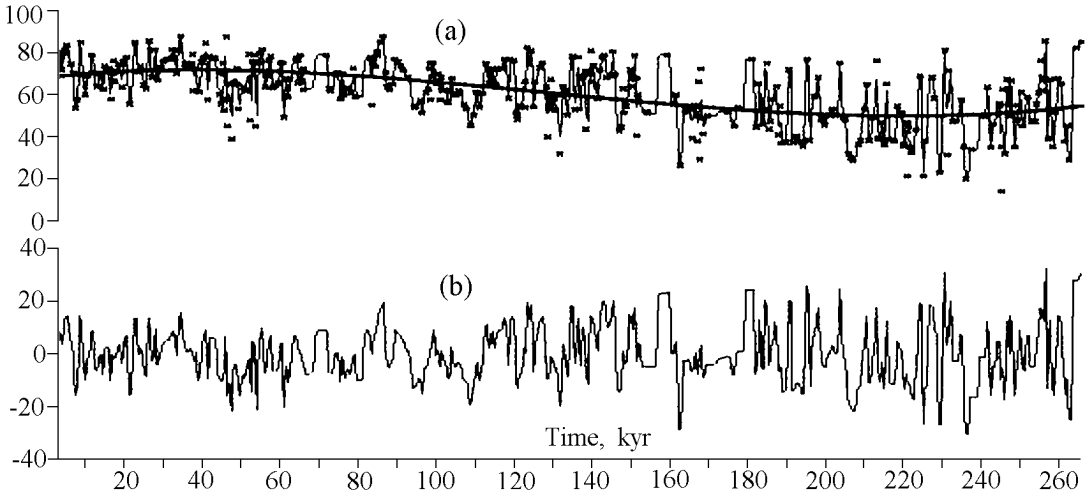

Figure 33. Bushveld. The first variant of the paleomagnetic record. Paleomagnetic inclination after the inclination sign has been changed in the R-polarity interval. a) points "×" – initial data; solid thin line – after transition to a uniform step of 0.5 kyr with the help of a nuclear assessment with the radius of H=0.25; solid thick line – result of a subsequent smoothing of the curve with a uniform step by the 3rd order polynomial. b) difference between the smoothed curve and a signal after transition to a uniform time step.

has no difference in principle in both cases of the recording, with the second Curie point taken into account and ignored. We connect the difference, first of all, with inaccurate fixing of unblocking and blocking temperatures, with determination of the Curie points and time.

Despite errors of measurements and in processing of the results, the following intervals of the main oscillations can be distinguished with confidence practically in all variants of the paleomagnetic record (three records of inclination and two records of declination) (Tables 16, 17): 90–100, 50–65, 30–40, 19–20, 15–17, 10–8 and 5–7 thousand years. Intervals, aside of errors, reflect first of all, instability of rhythms in time (Figures 34, 37). Duration of the main rhythms (no less than 10 thousand years) spans frequently 5–10 oscillations. The intervals of oscillations of D and I that are fixed

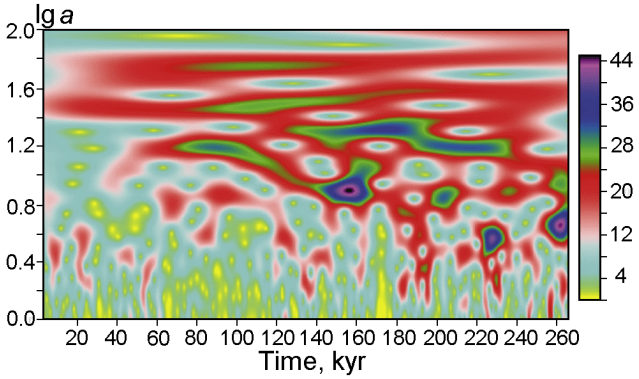

Figure 34. Wavelet diagram for the curve plotted in Figure 33b.

Table 17. Continued

D. Two Curie points, 556°C and 580°C. Inclination

Rhythm	Standard	"length"	Number of rhythms	Note
100–93	±4	1500–1700	2?	
89	±6	1240–1300	1?	
50	±3.5	1240–1340	2	
24–34	±3.5–12	1470–1700	8–9	bright
21–25	±4.5	1240–1310	3	
16–18	±2.5	1300–1430	7–8	weak (train?)
12–15	±4.5	1440–1590	10–11	bright
9–10	±3	1270–1640		5 splashes
6.3–7.2	±2	1300–1610		5 splashes
4.8–5.8		1300–1580		5 splashes

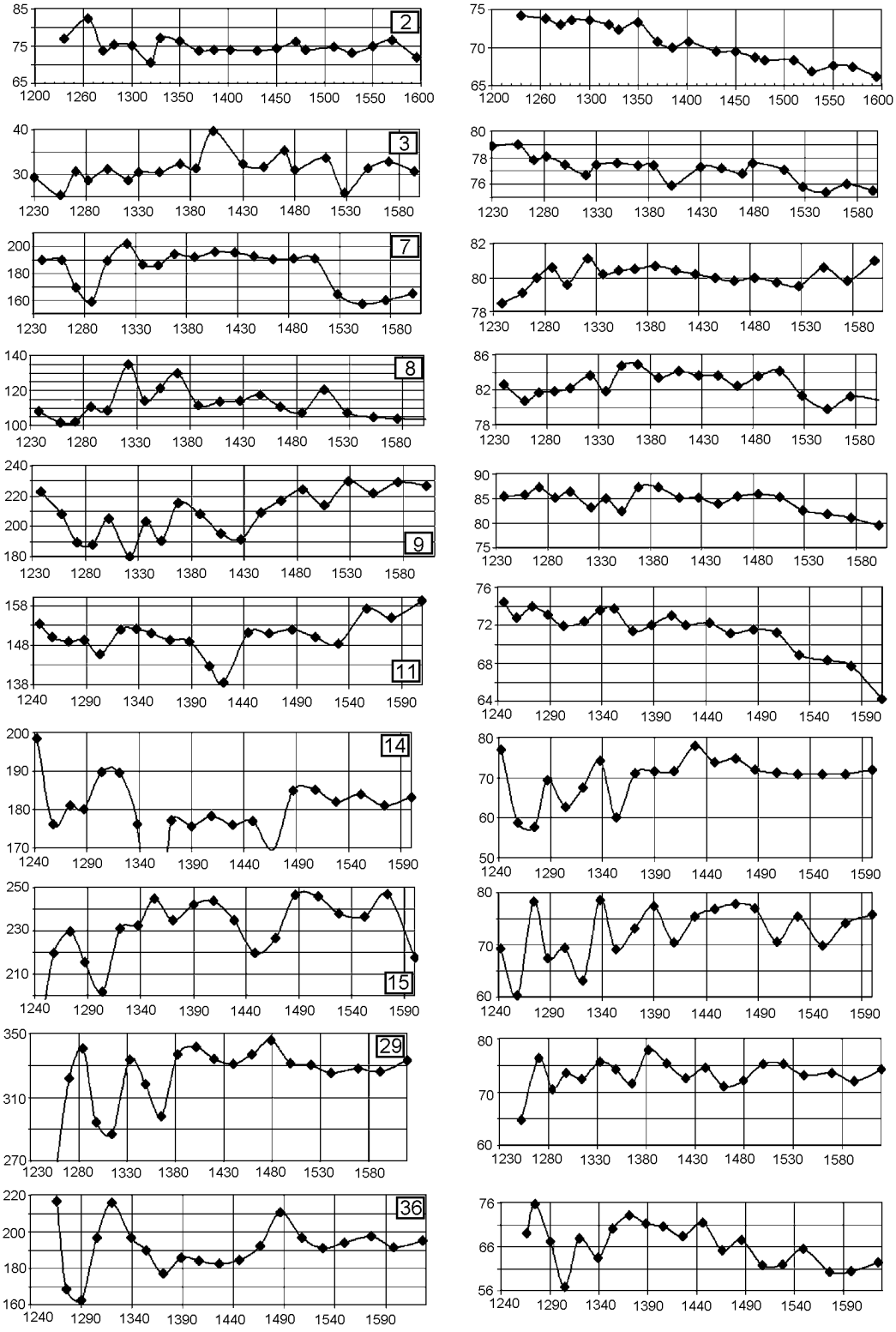

Figure 35. Behavior of declination and inclination of the field in the process of cooling of the Bushveld intrusion in each sample. Sample numbers are in rectangles.

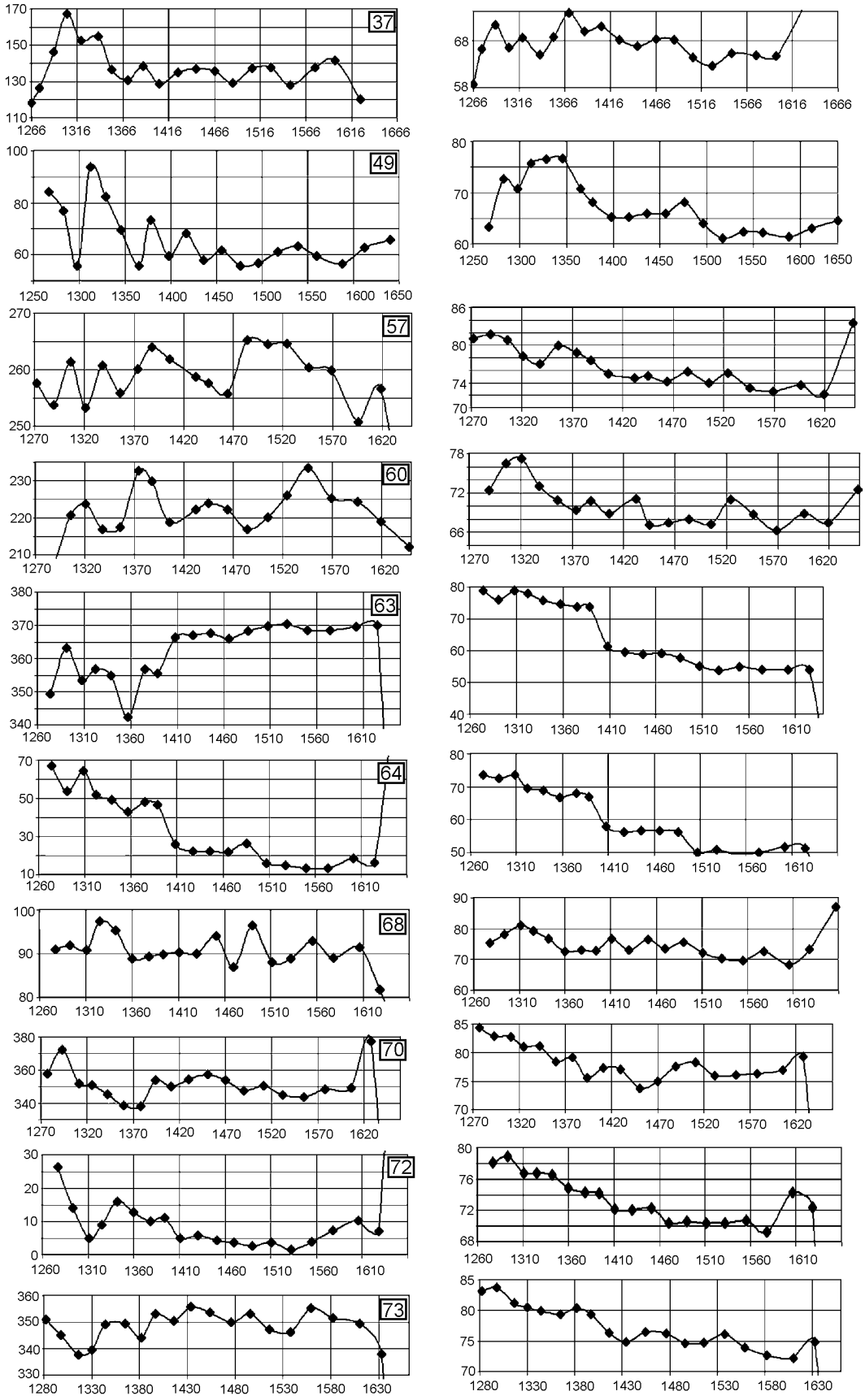

Figure 35. Continued.

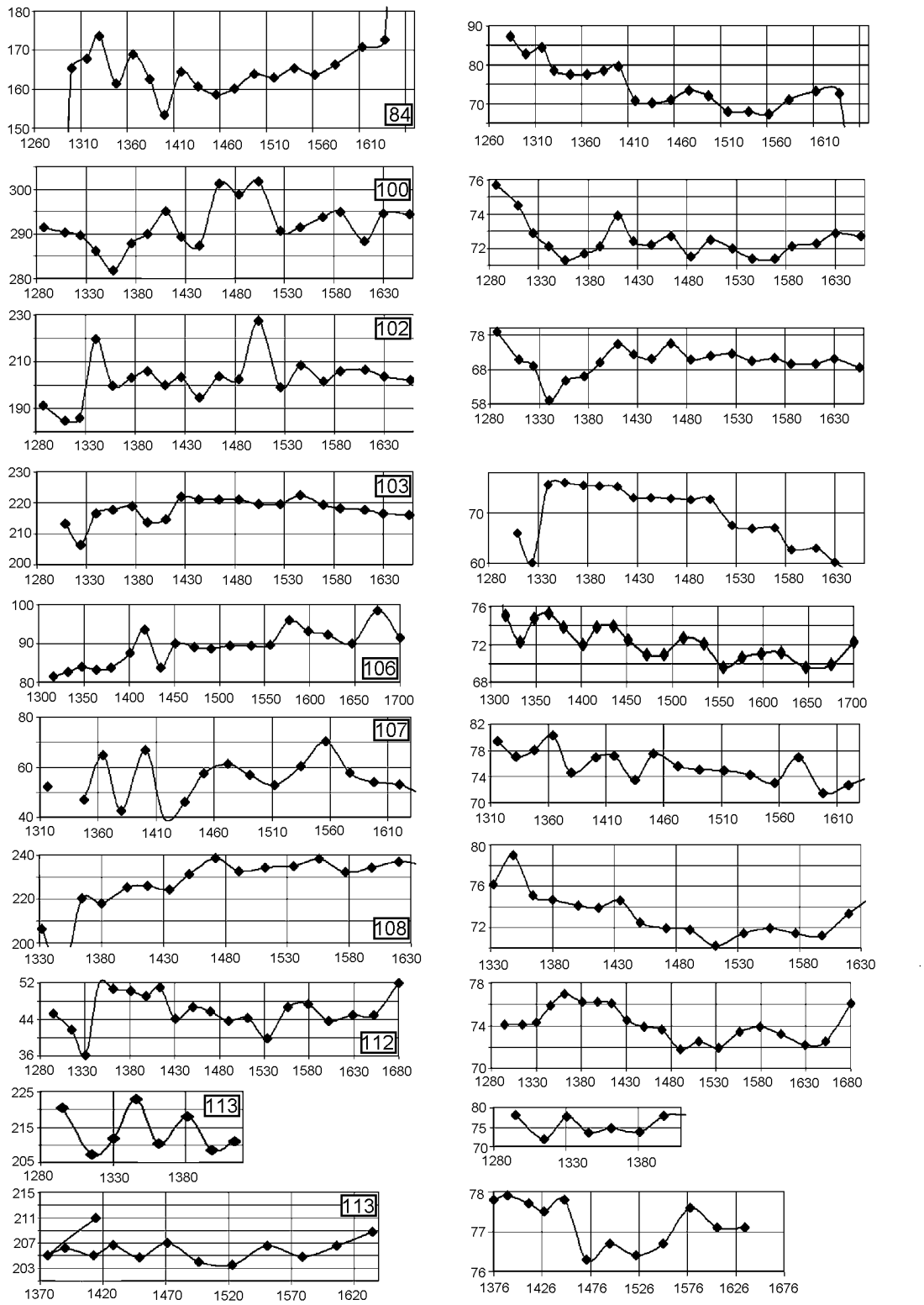

Figure 35. Continued.

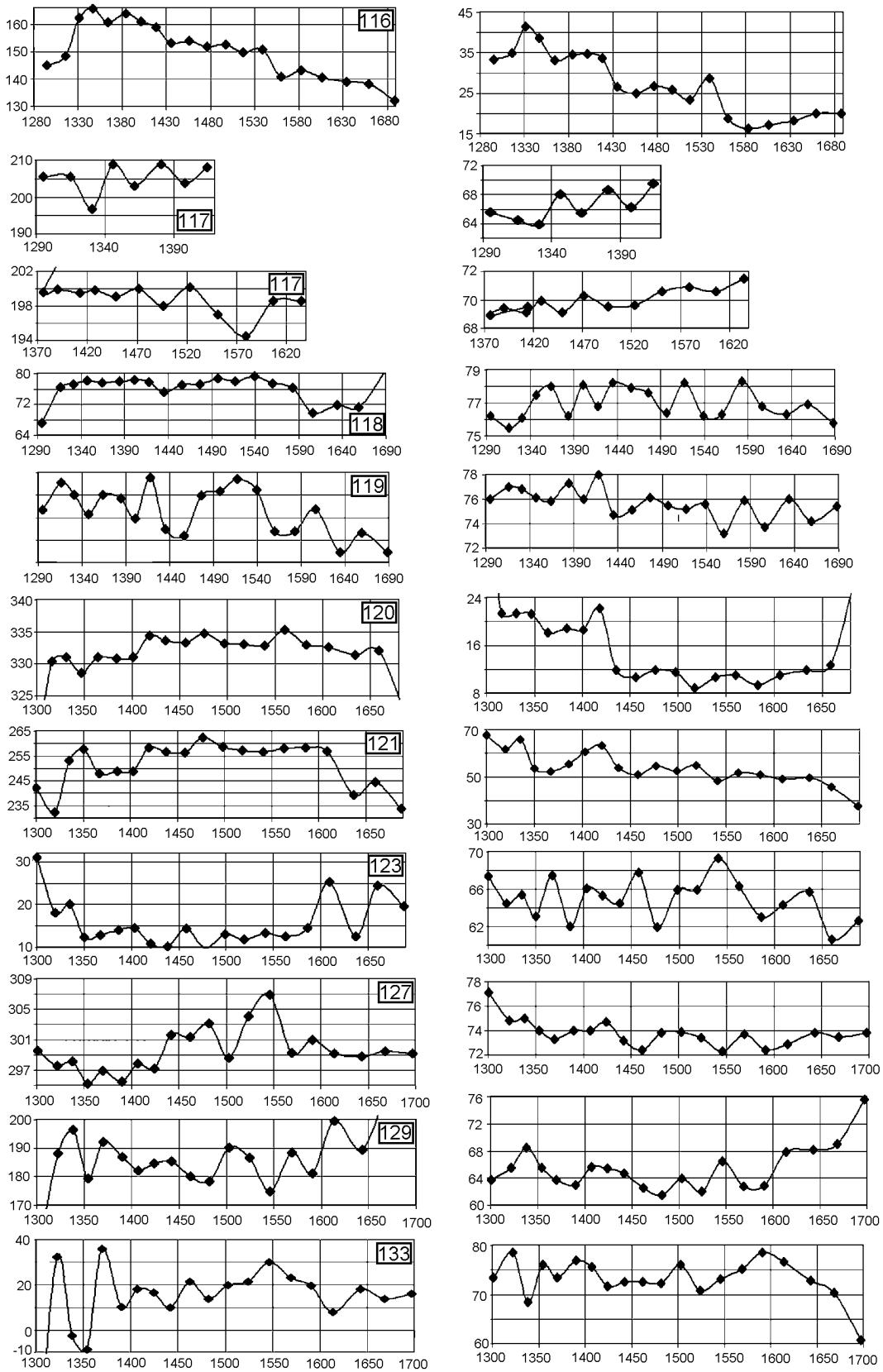

Figure 35. Continued.

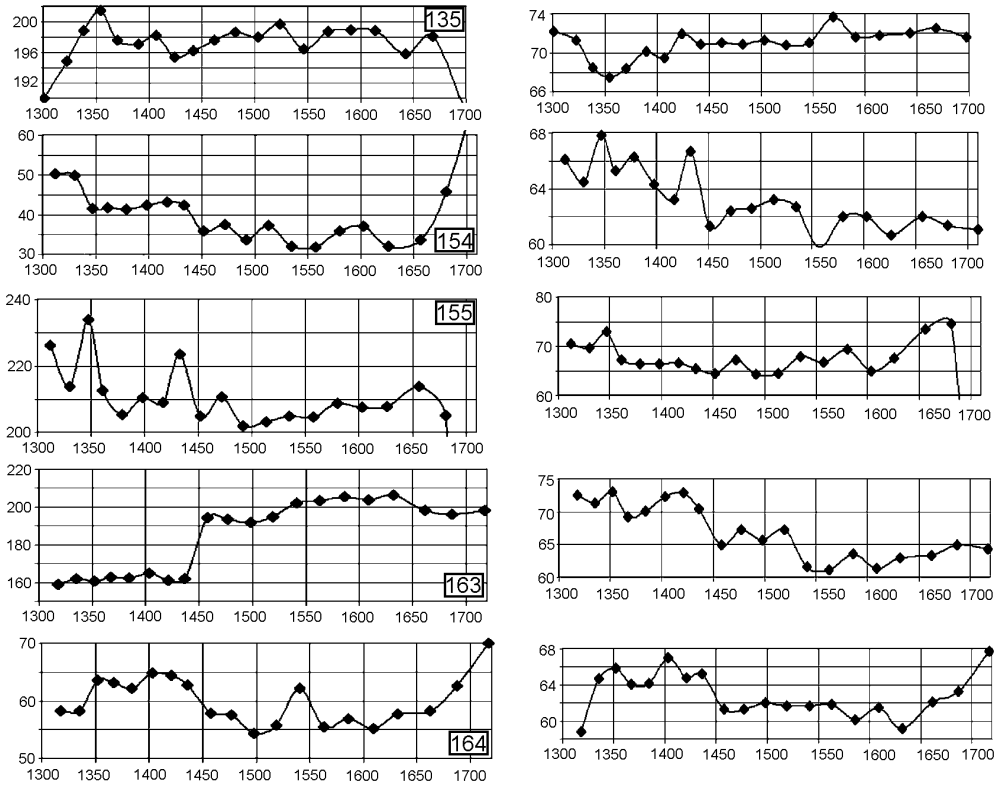

Figure 35. Continued.

on the wavelet diagrams (Figures 34 and 37) are confirmed by the maxima obtained by the maximum entropy method (Figure 38). However, as can be seen from comparison of Figures 37 and 38, the maximum entropy method fixes only the most intensive maxima of the oscillation amplitudes irrespective of whether it is a splash or a long oscillation, which is traced almost along the entire recording interval. In the last case the rhythm value is changing frequently with time, but the maximum entropy method is fixing the rhythm value with the maximum amplitude (for example, rhythm in Figure 37d is traced from 1440 kyr to 1590 kyr and changes during this period 12 kyr to 15 kyr years, whereas the maximum entropy method is fixing a rhythm of 12.5 kyr, relating to the maximum amplitude falling at 1480–1490 kyr; a similar situation is also for the rhythm of 24–34 kyr which is traced from 1480 kyr to 1660 kyr, a rhythm of 28 kyr with the maximum amplitude at 1640 kyr was fixed by the maximum entropy method etc.).

Conclusion

1. As a result of the paleomagnetic and petromagnetic study of the Monchegorsk, Kivakka and Bushveld intrusions we have shown for the first time that it is possible in principle to obtain a continuous record of the geomagnetic field behavior, fixed in the process of cooling of the gabbro-pyroxenite layered intrusions. Such intrusions are the most suited for this type of investigation: a) these are dry magmas, their cooling is in a conductive way, without participation of fluids which is simple to model knowing the main thermo-physical parameters, geometry and depth of forming the intrusion; it is possible to calculate temperature, time and velocity of cooling and this process is simple and homogenous at the cooling temperature below 600°C when the paleomagnetic recording begins; b) the mechanism of formation of magnetic minerals in the layered intrusions is known and is quite uniform – these are thin inclusions of the low-Ti titanomagnetites in plagioclases and pyroxenes as a result of a high-temperature exsolution of the latter; magnetites sealed in the silicates well preserved for billions of years and, accordingly, the paleomagnetic record is also retained. True, there is a certain difficulty here – the existing estimations of the plagioclase and pyroxene exsolution temperature with formation of the magnetite inclusions (550–600°C) are approximate. According to data of the thermo magnetic analysis and of the thermal demagnetization the low-Ti titanomagnetites are the main carriers of NRM in all the intrusions (T_c = 530–580°C). Usually their concentration is less than 0.1%. The NRM component acquired at the stage of cooling of the intrusion is thermoremanent and is distinguished

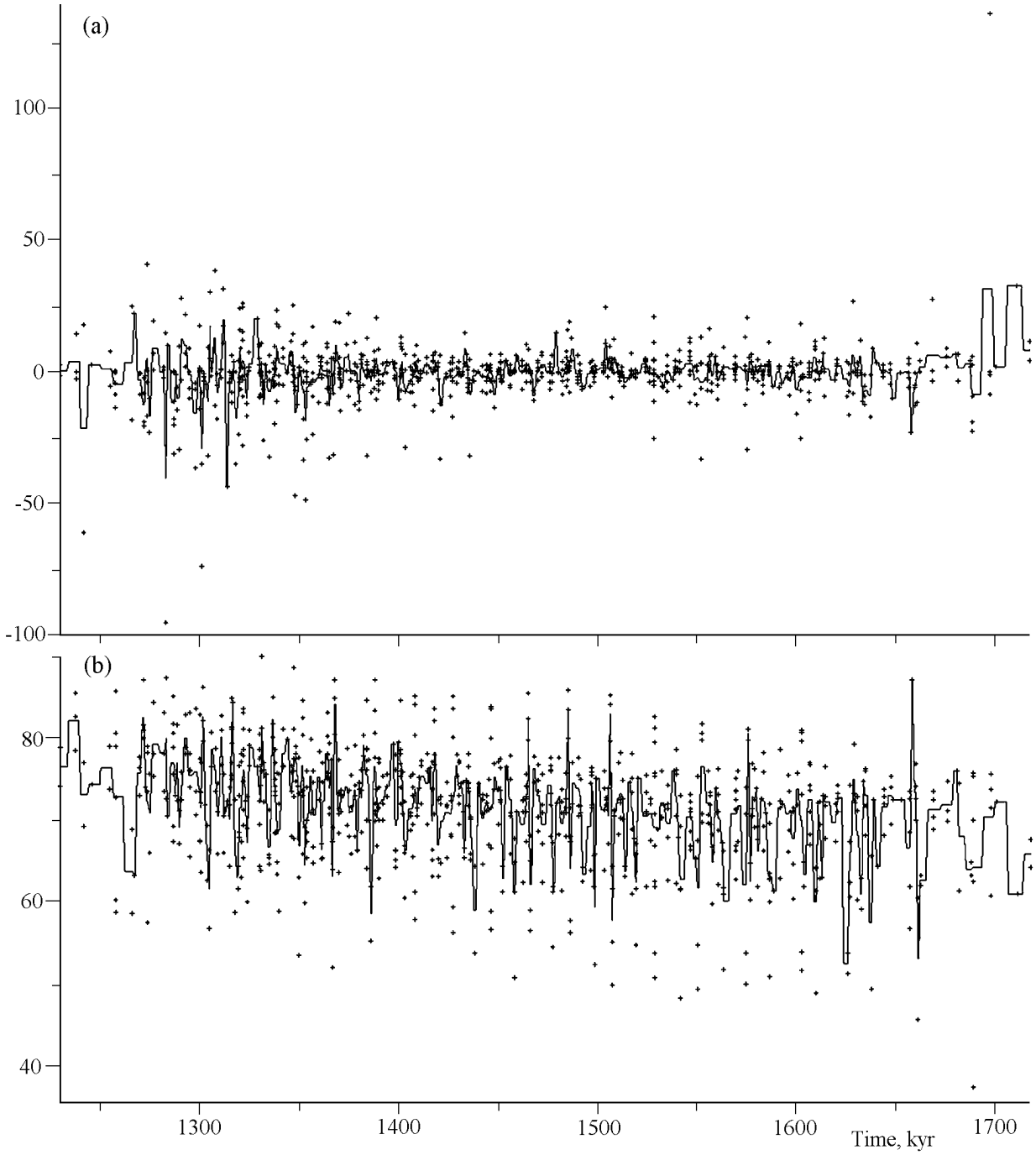

Figure 36. Behavior of declination (a, c) and inclination (b, d) of the field in the process of cooling of the Bushveld intrusion. The second variant of the record. a) Result of combining data of D for the first set of data (one Curie point is 580°C), after subtraction of the mean value from each sample. b) Result of combining data of I for the first set. c) Result of combining data of D for the second set (two Curie points, 556°C and 580°C), after subtraction of the mean value from each sample. d) Result of combining data of I for the second set. Points – initial data, line – result of averaging ($H = 0.25$) and transition to a uniform time step ($\Delta t = 0.5$).

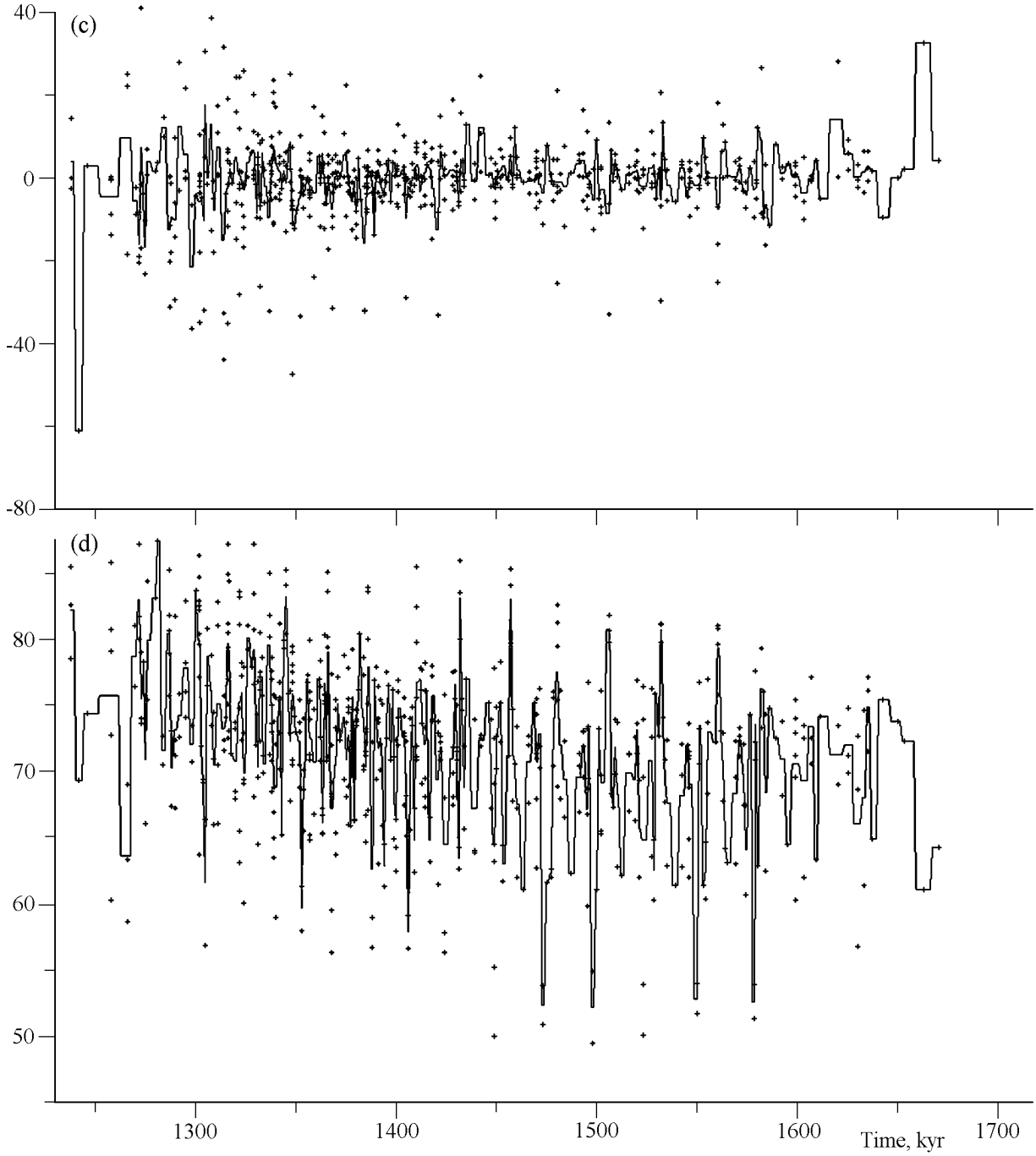

Figure 36. Continued.

by such characteristics as H_{cr}/H_c, J_{rs}/J_s, Q_n, shape of the curve $J_n(T)$, J_{rt}/J_{ri} and J_n/J_{ri} relationship the majority of samples above 500°C. Formation of a portion of titanomagnetites below their Curie points, i.e. below 520°C, which will acquire the crystallization remanent magnetization and partial thermoremanent magnetization during a further cooling is not ruled out. Calculations that we used refer only to a complete thermoremanent magnetization. It is not inconceivable that a similar effect is present in the objects studied by us and creates additional noise and biased errors.

2. We were reading the paleomagnetic record in two variants: a) *first variant* – a detailed sampling from the contact deep into the body, the isotherm of the Curie point of magnetic minerals present in the body shifts at different stages of cooling from the contact deep into the body or vice versa; b) *second variant* – a detailed thermal demagnetization of

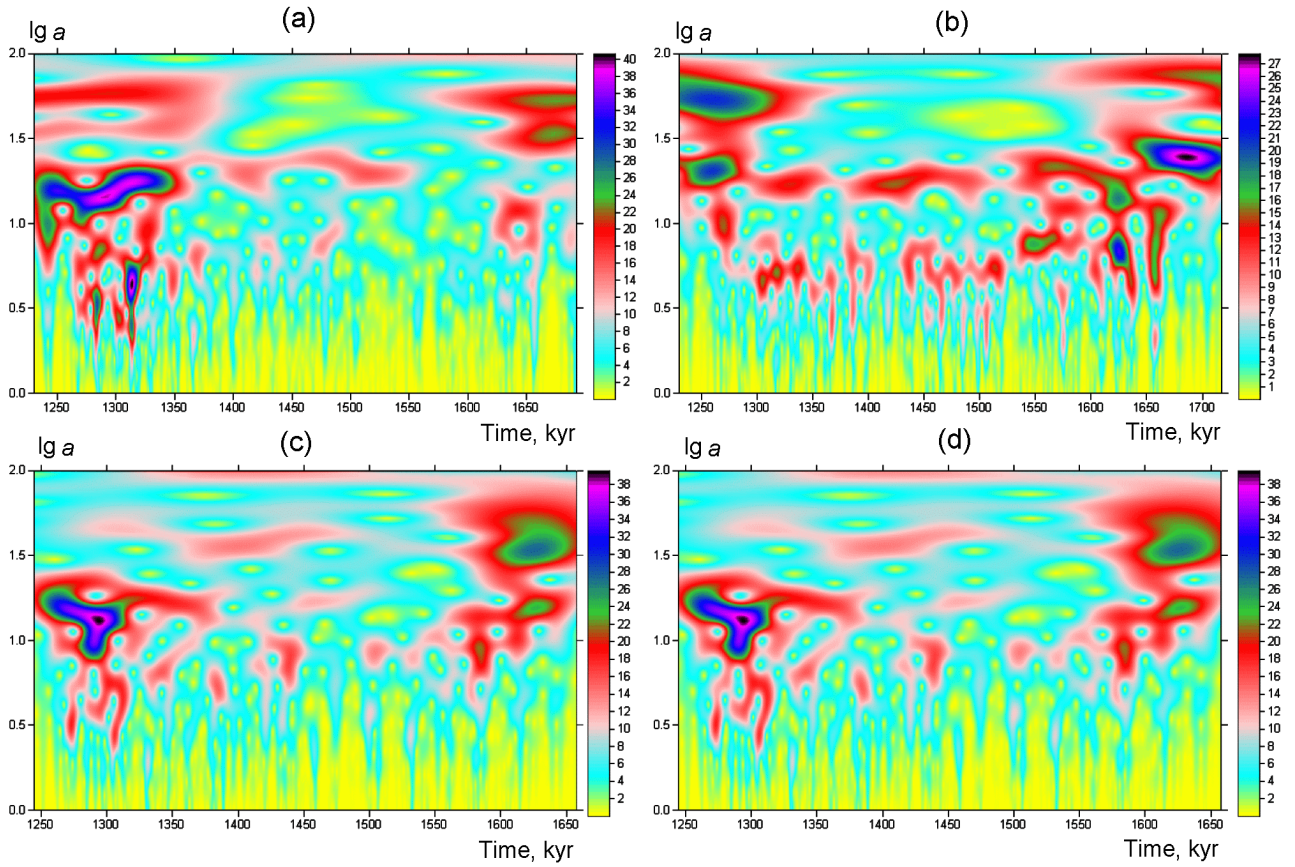

Figure 37. Wavelet diagrams of behavior of declination and inclination of the geomagnetic field in the process of cooling of the Bushveld intrusion. The second variant of the record. a) Wavelet diagram for D of the first set of data (one Curie point is 580°C), after averaging and transition to a uniform time step, a final part of data (after 1692.5 kyr) is excluded from processing due to strong peaks. b) Wavelet diagram for I from the first set of data after averaging and transition to a uniform time step and removal of a general linear trend. c) Wavelet diagram for D of the second set of data (two Curie points, 556°C and 580°C), after averaging and transition to a uniform time step, initial and final parts of data are excluded from processing due to strong peaks. d) Wavelet diagram for I of the second set of data after averaging and transition to a uniform time step and removal of a general trend by the 3rd order polynomial. Lga – logarithm of the time scale (period).

every sample permits to read the record of the geomagnetic field behavior in the process of cooling of the magmatic body at the sampling point from the Curie point of the magnetic mineral which is present in it to the blocking temperature at which a significant share of the thermoremanent magnetization can be still fixed within the range of accuracy of measurement. As a result of the petromagnetic study we have found that an appreciable and sometimes a considerable share of the ensemble of the magnetic grains are multidomain grains. Thermal demagnetization of such grains is close to their Curie points. This is of no significance for obtaining the first variant of recording. As to the second variant, due to the above reason it becomes possible to fix, as a rule, the record of the magnetic field behavior only above 500°C, and more frequently, above 540°C, when contribution of the single-domain and pseudosingle-domain magnetic grain contribution in the NRM begins to prevail. Hence, in case of magnetite (T_c = 580°C) with the thermal demagnetization step of 5° less than 10 points are obtained and this, of course, is insufficient for analysis of the record. Even the step of 3° will not save the situation. We had to average results on many samples to improve reliability. It is necessary to have a step of maximum 1° for the thermal demagnetization for which purpose a high-quality temperature control, a very high temperature uniformity and a high-quality shielding of the external magnetic field will be required. Even this 1° step does not ensure a *continuous recording*, both of our recording variants are *discrete* (in the first variant samples were taken from the Monchegorsk intrusion every 1–2 m that makes 100 years; in case of the Bushveld intrusion, 1 m of the section represents more than 500 years), though the process of cooling of the intrusion is undoubtedly continuous and, consequently, ensures a continuous paleomagnetic record. It is necessary to conduct a *continuous* thermal de-

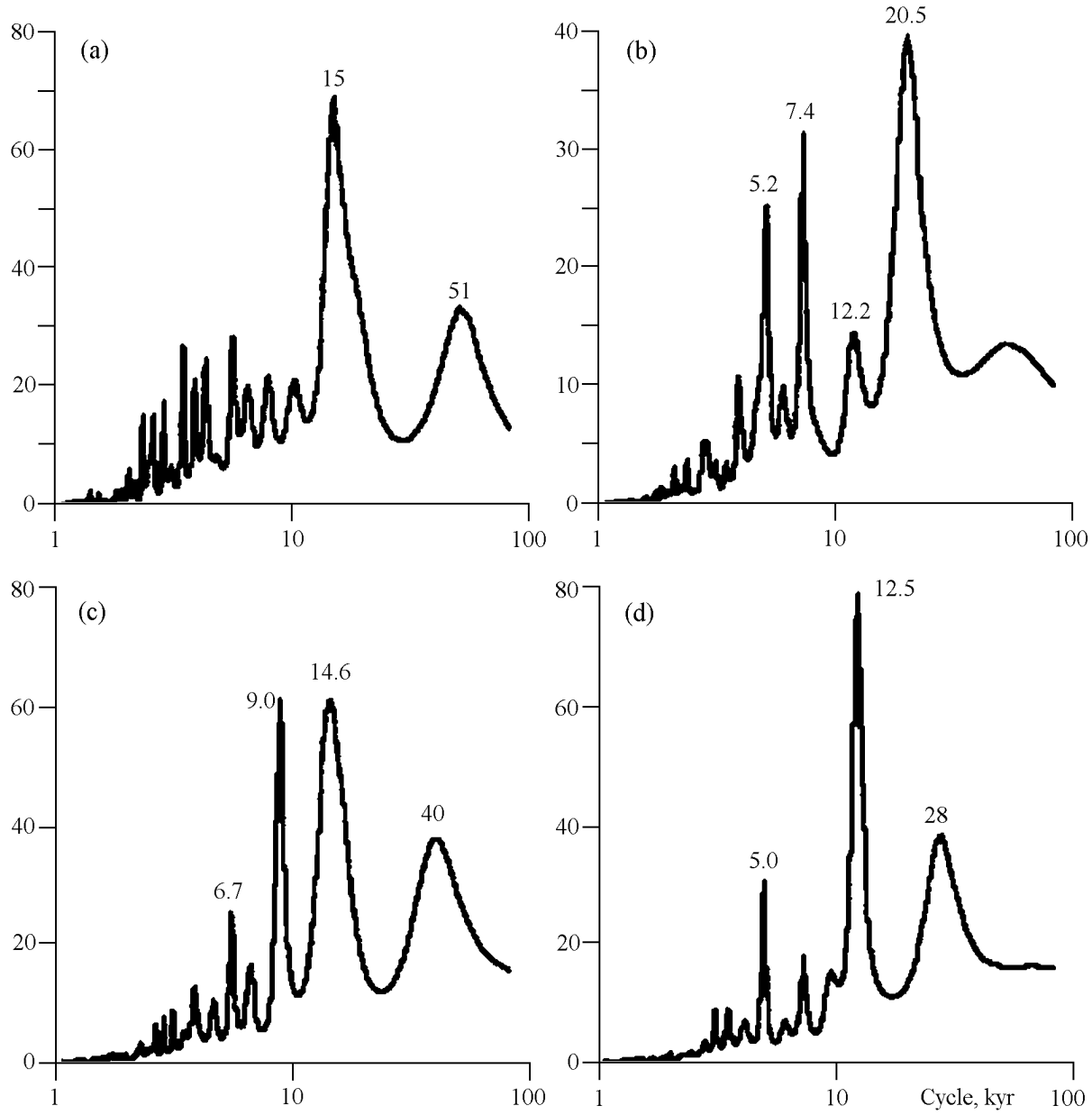

Figure 38. Spectra of power (maximum entropy method, $AR_{order} = 80$) of signals after averaging and transition to a uniform time step. (a) and (b) – D and I of the first set of data (one Curie point); (c) and (d) – D and I of the second set of data (two Curie points), after exclusions or peripheral intervals with peaks or of general trends (see Figure 37).

magnetization of the samples and this is now possible due to the fact that Yu. K. Vinogradov (Borok Observatory) developed a three-component thermomagnetometer performing a continuous recording automatically.

A more thorough sampling must be done for the first variant of the paleomagnetic recording, but even in this case the method will remain discrete.

Temperature accuracy determination is of great importance. In our experiments a 1° error in setting temperature in the furnace, in determination of the Curie point, in conversion of unblocking temperature during thermal demagnetization into blocking temperature during cooling of the intrusion etc. amounts to about 400 years in the most rapidly cooled Kivakka intrusion, 1000 years in the Monchegorsk intrusion and 3000 years in the larges Bushveld intrusion! Hence we have appreciable scatter in the time series of D, I, both in the first and in the second variants of the record.

In general, the second variant of obtaining the paleomagnetic record is more informative and efficient: a) it does not require a strict sampling across thickness of the body,

it is sufficient to select the unaltered localities (for example, great gaps appeared in the first variant of the paleomagnetic record due to the secondary alterations in the Kivakka intrusion), however, the intrusion must be a single uniformly cooled body (for modeling the cooling process); b) free choice of the sampling area and pieces of the unaltered rocks containing homogeneous magnetic minerals by composition, that is expressed in one or definitely prevailing Curie temperature, and in prevalence of the single-domain grains. All this almost impossible to observe in the first variant of obtaining the record; c) non-oriented samples can be used as it is possible to obtain relative alterations of the field direction as, for example, in the case of the Bushveld intrusion, where we were dealing with the specimens from the core which were not oriented in the horizontal plane, and obtained information about relative alterations of the paleomagnetic declination.

3. The secondary alterations appreciably distort the primary recording down to its complete destruction. We do not dwell on such phenomena as viscous remagnetization that is removed easily by thermal demagnetization. Naturally, so ancient formations as Early Proterozoic layered intrusions could not avoid various secondary phenomena during their long life such as heating, metamorphism, tectonic deformations etc., which had an effect on preservation of the primary record. Partly this is eliminated by the choice of the objects of the study. Thus, the whole blocks are preserved perfectly in the intrusions under study as was mentioned above (item 1). Samples for our studies were taken from such blocks. However, despite the choice of the objects, two out of three intrusions (Monchegorsk and Kivakka) were subjected to a considerable secondary heating (evidently, up to 400–500°C), which has sharply reduced the interval of the primary paleomagnetic record and even completely destroyed it here and there. This heating is dated to the Svecofennian tectonomagmatic activity (judging from the paleomagnetic data, age of this activity is 2–1.9 Ga).

4. Despite the difficulties listed above (it. 1–3), we succeeded in obtaining for the first time certain information about the state of the geomagnetic field in the process of cooling of three Early Proterozoic intrusions. Duration of the record obtained is ∼30–40 kyr (Kivakka intrusion), ∼70 kyr (Monchegorsk intrusion) and ∼400 kyr (Bushveld intrusion). From the viewpoint of magnetostratigraphy the record is characterized presence of chrons and subchrons of opposite polarity with duration of hundreds of thousand years to several dozens of thousand years; an excursion which lasted less than 2 thousand years has been fixed. A wavelet analysis was used to study the spectrum of the geomagnetic field variations peculiarities of their behavior in time (alteration of amplitude and rhythm in time, stability and duration of oscillations etc.). The spectra of variation recorded in the process of cooling of three intrusions are given in Figure 39. The spectra of record of three intrusions have both similarity and an appreciable difference comparable with one another, though the Monchegorsk and the Kivakka intrusions are older than the Bushveld intrusion by about 400 Ma and are located at a huge distance from it. The latter is not surprising if we recollect that even during the recording (dozens and hundreds of thousands years) some rhythms disappear and some appear, and the rhythm values vary in time. Duration of the rhythms varies from 1–2 oscillations (splashes) up to more than 10. For 50 million years and all the more for 400 million years (the age difference of the Monchegorsk, Kivakka and Bushveld intrusions) the spectrum of variations could have changed considerably. Besides, the distinguished rhythms have standard deviations, which exceed, as a rule, 1 thousand years; the technical errors (it. 2 of the Conclusion) are increasing the possible scatter of the results. At the same time, the spectra are comparable with one another.

Let us sum up all histograms of all three intrusions, declination and inclination, all variants of obtaining the records; to be more correct, let us calculate the average rhythms by intervals (Figure 40). As a result, the modes of stable oscillations: 3.2; 4; 4.4–4.7; 5; 5.5; 7; 7.5; 8–10; 14–15(?); 17.5–18.5; 20(?), 30–40, 52–64 and 90–100 are distinguished against a background of a uniform noise caused by a combination of actual short "splashes" (1–3 oscillations) and instability of rhythms in time plus errors in assessment of temperature and time (Figure 40). The last two rhythms 52–64 and 90–100 kyr are fixed only in a long record of the Bushveld intrusion. On the other hand, there are practically no rhythms below 5 thousand years in the record of the Bushveld intrusion, whereas rhythms of 2–3–4 thousand years a definitely observed in records of the Monchegorsk and Kivakka intrusions. However, accuracy in determination of the value of these rhythms is not reliable.

The pointed out features of the geomagnetic field behavior do not differ in principle from characteristics of the geomagnetic field in the Recent Cenozoic era. Hence, by the beginning of Proterozoic the liquid core of the Earth, which generates the geomagnetic field, was formed and was further changing insignificantly.

5. Let us point to some standard paleomagnetic results. The *Monchegorsk intrusion.* A paleomagnetic pole 265.3°E, 1.3°N, has been determined, which differs appreciably from APWP of the Baltic shield that is associated with the tectonic clockwise rotation through ∼ 30° and a tilt of the intrusion by 15°–20° to NW. The *Kivakka intrusion.* The prefolded component A_1 and synfolded/afterfolded component A_2 that were acquired at the stage of cooling of the intrusion are distinguished in the process of the thermal demagnetization of the samples. Judging by the trend of inclination, tilting of the body by 36° began approximately 85 thousand years after emplacement of the intrusion and it lasted for 20–25 thousand years. Position of the pole of the A_1 component in the stratigraphic system of coordinates (17.8°S and 247°E) is close to the mean coordinates of Fennoscandia pole of a similar age (they coincide after rotation of the intrusion through 30° counterclockwise). A great scatter of the paleomagnetic directions, first of all, is associated with an incomplete separation of the A_1 and A_2 components during the thermal demagnetization. The *Bushveld intrusion.* Orientation of the horizontal plane of the samples was restored on the basis of the viscous magnetization and from the high-temperature N-component of NRM we determined a mean paleomagnetic direction and a pole (12°N, 35.4°E), which coincides practically with the pole that was defined from the oriented samples of similar rocks taken from the

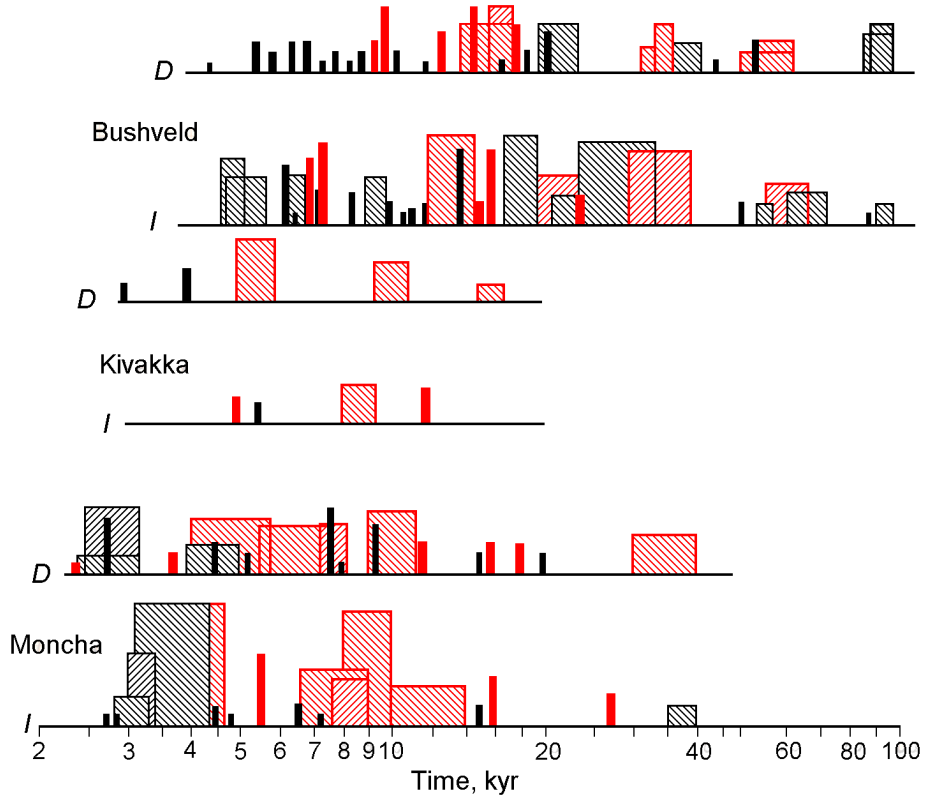

Figure 39. Summary of spectra of variations of the geomagnetic field direction in the process of cooling of the Bushveld, Kivakka and Monchegorsk intrusions. Results of the wavelet analysis (see Tables 10, 14, 16 and 17). Black bars are rhythms of oscillations of D and I. Crosshatched rectangles are intervals of rhythms changed in time. Height of the bars and rectangles reflects the number of oscillations (or the number of splashes) of one rhythm. Different methods of obtaining the paleomagnetic record are marked in different hatching. The most striking rhythms with the highest amplitude are marked with red.

natural outcrops [*Hattingh,* 1986a]. A tilt similar to that of the Kivakka intrusion has been noted at the stage of cooling of the Bushveld intrusion. Its angle is about 15° and it occurred after the normal polarity of the geomagnetic field has changed. Rotation of blocks, including the Monchegorsk and Kivakka intrusions (or their part) about the vertical axis occurred after tilting of the bodies but before their secondary heating.

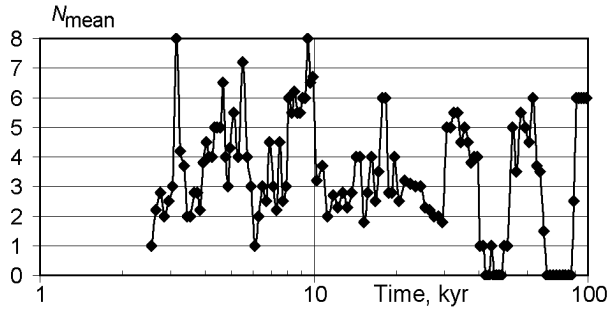

Figure 40. Results of the interval averaging of histograms Figure 39. Up to 20 kyr – average values on 6 histograms, from 20 kyr to 40 kyr – average values on 4 histograms (the Kivakka record is short and it does not cover the rhythms of 20 kyr and more); more than 40 kyr these are average values on 2 histograms (only Bushveld).

Acknowledgments. The authors would like to express their gratitude to V. N. Dech and S. R. Kotov for presenting a collection of specimens from the core of well WP-16; A. V. Shatsillo and D. M. Khvorov for their help in selection of the oriented samples from the Monchegorsk and Kivakka intrusions; M. V. Borisov, S. V. Bolikhovskaya, E. V. Koptev-Dvornikov, D. M. Khvorov, A. V. Chistyakov and E. V. Sharkov for their consultation and presentation of the geological and other materials; S. Kornev, Z. V. Sharonova and G. S. Yanova for their help in the paleomagnetic and petromagnetic measurements. This work was done due to a financial support of the RFFI, Grant no. 01-05-64240.

References

Amelin, Yu. V., L. M. Heaman, and V. S. Semenov (1995), U-Pb geochronology of layered intrusions in the eastern Baltic Shield: implications for the timing and duration of Paleoproterozoic continental rifting, *Precambrian Res., 75,* 31–46.

Amelin, Yu. V., and V. S. Semenov (1996), Nd and Sr isotope geochemistry of the mafic layered intrusions in the eastern Baltic shield: implications for the sources and contamination of Paleoproterozoic continental mafic magmas, *Contrib. Mineral. Petrol., 124,* 255–272.

Balashov, Yu. A., T. B. Bayanova, and F. P. Mitrofanov (1993), Isotope data on the age and genesis of layered intrusions in the Kola peninsula and Northern Karelia, northeastern Baltic shield, *Precambrian Res., 64,* 197–205.

Berk, K., J. F. Dewy, and U. S. F. Kidd (1980), Domination of horizontal movements, island arc and microcontinental collisions during the Later Permobile stage, *Recent history of the Earth* (in Russian), 620 pp., Mir, Moscow.

Buchanan, P. C., and W. U. Reimold (1998), Studies of the Rooiberg group, Bushveld complex, South Africa: No evidence for an impact origin, *Earth Planet. Sci. Lett., 155,* 149–165.

Buick, I. S., R. Maas, and R. Gibson (2001), Precise U-Pb titanite age constrains on the emplacement of the Bushveld Complex, South Africa, *J. Geol. Soc. London, 158*(1), 3–6.

Buiko, A. K., O. A. Levchenko, S. I. Turchenko, and E. P. Drubetskoi (1995), Geologu and isotopic dating of the Early Proterozoic Sumisko-Sariolian complex, North Karelia, *Stratigraphy, Geologic correlation, 3*(4), 16–30.

Cawthorn, R. G., and F. Walraven (1998), Emplacement and Crystallization Time for the Bushveld Complex, *J. Petrol., 39*(9).

Chui, C. K. (1992) *An Introduction to Wavelets,* Academic Press, San Diego, CA (Translation into Russian: Chui Ch., An Introduction to Wavelets, 412 pp., Mir, Moscow, 2001.).

Coe, R. S., and M. Prevot (1989), Evidence suggesting extremely rapid field variation during a geomagnetic reversal, *Earth Planet. Sci. Lett., 92,* 292–298.

Coe, R. S., M. Prevot and P. Camps (1995), New evidence for extraordinarily rapid change of the geomagnetic field durung reversal, *Nature, 374,* 687–692.

Crouzet, C., P. Rochette, and G. Menard (2001a), Experimental evaluation of thermal recording of successive polarities during uplift of metasediments, *Geophys. J. Int., 145,* 771–785.

Crouzet, C., H. Stang, E. Appel, E. Schill, and P. Gautam (2001b), Detailed analysis of successive pTRMs carried by pyrrhotite in Himalayan metacarbonates: an example from Hidden Valley, Central Nepal, *Geophys. J. Int., 146,* 607–618.

Crouzet, C., M. Fuller, I. Williams, H. Ito, V. A. Schmidt, and Yu. Wu (1978), Palaeomagnetic record of a late Tertiary field reversal, *Geophys. J. R. Astron. Soc., 53,* 373–412.

Daubechies, I. (1992), Ten Lectures on Wavelets, no. 61 in CBMS-NSF Series in Applied Mathematics, SIAM, Philadelphia (Translation into Russian: Daubechies I., Ten lectures on wavelets, 464 pp., 2001.).

Day, R., M. Fuller, and V. A. Schmidt (1977), Hysteresis properties of titanomagnetites: grain size and composition dapendence, *Phys. Earth Planet. Inter., 13,* 260–267.

Dodson, M. H., J. R. Dunn, M. Fuller, I. Williams, H. Ito, V. A. Schmidt, and Yu. Wu (1978), Palaeomagnetic record of a late Tertiary field reversal, *Geophys. J. R. Astron. Soc., 53,* 373–412.

Dodson, M. Y., and E. McClelland-Brown (1980), Magnetic blocking temperatures of single domain grains during slow cooling, *J. Geophys. Res., 85,* 2625–2637.

Dudarev, A. N., V. A. Kudryavtsev, V. G. Melamed, and V. N. Sharapov (1972), *Heat Exchange in Magmatogene Processes* (in Russian), 124 pp., Nauka, Novosibirsk.

Dunlop, D. J. (2002), Theory and application of the Day plot (M_{rs}/M_s versus H_{cr}/H_c), *J. Geophys. Res., 107*(B3), doi:10.1029/2001JB000487.

Eales, H. V., and R. G. Cawthorn (1996), The Bushveld Complex, in *Layered intrusions,* edited by R. G. Cawthorn, pp. 181–229, Elsevier Science.

Ein, A. S., and S. Ya. Sokolov (2000), Paleomagnetizm of the north Karelia basites, *Materials of the conference "Riftogenesis magmatism and metallogeny of Pre-Cambrian, Correlation of geological complexes of Fennoscandia"* (in Russian), pp. 47–49, Petrozavodsk.

Elming, S. A., L. J. Pesonen, M. Leino, A. N. Khramov, N. P. Mikhailova, A. F. Krasnova, S. Mertanen, G. Bylund, and M. Terho (1993), The continental drift of Fennoscandia and Ukraina during the Precambrian, *Tectonophysics, 223,* 177–198.

Engelbrecht, J. P. (1990), Contact metamorphic processes related to the aureole of the Bushveld Complex in the Marico District, western Transvaal, South Africa, *S. Afr. J. Geol., 93*(2), 339–349.

Enkin, R. J. (1994), A computer program package for analysis and presentation of palaeomagnetic data, *Pacific Geoscience Centre, Geol. Survey Canada, Sidney,* 16 p.

Hardle, W. (1989), *Applied nonparametric regression,* 349 pp., Cambridge University Press, Cambridge, New York, New Rochell, Melbourne, Sydney.

Hattingh, P. J. (1986a), The palaeomagnetism of the main zone in the western Bushveld Complex, *Earth Planet. Sci. Lett., 79,* 441–452.

Hattingh, P. J. (1986b), The palaeomagnetism of the main zone in the eastern Bushveld Complex, *Tectonophysics, 124,* 271—296.

Hattingh, P. J. (1989), The palaeomagnetism of the upper zone of the Bushveld Complex, *Tectonophysics, 165,* 131–142.

Hattingh, P. J., and N. D. Pauls (1994), New palaeomagnetic results from the northern Bushveld Complex of South Africa, *Precambrian Res., 69,* 229–240.

Khramov, A. N., M. A. Fedotova, B. N. Pisakin, and A. A. Priyatkin (1997), Paleomagnetism of Early Proterozoic intrusions and associated rocks of Karelia and Kola peninsula: contribution into development of Pre-Cambrian evolution model of the Russian-Baltic craton, *Fizika Zemli* (in Russian), (6), 24–41.

Khvorov, D. M., and A. Azzuz (2003), Phase relations of high-magnesian basalts: equilibrium of melt-olivine-orthopyroxene, *Geokhimiya* (in Russian), (8), 847–865.

Khvorov, D. M., E. V. Koptev-Dvornikov, and Ya. V. Bychkova (2000), Reconstruction of shape of the Kivakka layered intusion, *Obschie problemy petrologii* (in Russian), (1), 224–227, Syktyvkar.

Kogarko, L. N. (1995), *Alkaline rocks and carbonatites of the world,* Pt 2: Former USSR. Chapman, Hill, London.

Koptev-Dvornikov, E. V., B. S. Kireev, N. F. Pchelintseva, and D. M. Khvorov (2001), Distribution of cumulative paragenesises, rock forming and secondary elements in a vertical section of the Kivakka intrusion (Olang group of intrusions, Northern Karelia), *Petrologia* (in Russian), *9,* 3–27.

Kozlov, E. K. (1973), *Natural Series of Nickel Bearing Intrusions and Their Metallogeny* (in Russian), 288 pp., Nauka, Leningrad.

Krasnova, A. F., and E. G. Gooskova (1995), Palaeomagnetism of Precambrian basic intrusion and dykes of Northern Karelia, eastern Fennoscandian Shield, *Precambrian Res., 74,* 245–252.

Lavrov, M. M. (1979), *Pre-Cambrian ultrabasites and layered peridotite-gabbro-norite intrusions of the Northern Karelia* (in Russian), 79 pp., Nauka, Leningrad.

Levchenkov, O. A., A. A. Nikolaev, E. S. Bogomolov, and S. Z. Yakovleva (1994), Uranium-lead age of Sumia acid magmatites of Norhern Karelia, *Stratigrafia, Geologicheskaya korrelatsia* (in Russian), (2(1)), 3–9.

Mallat, S. (1998), *A wavelet tour of signal processing,* 577 pp., Academic Press. San Diego, London, Boston, N.Y., Sydney, Tokyo, Toronto.

Mertanen, S. (1995), Multicomponent remanent magnetizations reflecting the geological evolution of the Fennoscandian shield – a palaeomagnetic study with emphasis on the Svecofennian orogeny, *Geol. Surv. Finland, Espoo,* p. 46.

Mertanen, S., L. J. Pesonen, H. Huhma, and M. A. H. Leino (1989), Palaeomagnetism of the early Proterozoic layered intrusions, Northern Finland, *Geol. Surv. Finland, 347,* p. 40.

Mertanen, S., H. C. Halls, J. I. Vuollo, L. J. Pesonen, and V. S. Stepanov (1999), Paleomagnetism of 2.44 Ga mafic dykes in Russian Karelia, eastern Fennoscandian Shield – implications for continental reconstructions, *Precambrian Res., 98,* 197–221.

Nguen, T., and D. M. Pechesky (1985), Indications of crystallization remanent magnetization of the magnetite containing

rocks obtained experimantally, *Izv. AN SSSR, Fizika Zemli* (in Russian), (8) 48–62.

Nguen, T., and D. M. Pechesky (1987), Indications of chemical magnetization of magnetite formed during unmixing of titanomagnetite, *Izv. AN SSSR, Fizika Zemli* (in Russian), (5), 69–76.

Pechersky, D. M., K. S. Burakov, V. N. Vadkovsky, E. V. Sharkov, V. S. Zakharov, and Z. V. Sharonova (2002), Possibility of obtaining Early Proterozoic record of fine structure of the geomagnetic field: preliminary analysis of results of petromagnetic and paleomagnetic study of the Monchegorsk pluton, *Fizika Zemli* (in Russian), (6), 57–70.

Pechersky, D. M., K. S. Burakov, V. S. Zakharov, and E. V. Sharkov (2004), Behavior of geomagnetic field direction during cooling of the Monchegorsk pluton, *Fizika Zemli* (in Russian), (5), 64–85.

Pullaiah, G., E. Irving, K. L. Buchan, and D. J. Dunlop (1975), Magnetization changes caused by burial and uplift, *Earth Planet. Sci. Lett., 28,* 133–143.

Rochette, P., G. Menard and R. Dunn (1992), Themochronometry and cooling rates deduced from single sample records of successive magnetic polarities during uplift of metamorphic rocks in the Alps (France), *Geophys. J. Int., 108,* 491–501.

Saltikova, T. E. (1991), Geological Evolution of North Karelia, in *Deep fractures in the Paanajarvi–Kuusamo–Kuolajarvi area, Geological Survey of Finland,* no. 13, edited by A. Silvennoinen, pp. 11–17.

Scherbakov, V. P., and V. V. Scherbakova (2002), Errors in determination of paleodirections – domain structure of the rock ferromagnetic grains relationship, *Fizika Zemli* (in Russian), (5), 57–64.

Schoenberg, R., F. J. Kruger, and J. D. Kramers (1998), The formation of the PGE bearing Bushveld chromitites and the Merensky Reef by magma mixing: a combined Re-Os and Rb-Sr study, *Mineral. Mag, 62A,* (Goldschmidt Conference 1998, Toulouse), 1349–1350.

Sharkov, E. V. (1980), *Petrology of the layered intrusions* (in Russian), 183 pp., Leningrad.

Sharkov, E. V., V. F. Smol'kin, and I. S. Krasivskaya (1997), Early Proterozoic magmatic province of the high-magnesian boninite-like rocks in the eastern part of the Baltic shield, *Petrologia* (in Russian), *5,* 503–522.

Sholpo, L. E. (1977), *Use of the rock magnetism when solving geological problems* (in Russian), 182 pp., Nedra, Leningrad.

Silvennoinen, A. (1991), General geological setting and deep fracture structures in the Kuusamo–Kuolajärvi–Paanajärvi area, in *Deep fractures in the Paanajärvi–Kuusamo–Kuolajärvi area, Geol. Survey of Finland,* no. 13, edited by A. Silvennoinen, pp. 5–10.

Thermal field of the Europe (in Russian) (1982), 376 pp., Mir, Moscow.

Tikhonov, A. N., and A. A. Samarsky (1966), *Mathematical physics equations* (in Russian), 724 pp., Moscow.

Turcotte, D., and J. Schubert (1985), *Geodynamics* (in Russian), 57 pp., Mir, Moscow.

Valet, J.-P., T. Kidane, V. Soler, J. Brassart, V. Courtillot, and L. Meynadier (1998), Remagnetization in lava flows recording pretransitional directions, *J. Geophys. Res., 103,* 9755–9775.

Wager, L., and G. Brown (1970), *Igneous rocks* (in Russian), 550 pp., Mir, Moscow.

Williams, I., and M. Fuller (1982), A Miocene polarity transition (R-N) from the Agno batholith, Luzon, *J. Geophys. Res., 87,* 9408–9418.

D. M. Pechersky, A. A. Lyubushin, Institute of Physics of the Earth, Russian Academy of Sciences, 10 Bol'shaya Gruzinskaya ul., Moscow, 123995 Russia

V. S. Zakharov, Moscow State University, Vorobjovi Gori, Moscow, 119899 Russia

(Received 24 October 2004)